

AD-A238 971



LARGE ICE CRYSTAL CHARGE TRANSFER STUDIES

Final Report AFOSR-87-0379, June 1991

C P R Saunders

Pure and Applied Physics Department

UMIST

Manchester M60 1QD

England

DTIC  
ELICITE  
JUL 31 1991  
S D

DISPATCHED BY AIRMAIL  
Approved for Release  
Declassified

91-06577



## REPORT DOCUMENTATION PAGE

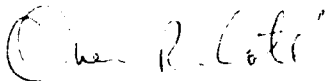
Form Approved  
OMB No. 0704-0188

PORT SECURITY CLASSIFICATION			1b. RESTRICTIVE MARKINGS			
SECURITY CLASSIFICATION AUTHORITY Unclassified			3. DISTRIBUTION / AVAILABILITY OF REPORT Approved for public release; distribution unlimited			
CLASSIFICATION / DOWNGRADING SCHEDULE						
FORMING ORGANIZATION REPORT NUMBER(S)			5. MONITORING ORGANIZATION REPORT NUMBER(S)  TR-91-07			
NAME OF PERFORMING ORGANIZATION Department of Physics UMIST		6b. OFFICE SYMBOL (If applicable) UMIST	7a. NAME OF MONITORING ORGANIZATION  EOARD			
ADDRESS (City, State, and ZIP Code) Main Building, Sackville Street, Manchester, M60 1QD, U K			7b. ADDRESS (City, State, and ZIP Code) 223/231 Old Marylebone Road London NW1 5TH U K			
NAME OF FUNDING / SPONSORING ORGANIZATION EOARD		8b. OFFICE SYMBOL (If applicable) EOARD	9. PROCUREMENT INSTRUMENT IDENTIFICATION NUMBER  AFOSR-87-0379			
ADDRESS (City, State, and ZIP Code)  223/231 Old Marylebone Road London NW1 5TH U K			10. SOURCE OF FUNDING NUMBERS			
TITLE (Include Security Classification)  Large Ice Crystal Charge Transfer Studies (Unlimited)			PROGRAM ELEMENT NO.	PROJECT NO.	TASK NO.	WORK UNIT ACCESSION NO.
PERSONAL AUTHOR(S) Saunders C P R						
TYPE OF REPORT Final		13b. TIME COVERED FROM Sep 87 TO May 91	14. DATE OF REPORT (Year, Month, Day) 91, 5, 31		15. PAGE COUNT	
SUPPLEMENTARY NOTATION						
COSATI CODES			18. SUBJECT TERMS (Continue on reverse if necessary and identify by block number)			
FIELD	GROUP	SUB-GROUP	Thunderstorms, Electrification, Charge transfer, Rime ice, cold chamber, aircraft charging, crystal scavenging, numerical modelling			
ABSTRACT (Continue on reverse if necessary and identify by block number) dies of charge transfer between ice crystals and a graupel pellet have been e in a laboratory cold room. The dependence of charge transfer upon liquid er in the cloud has been quantified and together with previously determined endencies on crystal size and velocity, relationships have been found bet- n the parameters that control the charge sign and magnitude. These results be used in numerical models of the electrification of thunderclouds. The rge transfer mechanism is discussed in terms of two competing mechanisms ding to positive and negative pellet charging. The validity of the exper- ntal techniques used has been verified by studying the charge to ice spheres ely falling through an ice crystal and supercooled droplet cloud. Other k has involved the collision efficiency of graupel pellets for ice crystals. heat transfer coefficient of riming graupel pellets, and the scavenging aerosol particles.						
DISTRIBUTION / AVAILABILITY OF ABSTRACT UNCLASSIFIED / UNLIMITED <input type="checkbox"/> SAME AS RPT <input type="checkbox"/> DTIC USERS			21. ABSTRACT SECURITY CLASSIFICATION			
NAME OF RESPONSIBLE INDIVIDUAL C P R Saunders			22b. TELEPHONE (Include Area Code) 44-01-200-3000		22c. OFFICE SYMBOL J6	

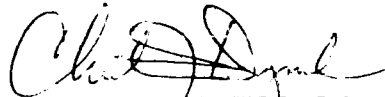
TR-91-07

This report has been reviewed and is releasable to the National Technical Information Service (NTIS).  
At NTIS it will be releasable to the general public, including foreign nations.

This technical report has been reviewed and is approved for publication.



OWEN R. COTE  
Chief, Geophysics and Space



CHESTER J. DYMEK, Lt Col, USAF  
Technical Director

Grant Number AFOSR-87-0379

## LARGE ICE CRYSTAL CHARGE TRANSFER STUDIES

C P R Saunders

Physics Department  
University of Manchester Institute of Science and Technology  
Manchester M60 1QD  
England

31 May 1991

# Final Scientific Report

1 September 1987 - 31 May 1991

Approved for public release, distribution unlimited.

Prepared for:

United States Air Force  
Air Force Office of Scientific Research  
Building 410  
Bolling AFB, DC 20332

and,  
European Office of Aerospace, Research and Development,  
London, England.

[illegible]

## CONTENTS

		Page
Chapter 1	Introduction to the work described in this report.	1
Chapter 2	The effect of liquid water on thunderstorm charging.	7
Chapter 3	Theories of thunderstorm electrification.	26
Chapter 4	Charge transfer to spherical and falling riming targets.	34
Chapter 5	A theoretical treatment of the trajectory of an ice crystal past a cylindrical target.	42
Chapter 6	The heat transfer of a riming cylinder.	50
Chapter 7	The scavenging of high altitude aerosol by small ice crystals.	58
Chapter 8	Thunderstorm charging: calculations of the effect of ice crystal size and graupel velocity.	67
Chapter 9	Discussion and suggestions for future work.	78
References		82

## CHAPTER 1

### INTRODUCTION TO THE WORK DESCRIBED IN THIS REPORT

The research described here has been carried out in the Atmospheric Physics Research Group Laboratories at The University of Manchester Institute of Science and Technology, (UMIST). The work detailed in this final report may be considered as a continuation of the work of an earlier UMIST-USAF research project called "Ice particle charge transfer studies" dated 87-9-30. The principal area of research has involved laboratory studies of the electrification of thunderclouds. The cold room facility in UMIST has been used to grow realistic clouds of supercooled water droplets and ice crystals which are caused to interact with a riming ice target representing a graupel (soft hail) pellet falling through a thunderstorm. The previous work showed that considerable charge was separated when ice crystals bounce off graupel and that the sign and magnitude of the charge was affected by temperature, liquid water content, ice crystal size and graupel velocity. Figure 1.1 shows the cold room with its upper chamber for ice crystal initiation, and a lower, crystal growth chamber. Ice crystals up to several hundred microns diameter are available for interaction with the vertical rods at the bottom of the chamber which move through the cloud, become covered in rime, and act as graupel pellet simulators. Any charge separated during crystal interactions with the riming target rod is measured through a slip-ring connection to the target. From a knowledge of the ice crystal concentration and collection efficiency, the charge transfer per crystal separation event may be determined, as shown in figures 1.2 and 1.3. The

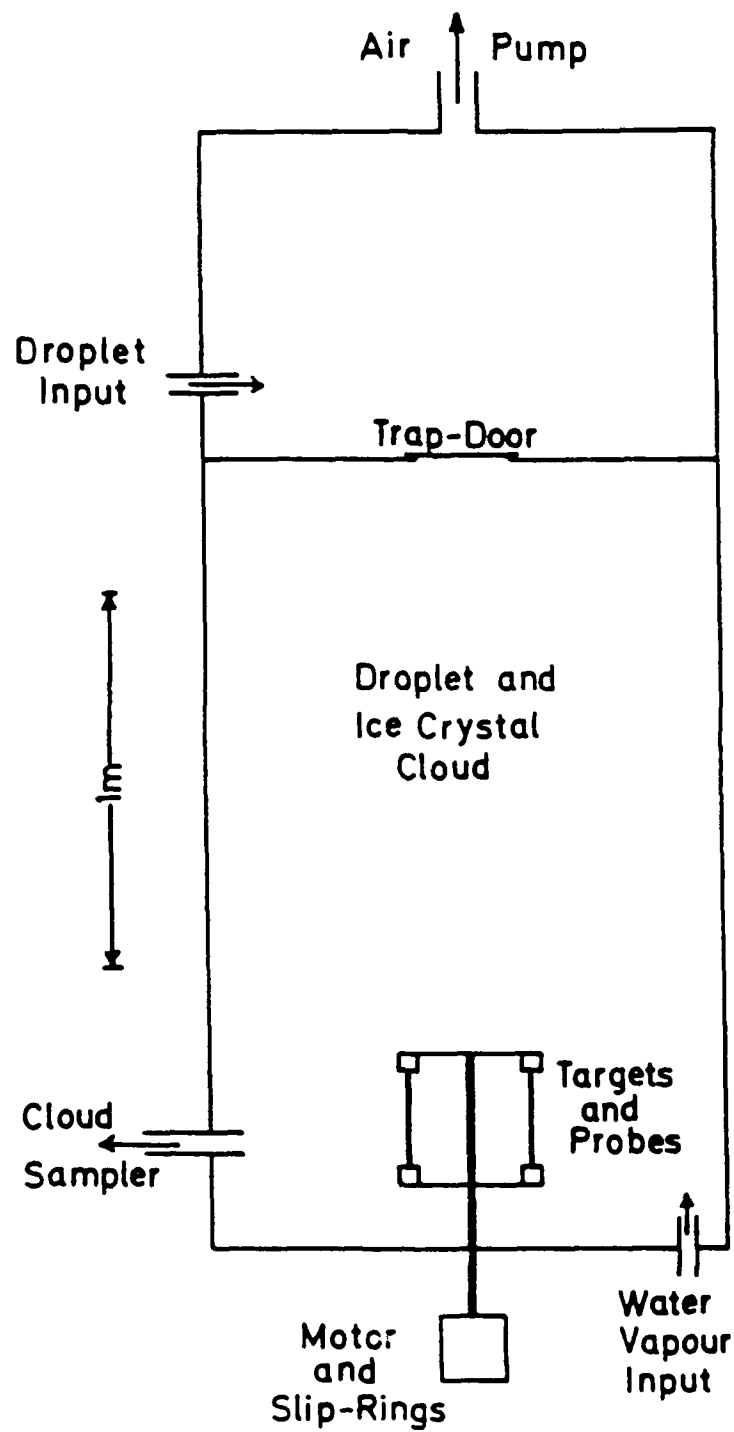


Figure 1.1 The cloud chamber inside the coldroom

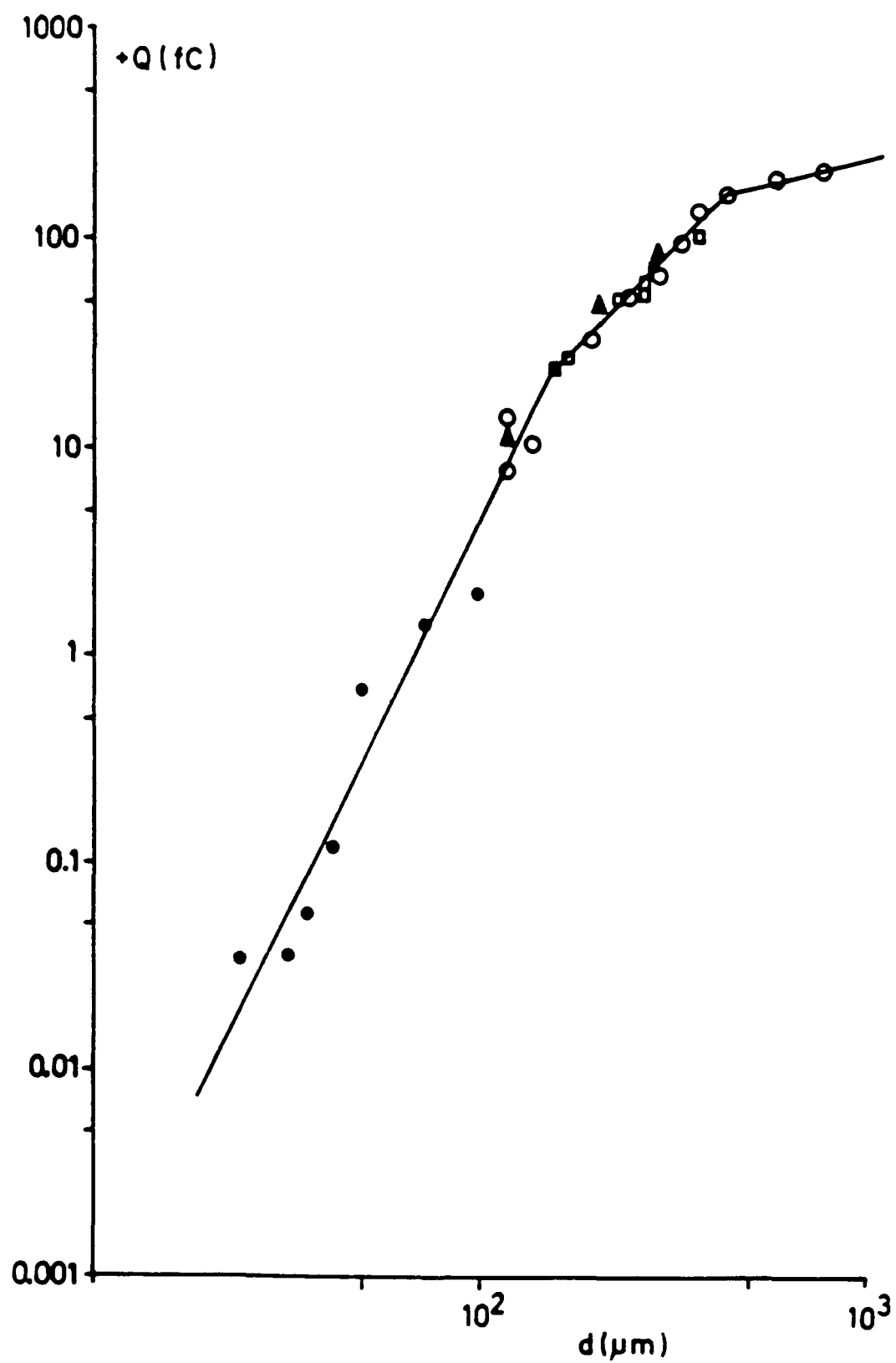


Figure 1.2 Positive charge to a riming target versus crystal size



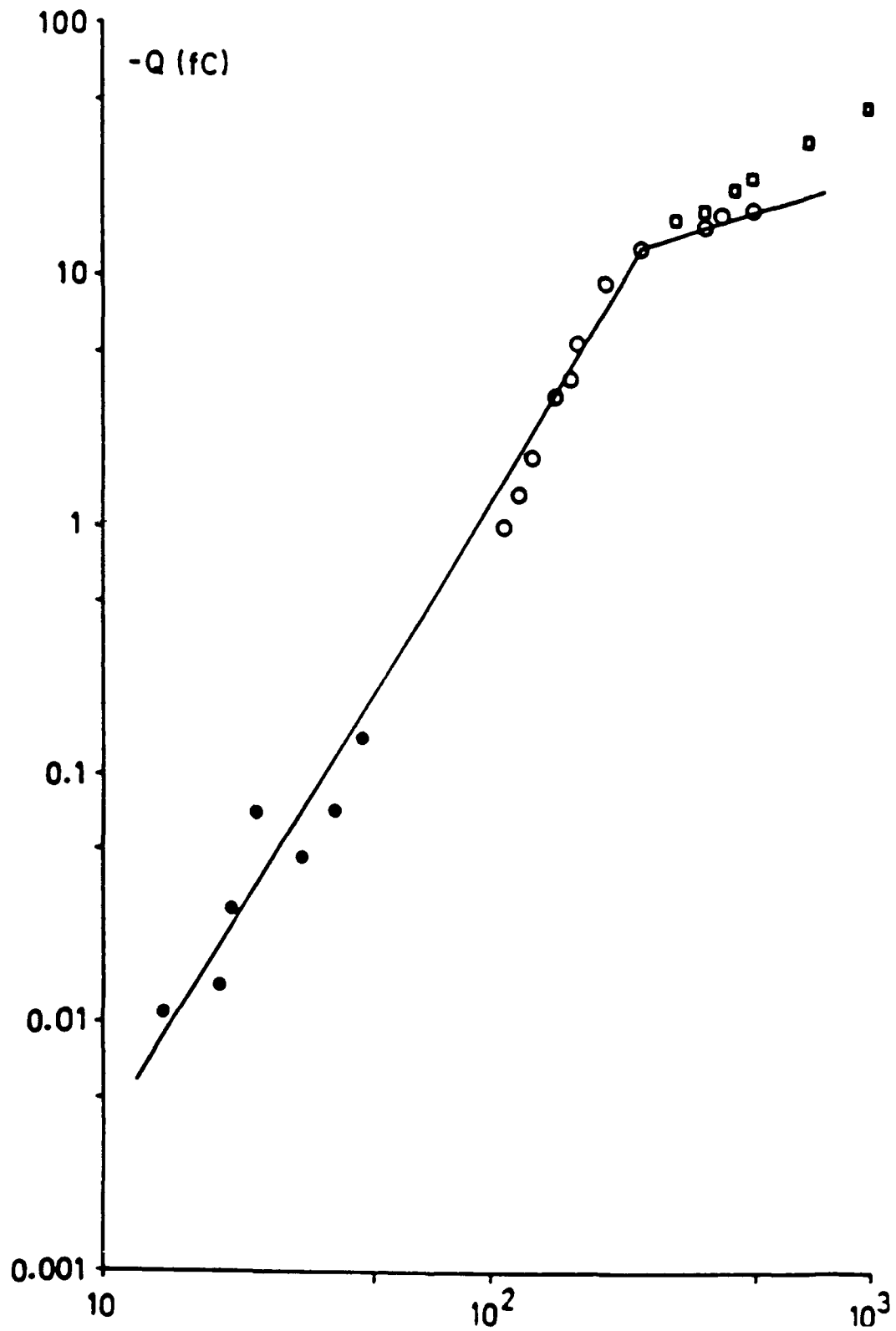


Figure 1.3 Negative charge to a riming target versus crystal size

results show that there is a charge-sign reversal temperature above which graupel charges positively and below which it charges negatively. The charge transfer is also velocity dependent as shown in Figure 1.4. These data were obtained with constant values of liquid water in the cloud. The reversal temperature is dependent on liquid water in a way which has been determined during the present work, the details being presented in Chapter 2. Relationships of the form  $q = A d^a V^b$  were determined in the earlier work for the positive and negative charging regimes, where  $A$ ,  $a$  and  $b$  are constants for particular ranges of ice crystal sizes,  $d$  is the crystal size and  $V$  is the velocity. These equations have now been extended to include liquid water content as a variable. The resulting parameterization of the charge transfer results to include all the controlling variables is now available for inclusion in numerical models of the electrical development of thunderstorms. A first attempt at this is described in Chapter 8.

Theories of the charge transfer mechanism have been plentiful in the past. Only a few have stood the test of time and these are included in a discussion of the present state of knowledge in Chapter 3. The conclusion is that more work is needed to discriminate between the remaining possibilities, or to come up with a mechanism or mechanisms which tie in better with the observations of the sensitivity of the sign of the charge transfer to the specific cloud conditions.

Figures 1.2 and 1.3 show that the charge transfer is limited in some way at larger crystal sizes and this observation led us to suggest that, following the initial charge transfer, when an ice crystal leaves the target surface, the adjacent

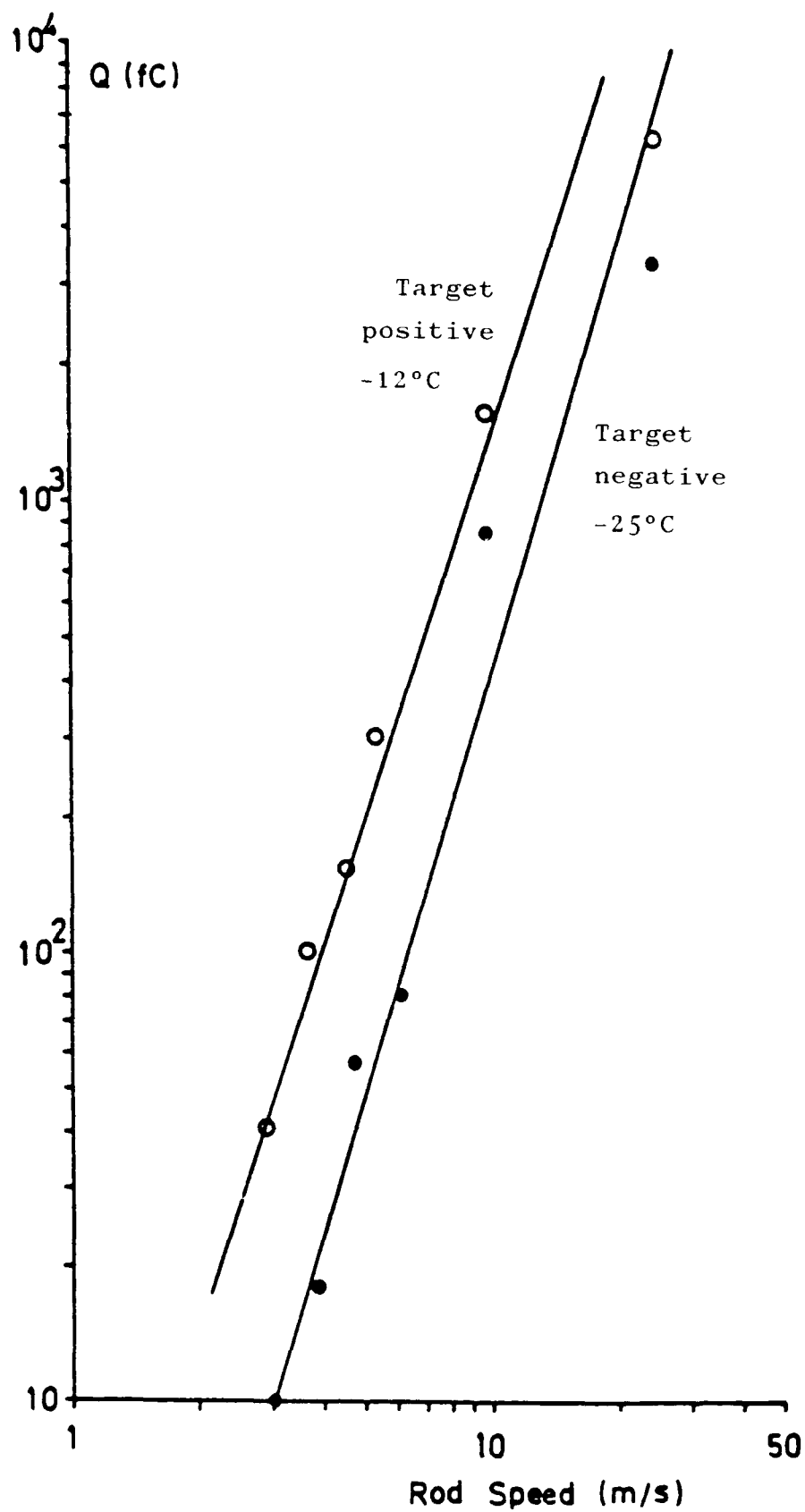


Figure 1.4 The velocity dependence for positive and negative charging

charges on the two surfaces are able to initiate a corona discharge which reverses some of the charge transfer. We predicted that this corona discharge would lead to the emission of light. A sensitive photo-diode was set-up to view the crystal interaction zone and light emission was noted. Figure 1.5 shows the number of photons emitted per femto-Coulomb of charge transferred as a function of ice crystal size. Several tests were made to check that the results were not spurious and the phenomenon is confirmed by Figure 1.5 which shows the original data reported in an earlier USAF interim report, together with further results which are in agreement. Also shown, are results obtained with a blue filter over the photo-diode confirming that the corona emission is associated with the blue nitrogen line. Not shown on the figure, is the zero result obtained with a red filter over the photo-diode. The corona associated with ice crystal impacts and separations is likely to lead to radio frequency emissions when ice crystals bounce off aircraft surfaces.

The charge transfer results obtained above, were the result of collisions of multiple ice crystals with the riming ice target. In order to check that this technique was valid, a separate experiment was set-up in which an individual ice crystal was levitated in a wind-tunnel while it grew to 200  $\mu\text{m}$ , it was then drawn past an ice target which was connected to an electrometer. The conditions were set-up for positive target charging and the results shown in Figure 1.6, when compared with those of Figure 1.2, confirm that both experimental methods are in broad agreement.

Possibly of great importance to the charging of aircraft,

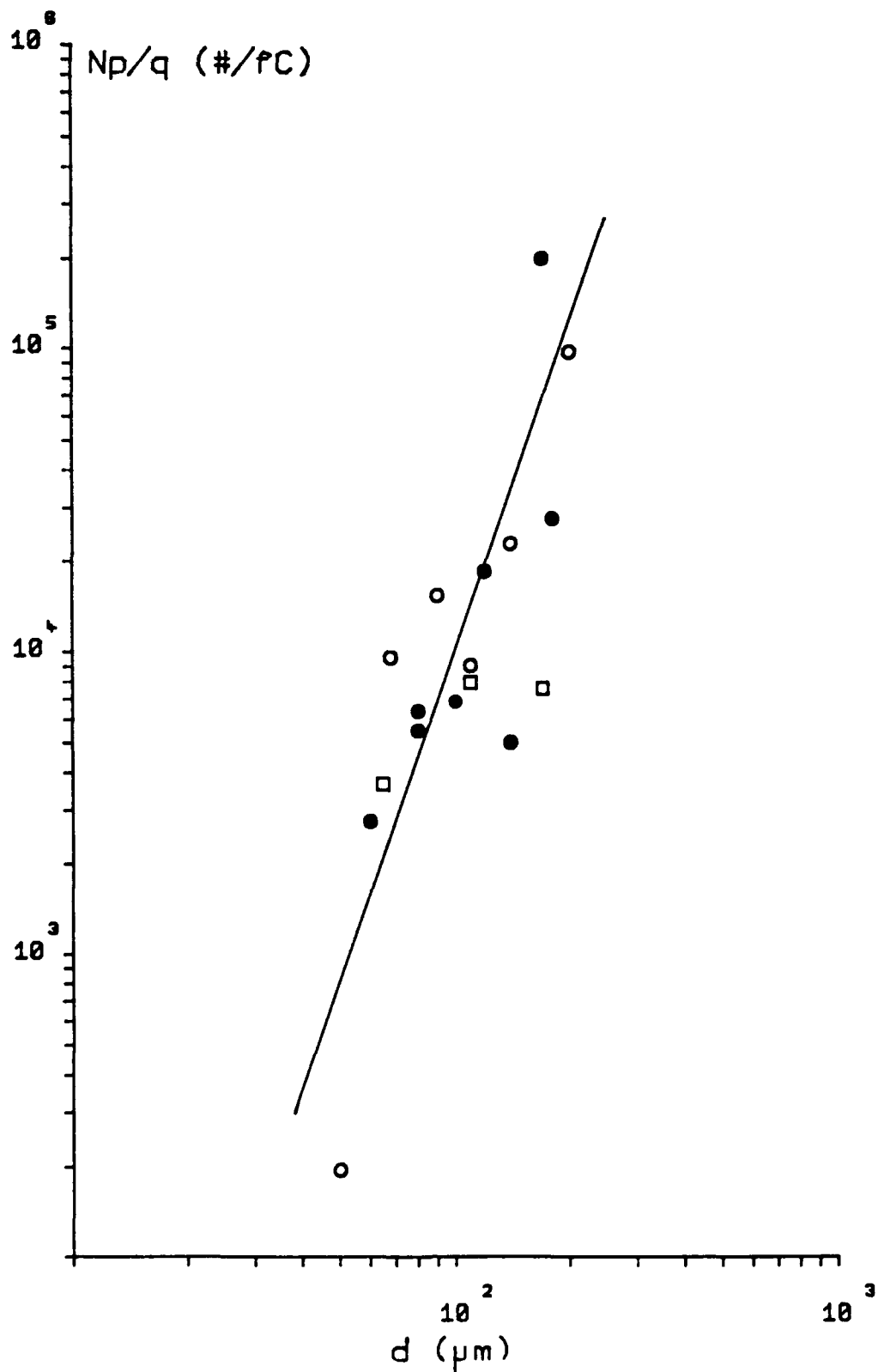


Figure 1.5 Light emission during during crystal interactions

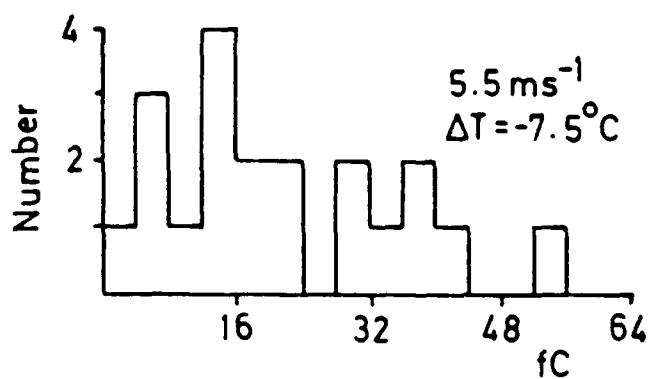
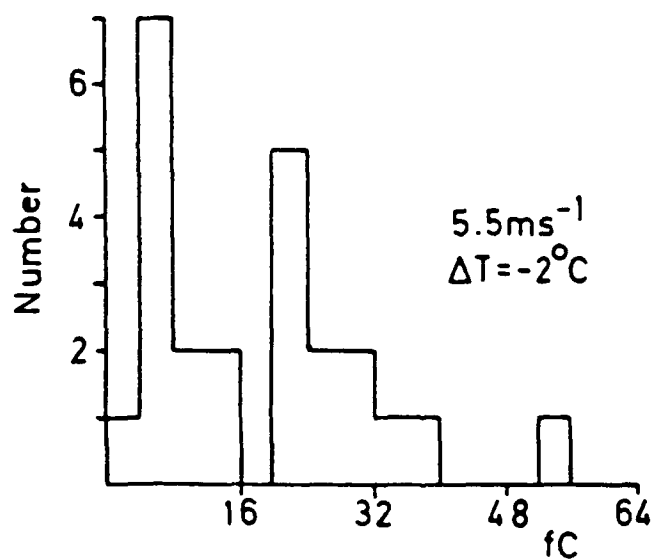
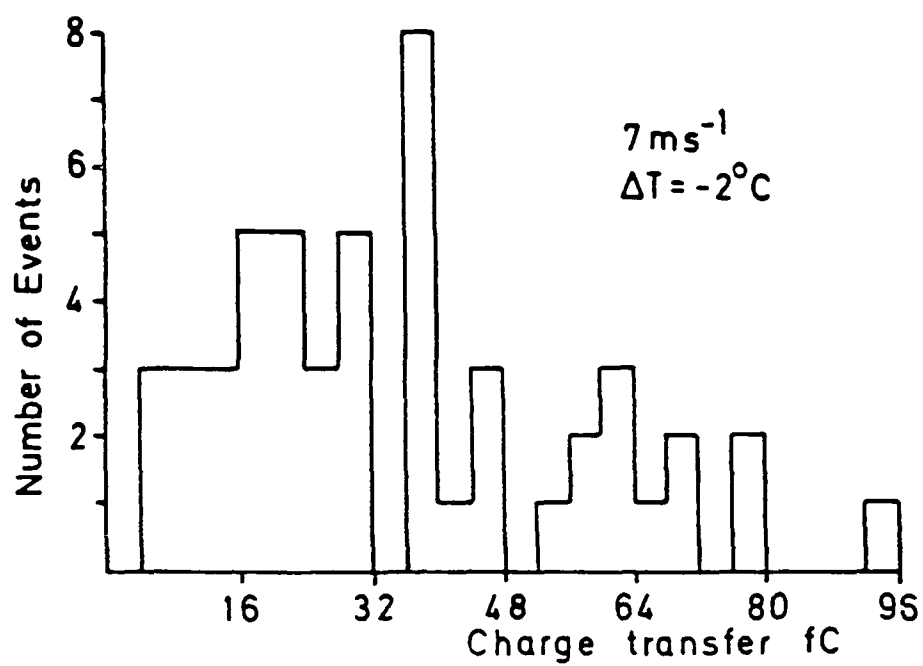


Figure 1.6 Individual charge transfer events

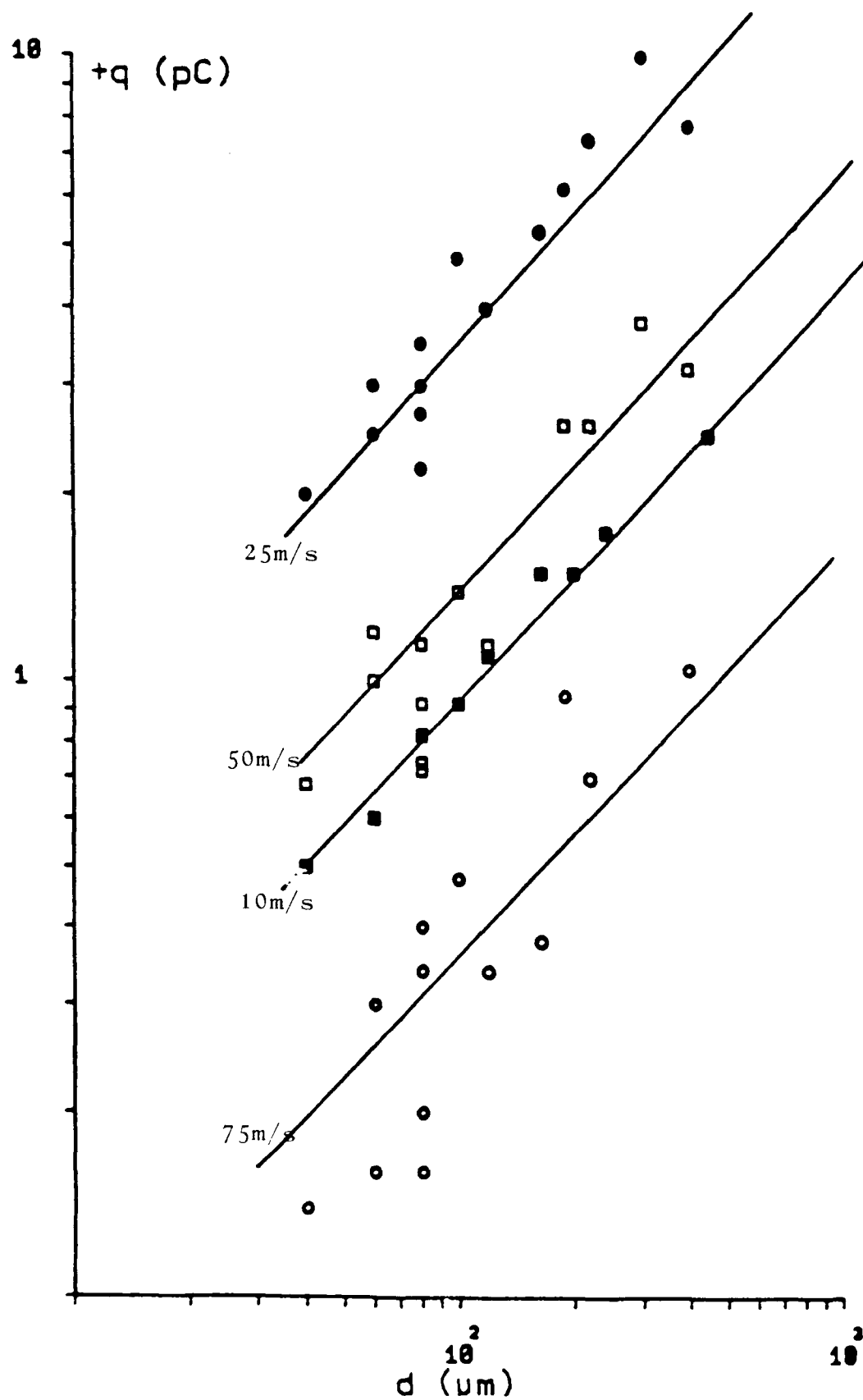


Figure 1.7 Charge per event versus crystal size for various velocities

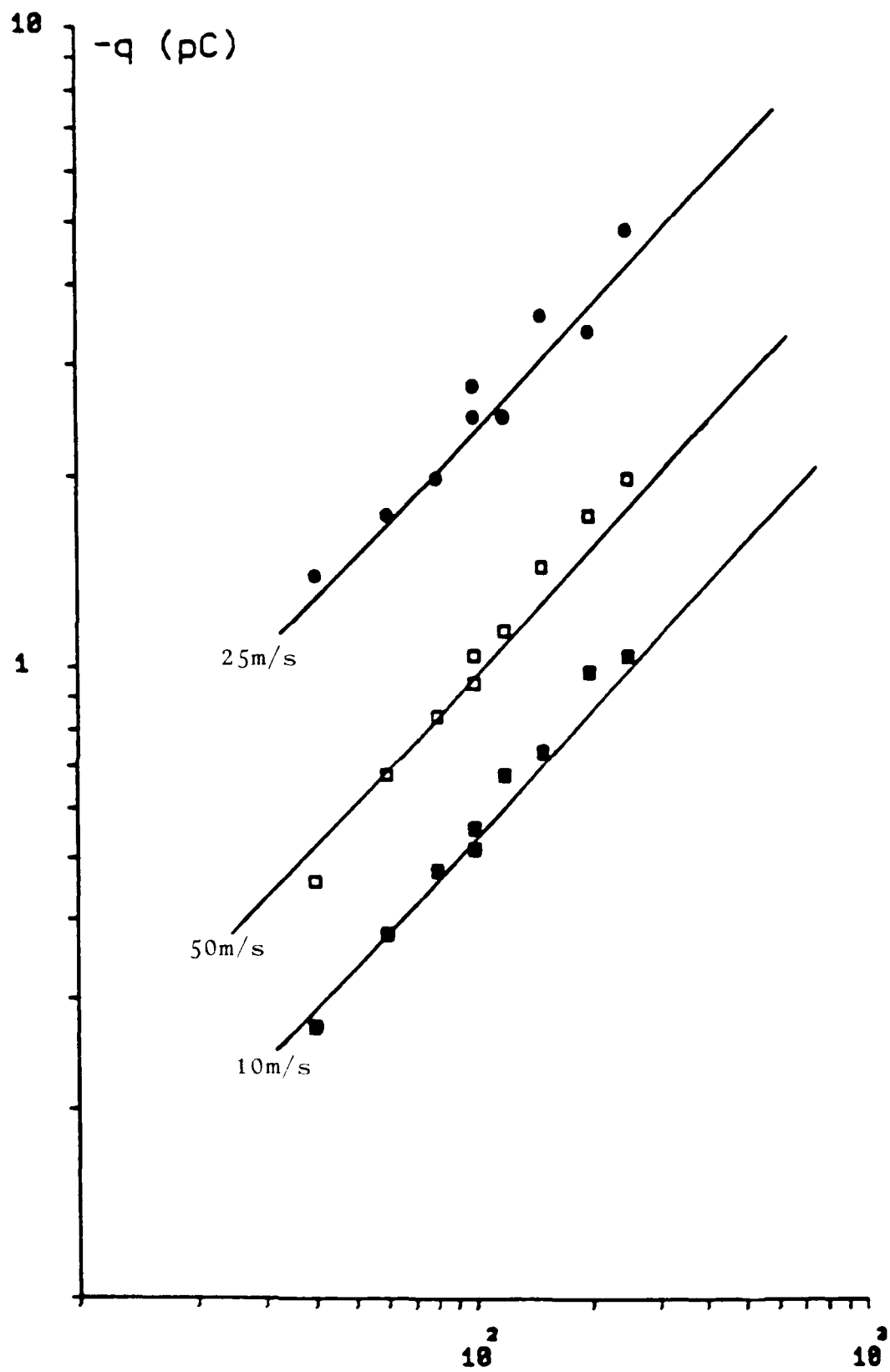


Figure 1.8 Charge per event versus crystal size  
for various velocities



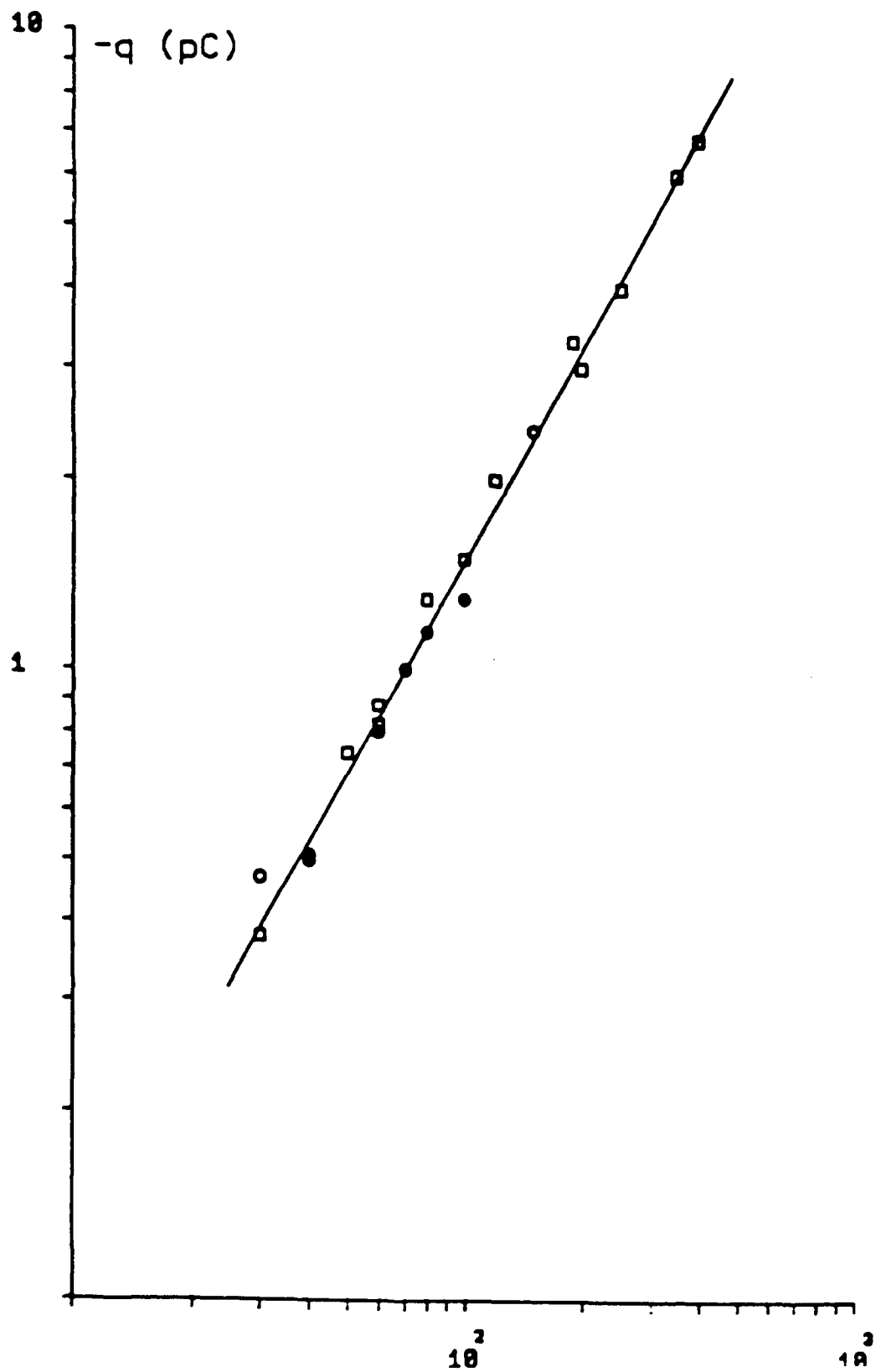


Figure 1.9 Charge per event for ice crystals  
at 110 m/s

is the impact of ice crystals upon the skin. Experiments were conducted to measure the charge transferred when ice crystals bounced off a target at high speeds both in the presence and absence of super-cooled water droplets. The expected increase of charge transfer with increasing velocity was observed but only up to a certain velocity, thereafter, the charge transfer decreased, as shown in Figures 1.7 and 1.8 for the case of a cloud of ice crystals and super-cooled droplets. Figure 1.9 shows the case for ice crystal interactions with the target in the absence of super-cooled droplets. The reduced charging at high speeds with water droplets and ice crystals in the cloud, was previously attributed to a decreased contact time at high speed. However, at low speeds ( $5 \text{ m s}^{-1}$ ), ice crystals alone give charge transfers of an order of magnitude less than when crystals and droplets are present together. But, at high speed, (Figure 1.9,  $110 \text{ m s}^{-1}$ ), the charge transfer due to ice crystals alone is substantial and is larger than the values for crystals and supercooled droplets at  $110 \text{ m s}^{-1}$  (extrapolated value from Figure 1.8). Thus the decrease of charge transfer with increase of velocity in the case with water droplets present, must be due to the presence of water on the surface of the target. Table 1.1 shows the values of cloud liquid water content required for wet growth at  $100 \text{ m s}^{-1}$  calculated from the heat balance equations of Macklin and Payne (1967).

Table 1.1

Air Temperature °C	Liquid Water Content ( $\text{g m}^{-3}$ ) for Wet Growth at $100 \text{ m s}^{-1}$
--------------------	--

-10	0.48
-15	1.03
-20	2.6
-25	3.8
-30	5.74

The actual liquid water content used in these experiments was maintained at  $0.1 \text{ g m}^{-3}$ . The table shows that wet growth could not have occurred. However, at high speeds, the rate of arrival of water droplets on the surface is higher than at low speeds so there is an increased possibility that an arriving ice crystal encounters a recently arrived droplet which has not had time to freeze and is captured by it. Thus, the decreased charge transfer at high speeds, in the presence of super-cooled droplets, is due to an increased crystal collection efficiency.

The experimental charge transfer work in the cold room has involved simulated graupel pellets in the form of riming rods which move round through the cloud. The rods are connected to an amplifier in order to measure the charge transfer and this effectively connects them to ground. This area of unreality in the simulations has led to concern and the situation has been checked by measuring the charge on ice spheres which have been dropped through the cloud of ice crystals. The results are presented in Chapter 4. Chapter 5 deals with the development of a computer model to calculate the trajectories of plate and columnar ice crystals in a fluid flow around a cylindrical target. The predictions were compared with experimental results.

Chapter 6 deals with the heat transfer to a riming target due to the release of latent heat from freezing droplets. Surface roughness is affected by rime density which in turn depends on impact velocity and temperature.

Chapter 7 is concerned with the scavenging of high altitude aerosol by ice crystals. An ice crystal cloud in the cold room was allowed to fall through a cloud of aerosol particles and the collection efficiency was compared with that predicted by scavenging theory.

Chapter 8 is the charging model calculation referred to above, while Chapter 9 concludes the report.

## CHAPTER 2.

### THE EFFECT OF LIQUID WATER ON THUNDERSTORM CHARGING

#### 2.1 Introduction

Laboratory studies have shown that thunderstorm charging caused by the interactions of ice crystals and graupel pellets is affected in sign and magnitude by temperature and cloud liquid water content; the presence of water droplets is a requirement for substantial charge transfer. Relationships showing the dependence of charge transfer on ice crystal size and velocity have previously been reported and now, in a continuation of the laboratory studies, the effect of liquid water content on the charge transfer has been investigated. Positive graupel charging occurs at temperatures above the "charge-sign-reversal-temperature" and vice-versa. The reversal temperature moves to lower temperatures when the liquid water content is increased. However, at low values of liquid water content, the sign of the graupel charging is inverted being positive at low temperatures and vice versa. Relationships between charge transfer, liquid water content, temperature, ice crystal size and velocity have been determined and may be used in numerical models of the development of thunderstorm electric fields. A one-dimensional model indicates that the charge separation rates noted here are adequate to account for thunderstorm electrification. Use of the equations with cloud parameter values taken from thunderstorm flights, predicts charge reversal levels around  $-13^{\circ}\text{C}$ , in agreement with the requirements of field analysis.

Observations of thunderstorms by Krehbiel et al (1979),

Lhermitte and Krehbiel (1979), Krehbiel (1986) and Williams (1989) have shown that the charge centers occur in well defined temperature bands. From airborne studies of thunderstorms, Dye et al (1986) suggest that the updraft-downdraft zone between  $-10^{\circ}\text{C}$  and  $-20^{\circ}\text{C}$  might be a preferred location for charge generation. These results confirm the requirement for a temperature sensitive charging mechanism. Laboratory studies of collisions between ice crystals and graupel pellets (soft hailstones), in the presence of supercooled water droplets, have shown that substantial charge is separated during such interactions (Reynolds et al (1957), Church (1966), Marshall et al (1978), Takahashi (1978), Hallett and Saunders (1979), Jayaratne et al (1983), Baker et al (1987), and Keith and Saunders (1989a, 1990)). In thunderstorms, when ice crystals bounce off riming hail pellets, the equal and oppositely charged particles separate in the updraft with the crystals being carried upwards relative to the hail. When such interactions occur at low values of cloud temperature, the laboratory studies show that the graupel becomes negatively charged which can account for the observations of a negative charge center in thunderstorms. The ice crystals are positively charged and are carried aloft to form a region of positive charge. Such a dipole fits the thunderstorm charge center observations first noted by Wilson (1920). Extensive laboratory studies of such ice crystal/graupel interactions by Jayaratne et al (1983) and Keith and Saunders (1990) have shown that the sign of the charge transfer is dependent on temperature and the liquid water content in the cloud. Jayaratne et al defined the "reversal temperature" as that temperature below which graupel pellets charge negatively,

and vice versa. The reversal temperature is dependent on liquid water content in such a way that higher values of liquid water promote positive pellet charging and thus shift the reversal temperature to lower temperatures. At altitudes below the reversal temperature level, graupel pellets charge positively and fall to form a weak, lower positive charge center. The negative crystals are carried aloft to re-inforce the negative graupel charge center. Such a thunderstorm tripole charge distribution has often been observed (Williams, 1989).

The experiments of Jayaratne et al (1983) showed that liquid water was essential for substantial charge transfer to occur during crystal interactions with a riming graupel pellet. With water droplets alone, no charge transfer occurred. When ice crystals alone interacted with an ice target, the charge transfer was not significant to thunderstorm electrification. Without water droplets in the cloud, they also noted that when the ice target grew by vapor deposition, it charged positively during crystal interactions, and when it evaporated, it charged negatively. Similar observations have been made by Buser and Aufdermaur (1977), Marshall et al (1978), Gaskell and Illingworth (1980) and Avila et al (1988), amongst others. Of note, is the fact that with water droplets present, the ice target is always growing, yet charge transfer of either sign may be obtained depending on the temperature and liquid water content of the cloud. Calculations of the heating of a riming pellet due to the release of latent heat, using the heat balance equation of Macklin and Payne (1967), confirm that at realistic liquid water contents and fall velocities for small graupel pellets, the riming surface is heated insufficiently to cause it to evaporate.

If the liquid water content were sufficiently high to cause wet growth, colliding ice crystals would be collected and there would be no charge transfer.

Aircraft penetrations of thunderstorms have shown that substantial electric charge is to be found on millimetre sized graupel pellets in the early stages of cloud development. For example, Gaskell et al (1978) and Christian et al (1980) measured charges of 50 pC on 3 mm diameter graupel. Our laboratory studies have attempted to simulate particle and cloud conditions that can lead to such charges. The laboratory experiments of Jayaratne et al (1983) and Keith and Saunders (1990) have, in general, been performed with 5 mm diameter metal rods which become ice covered and represent graupel pellets. Air, or target, speeds are chosen to be representative of the fall speed of 5 millimetre graupel, which is around  $3 \text{ m s}^{-1}$  (Locatelli and Hobbs, 1974). Earlier work by Reynolds et al (1957), Church (1966) and Takahashi (1978) was conducted with targets on rapidly rotating systems at speeds around  $10 \text{ m s}^{-1}$ . Saunders and Zhang (1987) and Keith and Saunders (1989b) showed that the high g forces experienced by the rime on rapidly rotating systems can lead to rime break-up which causes positive charging of the target and depletion of the local liquid water content. This may explain some of the differences between the results of Takahashi (1978) and the UMIST work. This will be discussed later, in more detail.

The work of Jayaratne et al (1983) and Keith and Saunders (1990) showed that the charge transfer is affected by ice crystal size and by velocity. Keith and Saunders presented results of their measured charge transfer,  $q \text{ C}$ , in the form:



$$q = Ad^aV^b \quad (1)$$

where  $d$  is the crystal size in metres and  $V$  is the speed in metres per second; the constant  $A$  and the coefficients  $a$  and  $b$  were determined for particular ranges of crystal size in the positive and negative charging regimes. The results are reproduced here in Table 2.1.

TABLE 2.1  
Values of the constants  $A$ ,  $a$  and  $b$ .

Crystal size $\mu\text{m}$	$A$	$a$	$b$
10-155	0.31	3.76	2.5
155-452	$2.44 \times 10^{-8}$	1.9	2.5
452-	$3.26 \times 10^{-13}$	0.44	2.5
10-253	$-8.11 \times 10^{-7}$	2.54	2.8
253-	$-3.72 \times 10^{-14}$	0.5	2.8

What was lacking from the earlier results was any quantitative determination of the dependence of charge transfer on liquid water content. The objective of the present work is to fill this gap by means of a series of charge transfer experiments performed at one value of velocity with crystals in a limited size range, but under various values of liquid water content, for both positive and negative charging. The results have been parameterized so that they can be used in numerical models of the rate of electric field development in thunderstorms.

## 2.2 EXPERIMENTAL METHOD

The objective of these experiments was to measure the charge transferred during ice crystal interactions with riming graupel pellets over a range of temperatures and liquid water contents. The experiments took place in a cloud chamber inside a large cold room which has been described by Keith and Saunders (1990). The substantial dimensions of the cloud chamber ( $0.9 \times 1.5 \times 2 \text{ m}^3$ ) permitted the clouds generated to be more uniform with more constant values of liquid water content than in the case of the experiments reported by Jayaratne et al (1983). A cloud of water droplets from a boiler was introduced into the chamber whereupon the droplets rapidly supercooled to the environmental temperature. Previous experiments using this technique had shown that any impurity in the droplets formed was at a low enough concentration to have no effect on the charge transfer. Ice crystals were initiated in the cloud by the brief insertion of a fine wire which had been cooled to liquid nitrogen temperature. The crystals grew in the supersaturated environment which was maintained by the continuous arrival of water vapor. The crystals could be sampled at intervals by drawing part of the cloud out of the chamber past a prepared formvar coated slide at a sufficiently high speed to ensure 100% collision. Later analysis provided water droplet and ice crystal size and concentration data.

A graupel pellet was simulated by a 5mm diameter metal target rod mounted on insulators inside a tube of 37 mm internal diameter (Figure 2.1). The target rod rapidly became covered in rime ice when the cloud was drawn past. A sensitive charge amplifier was connected to the target so that the current caused

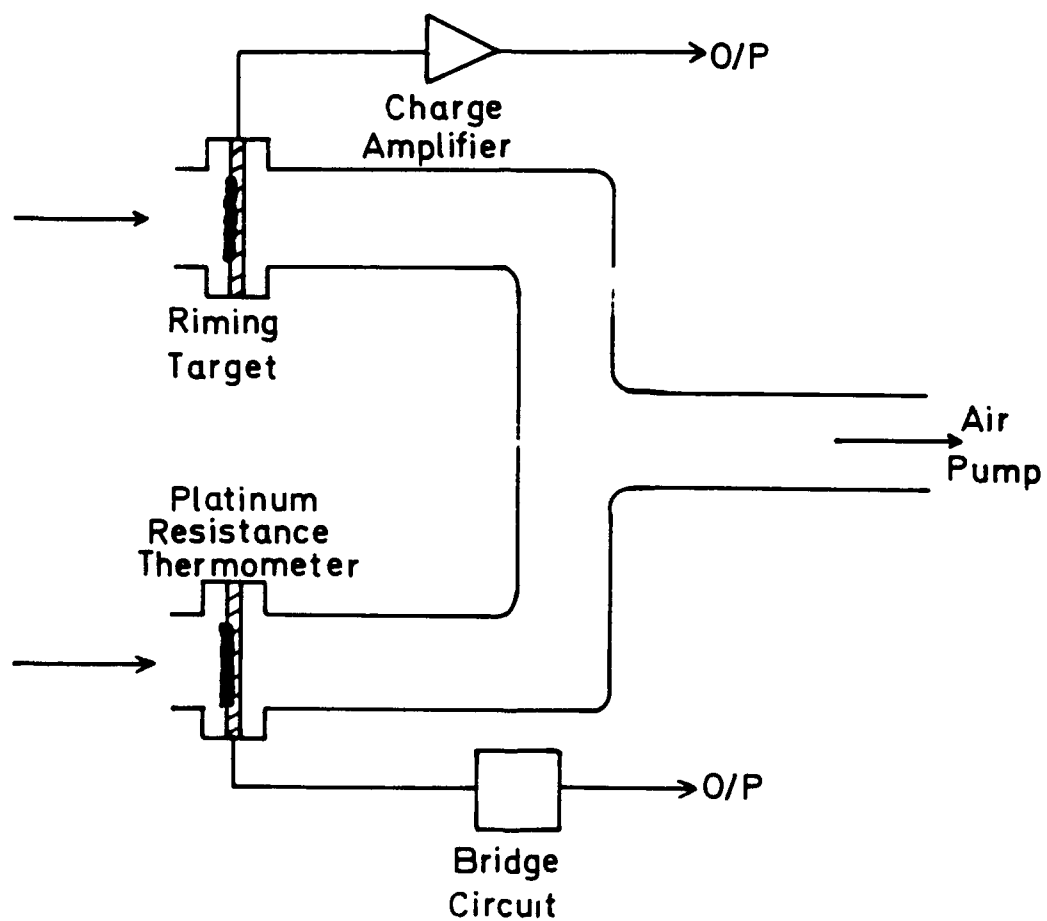


Figure 2.1 The twin tubes for the measurement of charge transfer and rime surface temperature

by a succession of ice crystal charging events could be monitored. With a sensitivity of 1mV equivalent to  $10^{-13}\text{A}$ , a time constant of 1 second and a noise level of 1 mV, individual charge transfers of 0.1 fC could be determined from a knowledge of the number of ice crystals interacting with the target. Keith and Saunders (1989c) determined the collection efficiency of ice targets for ice crystals under a range of conditions. In particular, they found values of the event probability (the collision efficiency times the separation probability) which permit calculations of the charge per crystal separation event to be made from a knowledge of the charging current, the crystal concentration and the velocity.

Previous work had shown that the presence of cloud liquid water is essential to significant charge transfer during crystal/graupel interactions. Furthermore, considerations of droplet spectra, riming rates and the behavior of freezing droplets on the riming surface (Jayaratne et al, (1983), Jayaratne and Saunders (1985), Baker et al (1989) and Keith and Saunders 1990)) have shown that it is important to know the rate of accretion of rime on the target because this controls the local surface conditions. This accretion rate is, in turn, controlled by the droplet collision efficiencies which are dependent on velocity and droplet and target sizes. The accreted rime comes from that portion of the droplet spectrum which collides with the target and may therefore be called the effective liquid water content in the cloud. This quantity is readily measured by monitoring the temperature rise of the riming target due to the latent heat released by freezing droplets. For this purpose, a second, similar tube to the target tube contained

a platinum resistance temperature probe mounted on a 5mm diameter rod having the same collision efficiency as the charge transfer target. The air speed through both tubes was the same, as confirmed by a pitot tube and by measurements of the charge transfer to both identical targets in a separate experiment. The effective liquid water content was determined from the heat balance equation for a riming cylinder derived by Macklin and Payne (1967). Their equation describes the balance between the rate at which heat is released by freezing droplets and the rate heat can be liberated to the environment by forced convection and evaporation, taking into account the effect of ventilation on the heat transfer process. The temperature probe had a sensitivity of 4 mV per  $^{\circ}\text{C}$ , and a resolution of  $0.06^{\circ}\text{C}$  corresponding to an effective liquid water content of  $0.03 \text{ g m}^{-3}$ .

In the charge transfer experiments, the rate of vapor input to the cloud was adjusted to give the required effective liquid water content in a range up to  $1.6 \text{ g m}^{-3}$ . The droplet cloud had a maximum size of  $33 \mu\text{m}$  with a modal diameter of  $12 \mu\text{m}$  as determined from analysis of formvar coated slides. The total liquid water content was measured by means of a hot-wire probe (Keith et al, 1986) which showed that the effective liquid water content was typically about half the total liquid water content. This was confirmed by an analysis of the collision efficiencies of the droplets using the size dependent results of Ranz and Wong (1952).

Previous experimental results by Keith and Saunders (1990) were used to formulate relationships between charge transfer, crystal size and velocity in the positive and negative charge transfer regimes above and below the reversal temperature. In

the present work, the effective liquid water content and temperature were varied while the crystal sizes were kept within the range 100 to 120  $\mu\text{m}$ . All the experiments were conducted at a velocity of  $3 \text{ m s}^{-1}$  which is appropriate to the fall speed of millimetre sized graupel pellets upon which significant charges have been measured in thunderstorms by Gaskell et al (1978), Gardiner et al (1985) and Dye et al (1986), amongst others.

### 2.3 RESULTS

Figure 2.2 shows the results of a typical experiment conducted in the temperature range  $-5^{\circ}\text{C}$  to  $-25^{\circ}\text{C}$  with positive charging to the target. The example shown was obtained at  $-10^{\circ}\text{C}$  with a vapor input rate adjusted to provide a particular value of effective liquid water content as determined by the heating of the target. The supercooled water droplet cloud was nucleated at time zero and the effective liquid water content achieved a fairly steady value of around  $0.4 \text{ g m}^{-3}$  after an initial rise during the first minute of the experiment. The charging current increased with time as the crystals grew and then decreased when the crystals fell out of the cloud. Formvar slide samples taken at intervals throughout the run were used to identify the moment when the ice crystals were in the range 100 to 110  $\mu\text{m}$ , at around 1.5 to 2 minutes after nucleation, whereupon the crystal concentration was determined and used to calculate the charge transferred per crystal separation event. Similar experiments were conducted over a range of temperatures and liquid water contents. Figure 2.3 shows the calculated charge transfers per ice crystal separation event obtained from several experiments over a range of values of effective liquid water content and

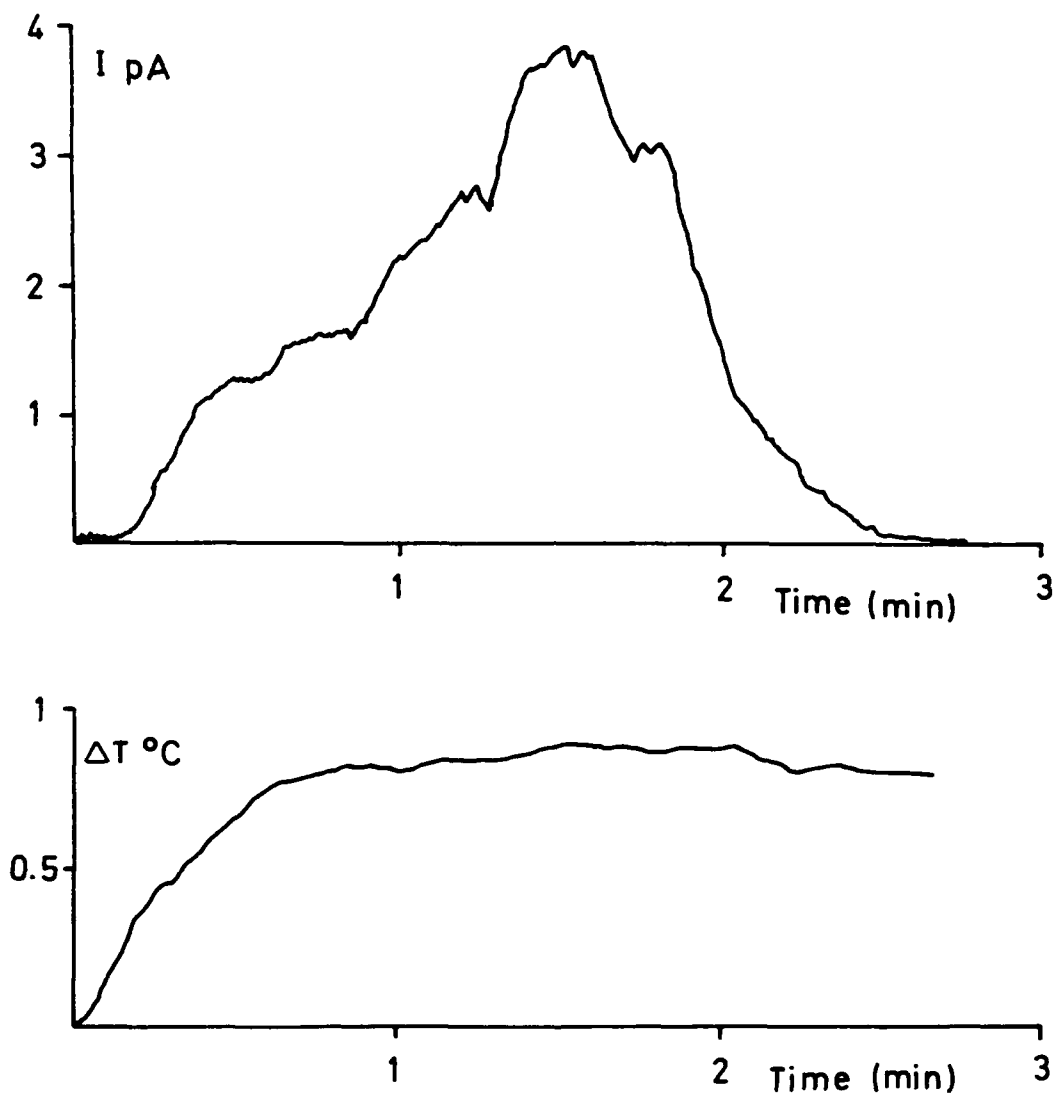


Figure 2.2 Positive current to the riming target and the elevation of the rime surface temperature throughout an experiment at  $-10^{\circ}\text{C}$ , for effective liquid water contents above  $0.22 \text{ g m}^{-3}$

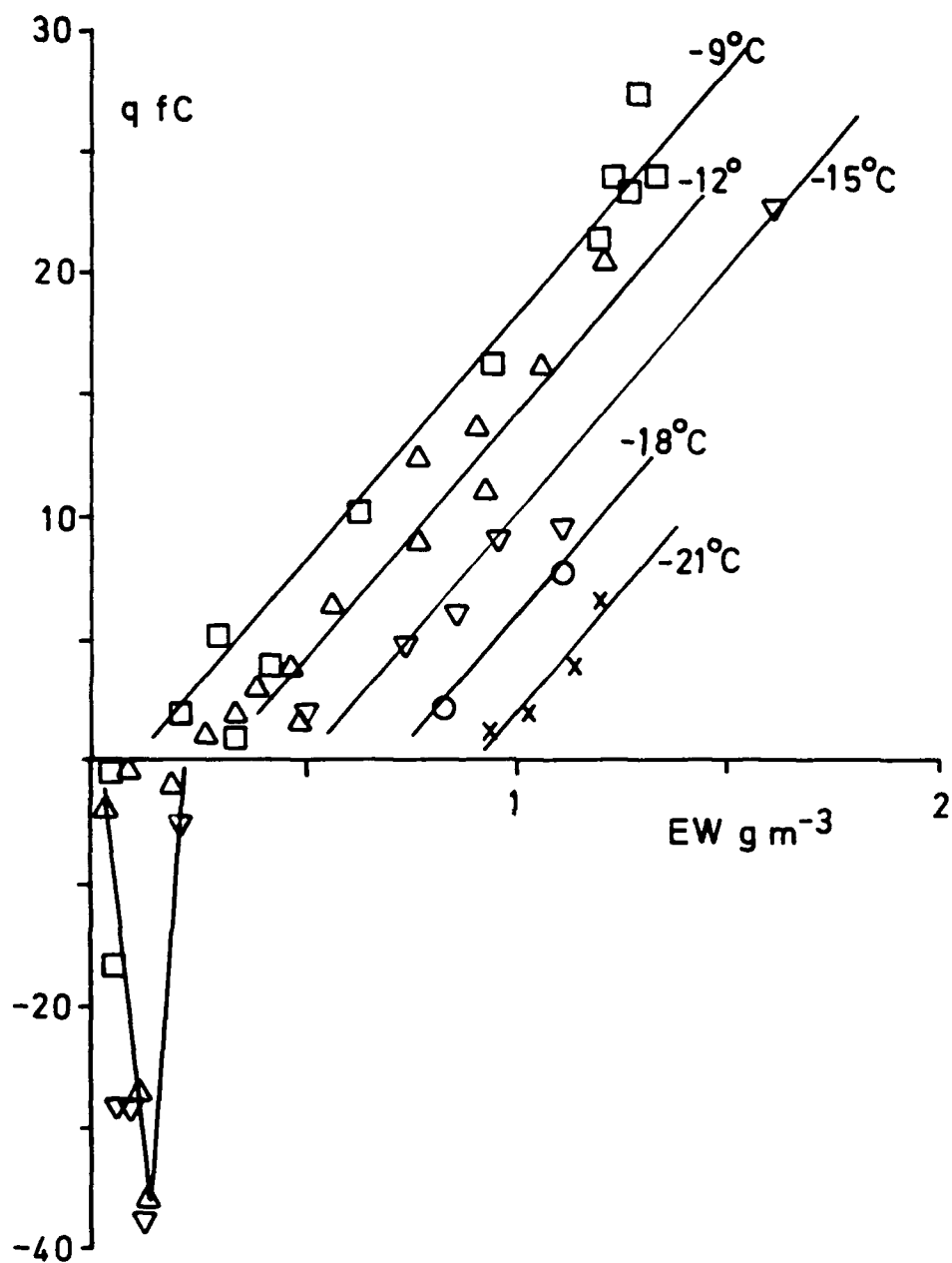


Figure 2.3 Charge transfer per crystal separation event to the riming target at temperatures down to  $-21^{\circ}\text{C}$  as a function of effective liquid water content.



temperature down to  $-21^{\circ}\text{C}$ . The lines drawn for positive target charging are best fits of charge versus effective liquid water content for particular small ranges of temperature. At low values of effective liquid water content, in the temperature range down to  $-16^{\circ}\text{C}$ , there is substantial negative target charging.

Figure 2.4 shows the negative current and rime heating data obtained at  $-24^{\circ}\text{C}$  which is typical of low temperature results. Figure 2.5 is the calculated charge per event for such cases. When the effective liquid water content lies between  $0.16\text{ g m}^{-3}$  and  $1.1\text{ g m}^{-3}$  the target charges negatively. This range corresponds to liquid water contents between about  $0.32$  and  $2.2\text{ g m}^{-3}$ . The charge transfer values were obtained over a temperature range down to  $-32^{\circ}\text{C}$  and the results indicate that negative charge transfer is independent of temperature.

## 2.4 DISCUSSION

The results follow the previously reported characteristics of positive charging to the target at temperatures above the reversal temperature and negative charging below; both cases require substantial liquid water, the value of which controls the reversal temperature. In addition, at low values of liquid water, there are positive and negative charging regimes at temperatures below about  $-20^{\circ}\text{C}$  and above about  $-16^{\circ}\text{C}$  respectively. The high positive values of charge transfer at low effective liquid water contents have not been reported in detail in previous UMIST studies but it has been possible to quantify them here because of the uniformity and longevity of the liquid

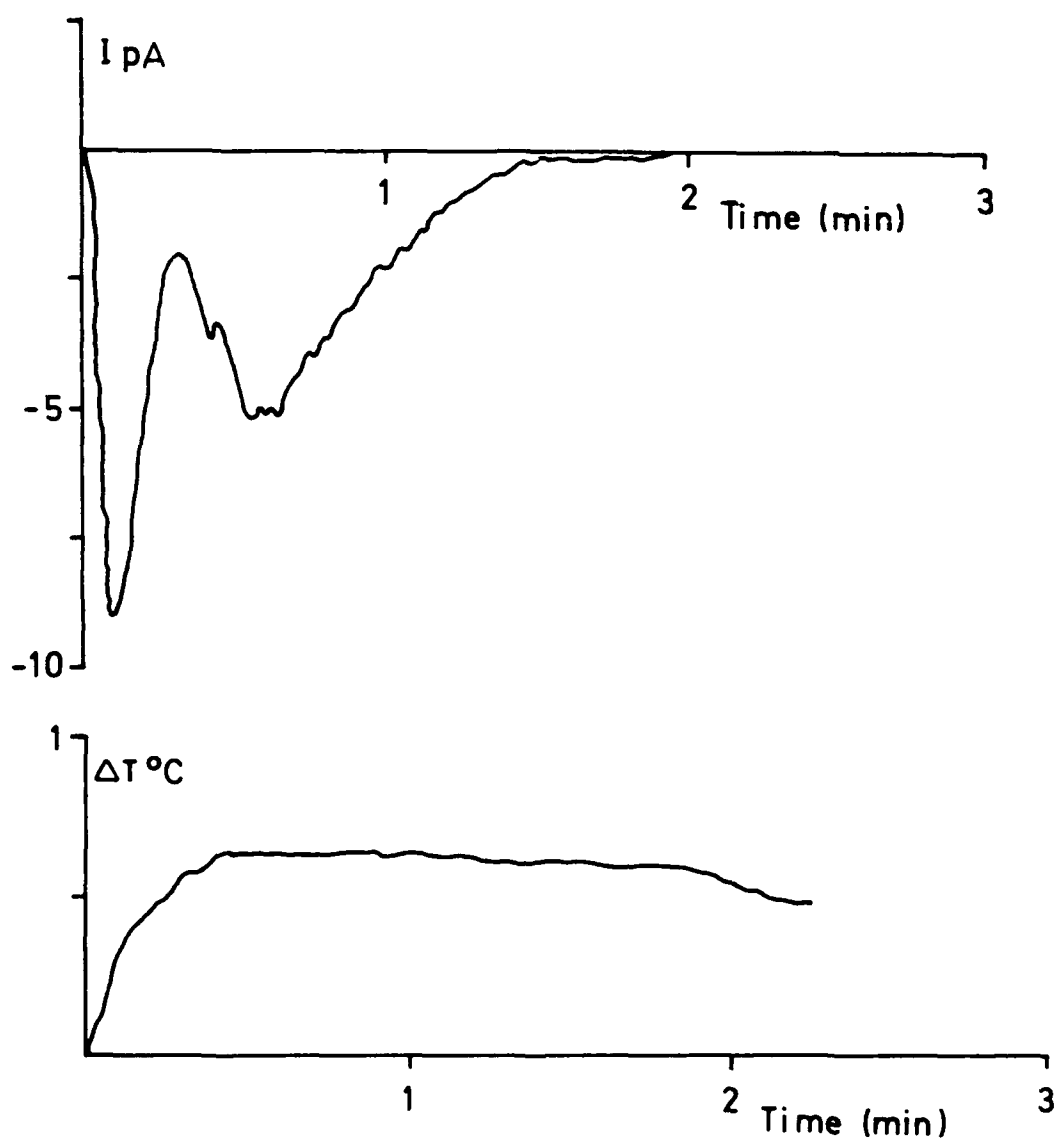


Figure 2.4 Negative current to the riming target and the temperature elevation of the rime surface at  $-24^{\circ}\text{C}$  with an effective liquid water content between 0.16 and 1.1 g m<sup>3</sup>

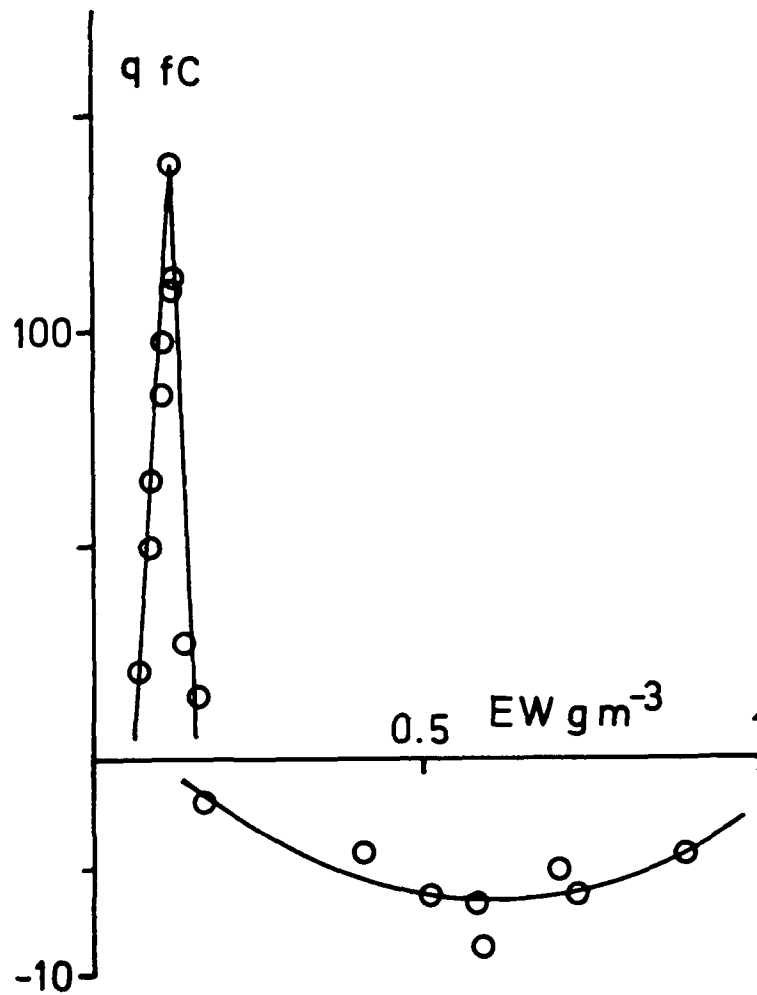


Figure 2.5 Charge transfer to the riming target per crystal separation event as a function of effective liquid water content at temperatures between  $-21$  and  $-32^{\circ}C$

water content in the present large cloud chamber. Church (1966) was the first to find that a riming target charges negatively at  $-15^{\circ}\text{C}$  in a low liquid water content cloud. Jayaratne et al (1983) also reported that when the liquid water content was reduced during a charge transfer experiment conducted above the reversal temperature, the target charging reversed sign from positive to negative. At low temperatures, the positive charge transfer at low liquid water contents was first reported by Reynolds et al (1957) who used a high ice crystal concentration which depleted the cloud droplets.

All the above results are consistent with the idea that under conditions suitable for vapor growth on the target, it charges positively due to crystals brushing past the negative surface charge caused by the temperature gradient across the surface layer. When riming occurs, a riming contact potential is set up, or charged dislocations are created, which lead to negative charging of the target. The positive and negative charging mechanisms are acting simultaneously, but depending on the local conditions, which are controlled by temperature, droplet size, freezing rate and the availability of water vapor from the environment and from that released by the freezing droplets, one or other of the mechanisms dominates.

The characteristics of the charge transfer results obtained in these and previous UMIST experiments are all represented by the figures shown here. Figure 2.3 shows data obtained at temperatures above  $-20^{\circ}\text{C}$ ; the positive charging at high liquid water content is due to interaction with the growing surface. The rime contact potential is reduced at these high temperatures, or dislocation production is limited by the slow freezing

process. The droplets freeze relatively slowly on the surface and thus provide vapor for surface growth leading to positive charging. With low effective liquid water contents, there are fewer drops on the surface and they freeze faster so there is less vapor available for surface growth; the contact potential effect, or increased dislocations due to more rapid droplet freezing, results in negative charging of the target. This also explains the negative charging observed by Jayaratne and Saunders (1985) at  $-10^{\circ}\text{C}$  with a cloud of small droplets, most of which were too small to strike the target. Figure 2.5 shows the low temperature results. Comparing the low liquid water content data in Figure 2.5 with that in Figure 2.3, the supersaturation is provided by the same amount of liquid water in both cases but is significantly greater at the lower temperature. The few droplets hitting the target cause a rime potential which is overcome by the increased surface growth, and positive target charging follows. For high effective liquid water contents, there are sufficient droplets to cause a wide-spread rime contact potential, or dislocation driven surface charge, which promotes negative target charging. This process is aided at low temperatures by rapid droplet freezing which limits the vapor available for surface growth. The result that the negative charging is independent of temperature is consistent with the fact that the rime contact potential maintains a fairly constant value at temperatures below  $-15^{\circ}\text{C}$ , according to Caranti and Illingworth (1980). Also, once established, the contact potential is not changed by further riming. Similarly, the surface charge density due to positively charged dislocations will remain constant during continued riming. The results

suggest that once the negative charging mechanism overcomes the positive one, there is no further temperature dependence.

Other results obtained in earlier studies fit in with the charging scheme outlined here. Figure 2.6 shows the current to a riming target due to ice crystals initiated at time zero, from the paper by Baker et al (1987). An initial positive peak was obtained at all temperatures in the presence of a high liquid water content and a high ice crystal concentration at the start of the experiment. The rapidly growing crystals keep the droplet sizes too small to strike the target; the well ventilated target experiences surface growth and the interacting crystals charge the target positively. This initial positive peak was not noted in the experiments of Keith and Saunders (1990) because the charge transfer data were obtained after the crystals had grown and reduced in concentration. Figure 2.6 also shows a second positive charging peak which the authors associated with rapid growth of the target following a temporary halt in the rotation of the riming apparatus. It seems likely that, while stopped, the target grew in the super-saturated environment and the pre-existing rime contact potential layer, or charged dislocation layer, was over-grown. When rotation re-commenced, the crystals interacted with the freshly grown surface and so the target charged positively. The collection of droplets rapidly restored the contact potential, or the positive surface charge layer, and negative charging followed.

## 2.5 Parameterization of the Data

Equations have been derived for the results shown in Figures 2.3 and 2.5. EW is the effective liquid water content in

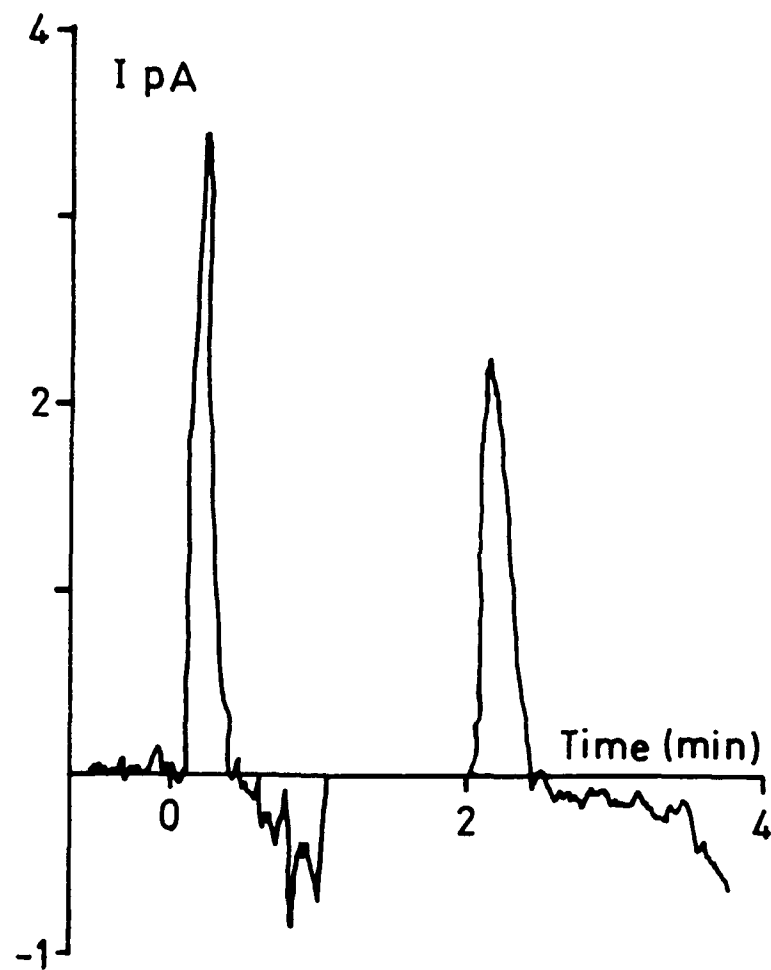


Figure 2.6 The current to a moving riming target due to crystal collisions as a function of time.  $T=-24^{\circ}\text{C}$ .  $V=3$  m/s. The cloud was seeded at  $t=0$ . Rotation was stopped at 1 min and re-started at 2 mins.

$g\ m^{-3}$ ,  $q$  is the charge to the hail pellet in fC and  $T$  is the ambient temperature in  $^{\circ}C$ .

From Figure 2.3:

$$\text{when } T > -16; \quad 0.026 < EW < 0.14; \quad q = -314.4EW + 7.9 \quad (2)$$

$$\text{when } T > -16; \quad 0.14 < EW < 0.22; \quad q = 419.4EW - 92.6 \quad (3)$$

$$\text{For positive charging,} \quad q = 20.22EW - 1.36(-T) + 10.048 \quad (4)$$

From Figure 2.5:

$$\text{where } T < -20; \quad 0.06 < EW < 0.12; \quad q = 2041.8EW - 128.7 \quad (5)$$

$$\text{where } T < -20; \quad 0.12 < EW < 0.16; \quad q = -2900.2EW + 462.9 \quad (6)$$

For negative charging, ( $EW < 1.1$ )

$$q = 3.02 - 31.76EW + 26.53EW^2 \quad (7)$$

Equation 4 is appropriate for positive target charging with the temperature dependence included in the formula. Equation 7 represents negative target charging which is not temperature dependent. In order to decide between the use of equations 4 or 7, the positive charging data of Figure 2.3 have been used to determine the effective liquid water contents and temperatures for which the charge transferred is zero. An equation for the critical values of effective liquid water content was determined and is given by:

$$CEW = -0.487 + 6.64 \times 10^{-2} (-T) \quad g\ m^{-3} \quad (8)$$

Figure 2.7 represents the charging zones described by the above equations with the diagonal line representing the boundary between positive and negative charging. For the low liquid water content regimes, the sharp cut off at  $-16^{\circ}C$  and  $-20^{\circ}C$  is more likely to be a smooth transition with charge sign reversal around  $-18^{\circ}C$ .

The data obtained in the present experiments were obtained with ice crystals around  $110\mu m$  in size at speeds of  $3\ m\ s^{-1}$ . The



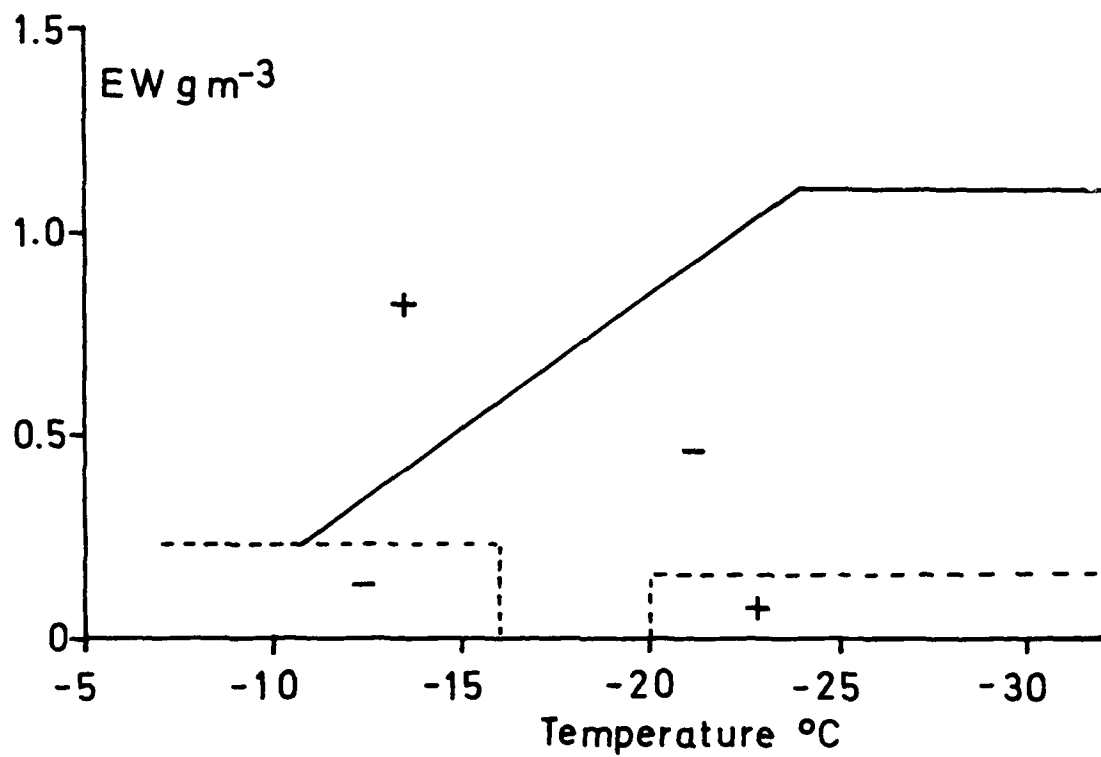


Figure 2.7 The positive and negative target charging zones as a function of temperature and effective liquid water content

dependence of charge transfer on velocity and crystal size is summarised in Table 2.1. The two sets of results may be combined in order to generate equations which allow calculations of charge transfer for a range of values of temperature, effective liquid water content, crystal size and velocity. The equations are of the form:

$$Q = B d^a v^b q f C \quad (9)$$

where the constants B, a and b are given in Table 2.2. d is the crystal size (m), V the speed ( $\text{m s}^{-1}$ ), and q is determined from equations (2) to (7) as appropriate. The values of the constants are given in Table 2.2.

TABLE 2.2

B	a	b	Situation	Crystal Size $\mu\text{m}$
$4.9 \times 10^{13}$	3.76	2.5	High EW positive charge	< 155
$4 \times 10^6$	1.9	2.5	"	155 - 452
52.8	0.44	2.5	"	> 452
$5.24 \times 10^8$	2.54	2.8	High EW negative charge	< 253
24	0.5	2.8	"	> 253
$4.915 \times 10^{13}$	3.76	2.5	Low EW positive charge	< 155
$4.039 \times 10^6$	1.9	2.5	"	155-452
52.8	0.44	2.5	"	> 452
$5.24 \times 10^8$	2.54	2.8	Low EW negative charge	< 253
24	0.5	2.8	"	> 253

Because the liquid water content charge dependencies were determined with  $110\mu\text{m}$  crystals, a further experiment was conducted to check the validity of these equations for large crystals. Ice crystals up to  $400\mu\text{m}$  in diameter were grown, the charge transfer was measured then compared with the calculated values. The agreement was within 1.7%. Also, a correlation coefficient of 0.9 was determined between every data point obtained in these experiments with its corresponding calculated value. Takahashi (1978) presented results of charge transfer to a riming target as a function of cloud liquid water content and temperature for ice crystals in the range 10 to  $100\mu\text{m}$ . Target charging was positive above  $-10^{\circ}\text{C}$  and at both low and high values of liquid water content below  $-10^{\circ}\text{C}$ . At intermediate liquid water contents around  $1\text{ g m}^{-3}$ , below  $-10^{\circ}\text{C}$ , the target charged negatively. The significant differences with the present work are that we find negative charging at higher temperatures than  $-10^{\circ}\text{C}$  at low liquid water contents, and Takahashi's liquid water content values for negative charging are about twice our values. He performed all his experiments at  $9\text{ m s}^{-1}$  which involved a rapidly rotating apparatus moving needles through a cloud of crystals. Saunders and Zhang (1987) and Keith and Saunders (1989b) showed that high speed rotation rates can lead to rime break-up and the ejection of fragments which charge the target positively. This may have prevented Takahashi observing negative charging above  $-10^{\circ}\text{C}$ . They also noted that the local cloud can be depleted by the rapid rotation of the riming apparatus which leads to a lower liquid water content at the riming target. Takahashi measured the liquid water content by weighing the rime collected on fine wires moved rapidly through

the cloud. However, his charge transfer apparatus was more substantial than the fine wires and so the cloud could have been depleted around his target leading him to over-estimate his liquid water contents. When comparing Takahashi's data with the present work it is to be noted that his charge data are presented in terms of charge per ice crystal collision with no consideration of ice crystal separation probabilities. Data here are given in terms of charge per separation event.

The charge transfer equations may be used to consider results obtained in studies of thunderstorms. For example, Dye et al (1988) flew an instrumented aircraft through a thunderstorm and presented results of charge on particles and an analysis of charge center location together with a discussion of how charge transfer by particle collisions could have caused the observed fields and charges. In a thunderstorm traverse at  $-12^{\circ}\text{C}$ , they noted that 3 mm graupel carried charges less than about 1 pC. From their data they calculated that in a five minute fall time, a graupel particle would have made between 30 and 140 collisions with smaller ice particles. The relative fall speeds of 3 mm graupel and 1 mm ice crystals is around  $2.5 \text{ m s}^{-1}$ . The event probability for this case is around 0.7 (Keith and Saunders, 1989c) giving a requirement of between 20 and 100 separation events leading to charge transfers of between 50 and 10 fC per event. They observed liquid water contents up to  $0.8 \text{ g m}^{-3}$  with a mean value around  $0.5 \text{ g m}^{-3}$ . The liquid water content, for the realistic droplet size distribution in our experiments, is around twice the effective liquid water content which therefore takes a value of  $0.25 \text{ g m}^{-3}$ . The charge transfer, calculated from our equations, for a relative speed of  $2.5 \text{ m s}^{-1}$ , with  $1000\mu\text{m}$

crystals, at  $-12^{\circ}\text{C}$  is  $-32 \text{ fC}$  which agrees well with the thunderstorm values.

Dye et al (1988) also noted a region of negative charge at  $-12^{\circ}\text{C}$  and one of positive charge at  $-20^{\circ}\text{C}$ . They argued that this implies a charge sign reversal at a temperature higher than  $-20^{\circ}\text{C}$ . With effective liquid water contents in the clouds they penetrated of up to  $0.4 \text{ g m}^{-3}$ , the reversal temperature, determined from equation 8, is  $-13^{\circ}\text{C}$ . A reversal temperature of  $-11^{\circ}\text{C}$  corresponds to the average effective liquid water content of  $0.25 \text{ g m}^{-3}$ . These predictions from the laboratory work appear to agree with the thunderstorm observations.

The principal objective of this work was to provide a complete data set of charge transfer as a function of liquid water content and temperature for ice crystal collisions with hail pellets. These data are now available for inclusion in numerical models of thunderstorm electrification. The charging rate of a typical thunderstorm was calculated using the equations presented above. The theoretical, one dimensional, cloud model described in Chapter 8 was adapted for calculations of thunderstorm electric charge separation rates. The model was modified further to include the charge transfer equations and was used here for the case of a thunderstorm which caused severe hail damage in the Thracian lowlands, for which sounding data are available. The calculations indicate a charge reversal temperature of  $-17^{\circ}\text{C}$  for a liquid water content of  $1.4 \text{ g m}^{-3}$ . Latham and Mason (1961) summarised the requirements of a viable thunderstorm charging mechanism and concluded that a minimum charging rate of  $2 \times 10^4 \text{ fC m}^{-3} \text{ s}^{-1}$  was needed to account for the observed rates of electrical development in typical

thunderstorms. The calculations show that this rate was exceeded at temperatures below  $-18^{\circ}\text{C}$ , confirming that the results from the present laboratory work offer satisfactory thunderstorm charging rates. However, there are limitations of one dimensional numerical models and, in order for a proper assessment of these results, three dimensional models which include thunderstorm dynamics are required.

## CHAPTER 3

### THEORIES OF THUNDERSTORM ELECTRIFICATION

#### 3.1 Introduction

A discussion is presented of the various charge transfer theories. The results are consistent with the idea of two competing mechanisms whose relative success depends on the temperature and liquid water content. Positive graupel charging occurs when the graupel surface grows from the vapor and the crystals interact with a negative surface charge caused by a temperature gradient across the rime ice surface layer. Negative graupel charging occurs when the surface growth effect is swamped by freezing droplets which create either a pseudo contact potential with which the crystals interact, or a positive surface charge, due to dislocations in the rime ice, which is removed during glancing crystal interactions.

#### 3.2 THEORIES OF THUNDERSTORM ELECTRIFICATION

Many theories have been put forward and most of them agree that charges are carried on cloud and precipitation particles. Vonnegut (1953) and Moore et al (1989), rely on convective motion to bring charge into the cloud where it is captured by particles; however, a definite link with temperature seems to be lacking in this mechanism. Much effort has been expended on developing a theory of the inductive process whereby particles interacting in the pre-existing electric field separate charge to enhance the field (Elster and Geitel (1913), Latham and Mason (1962), Sartor (1981), Levin (1976)). Likely candidates here are ice crystals

or water droplets bouncing off graupel pellets. However, Gaskell (1981) and Illingworth and Caranti (1985) showed that the surface conductivity of ice is insufficient to permit substantial charge to flow to the interaction point during the brief contact time of ice crystals and graupel pellets. Mason (1988) has suggested that water droplets making grazing impacts with graupel pellets of low density, and hence low fall velocity, will bounce off and separate charge. Such a mechanism needs further laboratory investigation. However, the measurements of Gaskell et al (1978) and Christian et al (1980) in thunderstorms, have shown that small graupel pellets carry charges larger than can be accounted for by the existing electric field. So, the inductive mechanism can only become important later in storm development when the electric field has increased, but it cannot account for the initial electrification.

The most likely process of thunderstorm electrification is one involving ice crystal collisions with graupel pellets in the presence of supercooled water droplets, as investigated here, and which has been shown to separate substantial charge. Several mechanisms have been proposed to account for the charge transfer, but none of them is entirely satisfactory. Reynolds et al (1957) conjectured that the presence of supercooled water was essential because it warmed the rime surface to provide a temperature difference between the crystals and the surface. This led to considerable analysis of temperature gradient driven charge transfer by Latham and Mason (1961). However, the magnitude of the charge available by this mechanism proved to be less than that observed. Also, Gaskell and Illingworth (1980) and Jayaratne et al (1983) showed that the sign of the charge



transfer was independent of the temperature difference between the interacting particles. Gaskell and Illingworth reversed the sign of the charge transfer to ice targets by keeping the temperature difference between the interacting particles constant while causing the target to grow or evaporate. Jayaratne et al performed the converse experiment; the sign of the charge transfer remained the same even when the temperature gradient was reversed. These experiments indicate that temperature differences between the interacting particles cannot drive thunderstorm electrification. However, neither of these results preclude the possibility of temperature gradients within the surface being important, as will be discussed later.

Jayaratne and Saunders (1985) noted that the positive charging of a riming target at  $-10^{\circ}\text{C}$  could be reversed by changing the drop size distribution while keeping the liquid water content constant. Their analysis indicated that the nature of the ice crystal surface was playing a controlling role in the charge transfer. Hitherto, only the surface conditions of the target graupel pellet had been considered. Analysis by Baker et al (1987), of the relative diffusional growth rates of crystals and the riming graupel pellet with which they interact, showed that all the characteristics of the laboratory charge transfer results of Jayaratne et al (1983) could be accounted for if the faster growing particle charges positively. There was no physical mechanism for the charge transfer here, but differences in the growth rates of the particles will be controlled by temperature, liquid water content, local supersaturation and the droplet freezing time on the riming surface. A possible growth rate dependent mechanism relying on melted layers on the surfaces

of the ice particles has been presented by Baker and Dash (1989). Water molecules become oriented in the surface layers leading to an excess of negative ions near the surface which provides a charge source. Baker and Dash argue that the layers on the two particles have different thicknesses which depend on the local growth conditions. Experimental confirmation is required for their prediction that during contact, charge is transferred by mass transfer from the thicker to the thinner layer and that the direction is in agreement with the UMIST laboratory results. However, the evidence for a liquid-like-layer on ice (Fletcher, 1973) suggests that it becomes thinner with decrease in temperature which would lead to reduced charging at low temperature; yet our charge transfer values are substantial at temperatures below  $-30^{\circ}\text{C}$ .

Caranti et al (1985) and Avila et al (1988) postulated that in the area around a freezing drop on a riming substrate, the vapor provided by the drop, whose temperature rises to  $0^{\circ}\text{C}$  during the freezing process, causes the growth of ice crystals on the surface. These crystals may be knocked off by the airborne ice crystals when they make glancing collisions with the target, thus charging the ice target positively. Findeisen (1940) noted that when an air-stream removed frost fragments from an ice target, it charged positively. A qualitative theory based on this idea involving temperature gradients along the frost fibers was put forward by Avila et al (1988). The effect is consistent with the results obtained by many scientists, quoted earlier, that during ice crystal interactions, growing ice targets charge positively and evaporating targets charge negatively. When a frost fiber on the ice surface grows from the vapor, its outer tip is warmed by

latent heat released by depositing molecules; conversely, if it evaporates, its outer tip will be cooled. According to the temperature gradient theory of Latham and Mason (1961), protons in ice are more mobile than the negative ions and so the warmer end of the fiber becomes negatively charged. Thus, in the case of growth, the fiber tips will become negatively charged and grazing crystals will remove negatively charged fibers leading to the observed positive charging of the target. There is evidence from Cross and Speare (1969) and Cross (1971), who took scanning electron microscope photographs, that an evaporating ice surface becomes covered in fine fibers of ice. The tips of evaporating ice fibers will be cooled relative to their bases on the ice substrate and a temperature gradient along the fiber will lead to the fiber tip becoming positive with respect to its base. If this fiber were to be removed by a passing crystal, the ice substrate would charge negatively as observed. Although it is established that the breaking of ice fibers under growing or evaporating conditions can lead to charge transfer, it is not clear whether such fibers occur under natural conditions of growth on graupel pellets. Laboratory studies have shown that it is possible to change the sign of target charging within seconds, from negative to positive, by introducing a vapor source which causes target growth. In this case, a fiber on the ice surface in the recently saturated environment is initiated and then grows at a rate of order  $1\mu\text{m}$  per second and so is less than  $10\mu\text{m}$  long when it encounters the passing ice crystals. Such a fiber is very different from the substantial frost fibers noted by Findeisen and may not be removed at all by the crystals. An alternative to the idea of temperature gradients along fibers is

the possibility of temperature gradients in the surface itself due to depositing molecules warming the whole surface relative to the bulk of the ice beneath. The surface then has a negative charge and incident crystals will become negatively charged during contact due to charge transfer, or by the transfer of charged material.

It has been evident for some time that there are at least two competing mechanisms of charge transfer during ice crystal and graupel interactions. The precise, local conditions on the rimer surface, controlled by temperature and liquid water content, causes one or the other of the mechanisms to dominate. In thunderstorms, graupel pellets of 5 mm diameter, falling at  $3 \text{ m s}^{-1}$  at  $-20^{\circ}\text{C}$ , in liquid water contents up to  $2.5 \text{ g m}^{-3}$ , do not warm sufficiently by riming to cause surface evaporation, (Macklin and Payne, 1967). Thus the competing negative mechanism is not due to target evaporation. Caranti and Illingworth (1980) detected a negative contact potential on a rimed ice surface which increased at lower riming temperatures down to  $-15^{\circ}\text{C}$  and was not affected by target growth or evaporation. Ice is a proton conductor and so strictly, "contact potential" which deals with electron Fermi levels, is not an applicable concept. Caranti (1982) states, "the contact potential difference between two pieces of ice will be understood as the potential difference measured using the Kelvin vibrating capacitor method. This contact potential is not necessarily related to the Fermi levels or work functions of the pieces of ice because it is quite likely that the charges that flow during contact will not be electrons". Earlier, Buser and Aufdermaur (1977) proposed the existence of electronic surface states on ice leading to electron exchange

during contact. Gaskell and Illingworth (1980) pointed out that such states may be associated with the liquid-like layer on ice (Fletcher (1973)), which provides a substantial surface density of ions. Caranti et al (1985) reported an effective work function for ice of 4.3 eV by measuring charge transfer when ice spheres collided with metal surfaces. A negative rime contact potential is commensurate with the negative charging of graupel pellets during ice crystal interactions if the contact potential of the ice crystals is positive with respect to the rime surface. They noted that the rime contact potential was maintained for many hours after riming ceased, whereas Jayaratne et al (1983) and Keith and Saunders (1990) found that charge transfer fell to insignificant values when there were no droplets present, and crystals alone interacted with the target. This difference may possibly be accounted for by the collection of ice crystals on the rimer which cover up the rime surface and so prevent subsequent crystal interactions with the surface carrying the contact potential.

Keith and Saunders (1990) have noted that there are positive charges trapped on dislocations in ice; presumably the negatively charged point defects diffuse into the bulk of the ice leaving the surface with a positive charge. If such positive charges appear on the rimer surface they could lead to charge transfer during ice crystal collisions. The density of dislocations in rime ice is dependent on droplet freezing rate (McCappin and Macklin, (1984)) and hence there is a link with temperature; the droplets freeze faster at lower temperatures and so produce more dislocations. Ice crystals grow slowly from the vapour and so have a low concentration of dislocations, (McKnight and Hallett,

(1978)) which leads to a charge density difference across the rime/ice crystal interface. The dislocation concentration and charge data are available from work by Bryant and Mason (1960), Higashi et al (1968), Fukuda and Higashi (1969), Itagaki (1970,1972,1983), and Sinha (1978). Keith and Saunders used their results to show that adequate charge is available on dislocations to account for the observed negative charge transfer to the rimer.

### 3.3 CONCLUSION

Thus the two charge transfer regimes may be accounted for by the positive charging of the rimer due to surface growth, with possible break-off of fibers, and negative rimer charging by either a contact potential difference or a difference in concentration of charged dislocations on the interacting surfaces. All charge transfer processes work simultaneously, but one or the other dominates depending on temperature and liquid water content.

## CHAPTER 4

### CHARGE TRANSFER TO SPHERICAL AND FALLING RIMING TARGETS

#### 4.1 Introduction

The extensive laboratory investigations of thunderstorm charging which have been performed in the UMIST laboratory over the last few years, have involved the use of simulated graupel pellets. These have taken the form of 5 mm diameter metal rods which are moved through the cloud on a rotating frame. The rods rapidly rime up and subsequent interactions with ice crystals leads to charge transfer which is detected by measuring the current flowing from the rod. The question arises as to whether the rod technique adequately represents the thunderstorm situation where the falling graupel pellet is approximately spherical and tumbles or oscillates as it falls.

Furthermore, there is a fundamental difference between the situation in the laboratory and that for a free falling graupel pellet. Our riming target is connected to an amplifier which effectively maintains the target potential at ground, any build up of charge on the target is prevented because the charge passes to ground through the circuit. However, a natural falling pellet is isolated and any charge transfers to it result in a build up of charge on the pellet which may influence subsequent charging events in a way which is not modelled in our laboratory studies.

The purpose of the work described in this Chapter was to discover whether the shape of the target and any initial charge carried, has any influence on the sign and magnitude of the charge transfer in order to know whether the experimental data are valid when used in thunderstorm electrification models.

## 4.2 Experimental Procedure

The charging experiments were performed in the large cloud chamber situated within a cold room as described in Chapter 2. The cloud was formed by introducing vapor from a boiler situated beneath the floor of the chamber. The droplets quickly super-cooled to the ambient temperature. Ice crystals were produced by introducing into the chamber a thin wire cooled to liquid nitrogen temperature, whereupon they grew rapidly at the expense of the evaporating droplets. The size and concentration of the ice crystals was determined by the formvar technique. Figure 4.1 shows the cloud chamber and apparatus.

The event probability of a spherical target for ice crystals was determined. The event probability is the product of the collision efficiency and separation efficiency and is therefore a measure of the collection efficiency of the target. Keith and Saunders (1989c) determined the event probability of a cylindrical target for ice crystals and those results were now used to find the event probability of the spherical target by comparing the charging current to a 5 mm diameter sphere with that to a 5 mm cylindrical target, both targets being moved simultaneously through the mixed cloud while their charging currents were noted.

Ice spheres were used to simulate real graupel pellets; they fell through the mixed cloud of super-cooled water droplets and ice crystals and at the bottom of the chamber they fell into a Faraday can connected to an electrometer so that their charge could be measured. The ice spheres were formed by filling plastic moulds with distilled water which were then frozen. The spheres, of diameter 6, 7, 8, 9 and 10 mm, could be kept, until



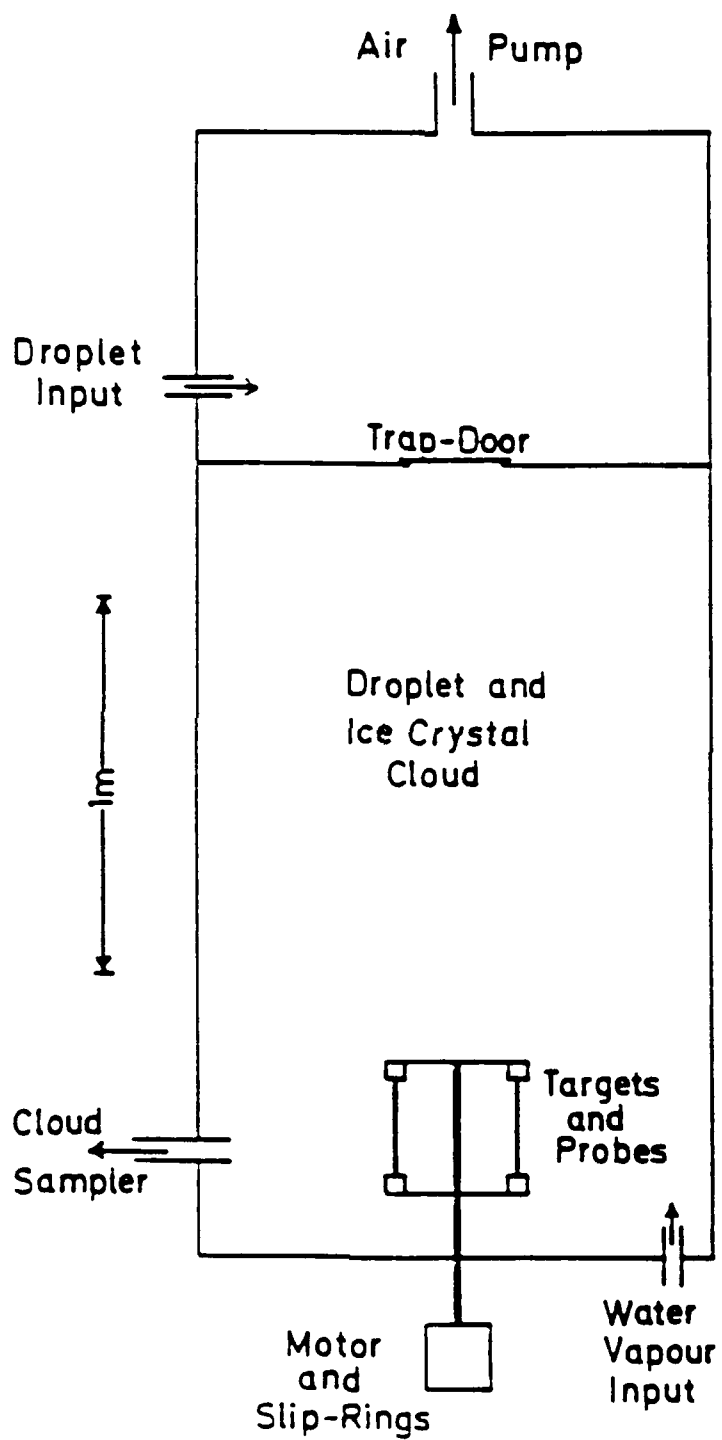


Figure 4.1 The ice crystal growth chamber and riming rods

required, in a sealed container in a freezer for several weeks without significant degradation. The terminal velocity of the ice spheres was determined by dropping them through a series of induction rings of known separation. The transit time between successive rings was measured and it was found that the spheres reached their terminal velocity after falling 1 metre which gave them sufficient time to reach their terminal velocity before entering the lower cloud chamber. The experiment was conducted by first sampling the cloud so that the ice crystal size and concentration could be determined. A sphere was then dropped through the mixed cloud and its net charge acquired during the descent was recorded. A separate experiment was performed to determine that the spheres, which fell from a grounded release mechanism, had insignificant initial charge. The five spheres of different diameter were dropped in turn within 20 seconds, so that the cloud particle concentration did not change significantly during the experiment. The charge per crystal separation event was estimated from the net charge, the number of charging events and the event probability of the falling target. The experiment was repeated under different conditions of temperature, liquid water content and ice crystal size and concentration.

The previous experiments by Keith and Saunders and others used a conditionally neutral target in that the charge acquired during crystal interactions flowed to ground via the electrometer thus keeping the riming target at ground potential. In the present experiments, the sphere builds up a charge during descent in a realistic way, and this may affect subsequent charge transfers. In order to determine whether the charge transfer was

influenced by the acquired charge, the spheres were given an initial charge which ranged from +0.33 pC to +45 pC by raising the metal dropping support to an appropriate voltage. These charged spheres were then released to fall through an induction ring whose induced voltage pulse was used to determine the initial charge. They then fell through the cloud, collected supercooled water droplets, and interacted with ice crystals in the usual way. At the bottom of the chamber, their charge was measured and the charge generated during the descent was calculated, from which the charge per event was calculated.

#### 4.3 Results

##### 4.3.1 Determination of the event probability of ice spheres.

A 5 mm diameter metal sphere replaced one of the arms of the rotating apparatus shown in Figure 4.1. The sphere and the 5 mm diameter cylindrical target were moved through a cloud of ice crystals and water droplets while the two charging currents were noted. The event probability of the sphere  $EP_S$  was then determined from the relationship:

$$EP_S = (I_S/I_C)(V_C/V_S) EP_C$$

where  $I_S$  and  $I_C$  are the charging currents to the cylinder and sphere;  $V_C$  and  $V_S$  are the volumes swept out and  $EP_C$  is the event probability of the cylindrical target.

Figure 4.2 shows the event probability of the sphere, as determined from the above equation, and that of the cylinder as determined from the work of Keith and Saunders (1989c) for data obtained over a range of crystal sizes and impact velocities. The event probability of the sphere is about 10% greater than

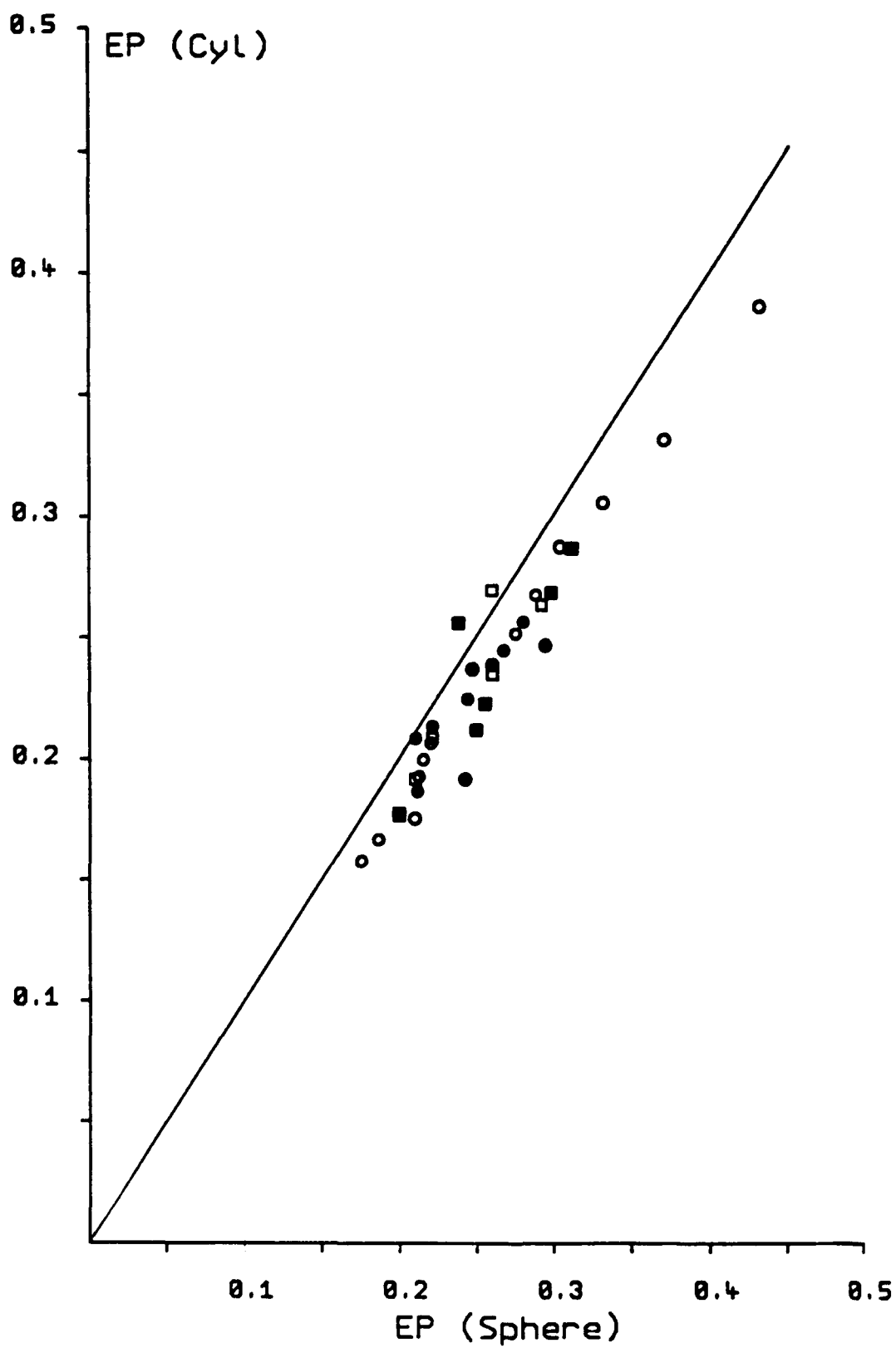


Figure 4.2 The event probabilities of a cylindrical and spherical target.

that of a cylinder of the same size independent of crystal size and velocity.

#### 4.3.2 Determination of the charge per event for an initially uncharged spherical target.

The positive charging regime was investigated with cloud temperatures in the range  $-6$  to  $-17^{\circ}\text{C}$ . The crystal size ranged from  $60$  to  $695\text{ }\mu\text{m}$  and the maximum cloud liquid water content was  $3.2\text{ g/m}^3$ . Figures 4.3a to 4.3e show the comparison between the measured charge per event for the falling ice spheres and values calculated from the equations developed in Chapter 2 for cylindrical targets; the sphere and cylinder diameters were  $6, 7, 8, 9$  and  $10\text{ mm}$ . The 1:1 line is also shown. The charge per event for the ice spheres is calculated from the measured charge, the event probabilities taken as 10% greater than those for cylindrical targets, the sphere fall velocity and the crystal concentration. For the calculations involving the cylindrical target, the value of the effective liquid water content was determined by the temperature rise of a riming target (as described in Chapter 2) in an airstream at the same velocity as the falling sphere. At temperatures below  $-20^{\circ}\text{C}$  the charging to the sphere is negative unless the liquid water content is quite high. The experiments were repeated at temperatures between  $-20$  and  $-29^{\circ}\text{C}$  with a variety of crystal sizes and liquid water contents. Figures 4.4a to 4.4e again show a comparison between the observed results and those calculated for the same conditions; the line shown is a 1:1 correlation.

The effect on the charge transfer to the falling sphere of the build up of charge upon it may be seen in figures 4.5 and 4.6

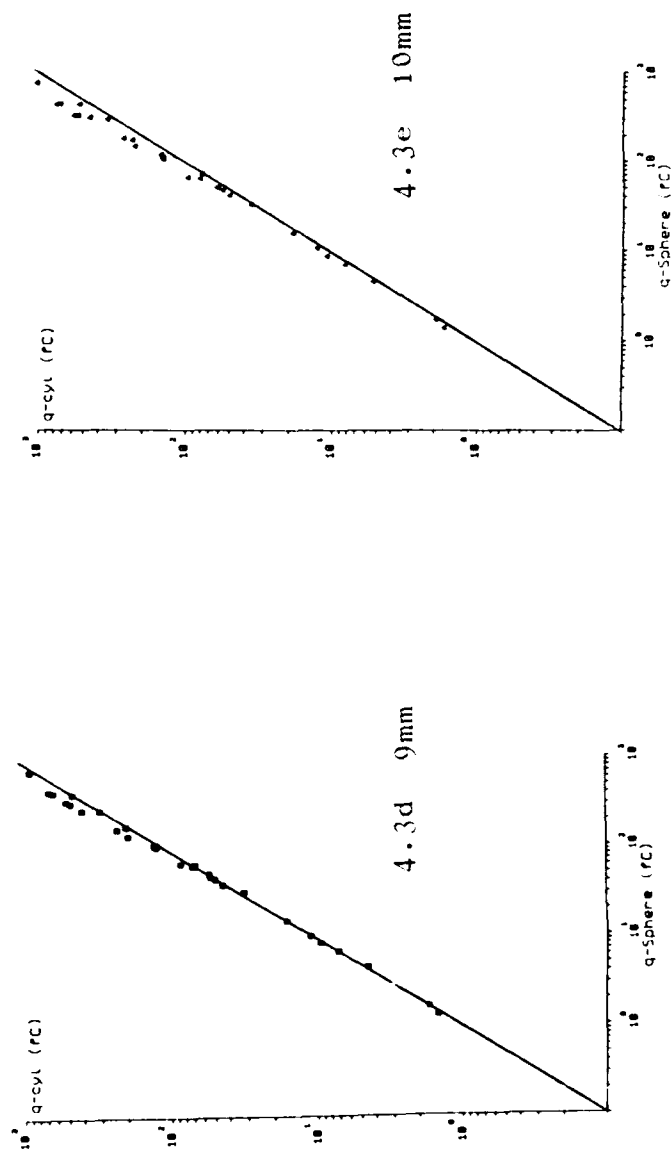
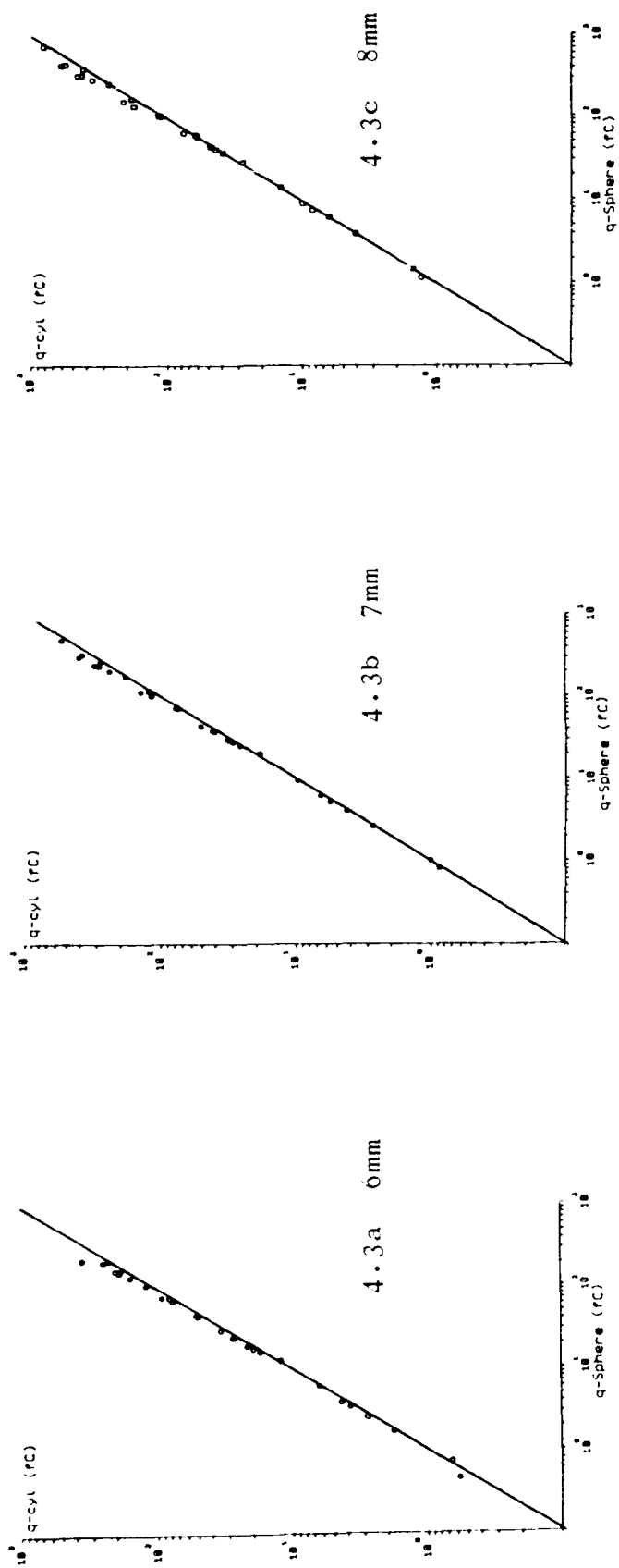


Figure 4.3  
 Falling sphere  
 charge versus  
 calculated charge  
 to a cylinder.  
 Positive charge  
 regime

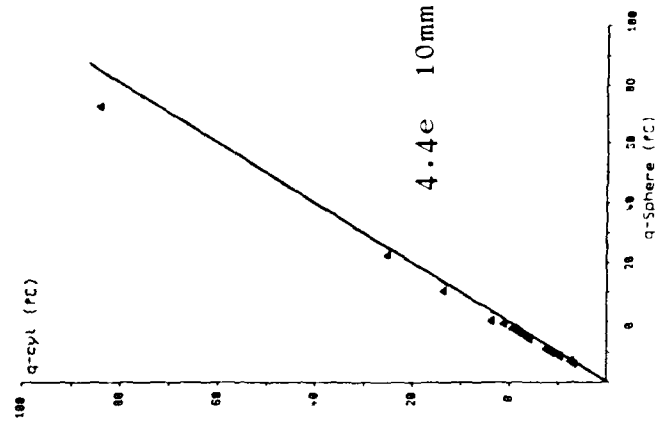
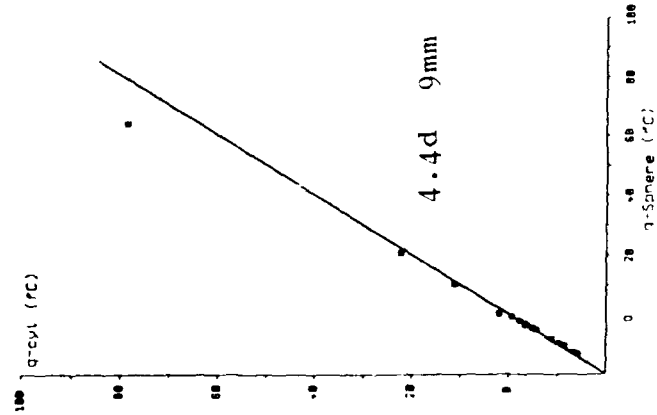
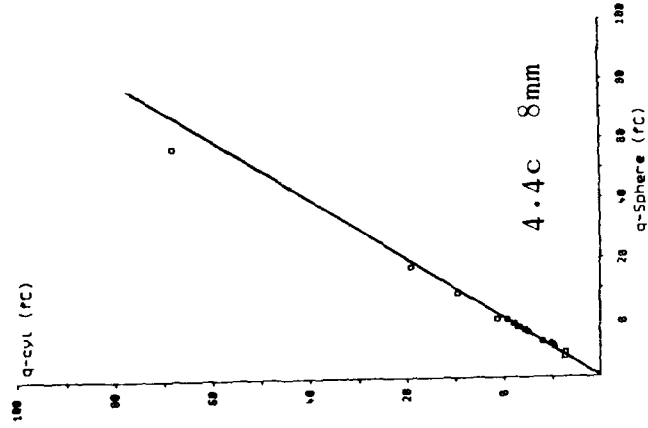
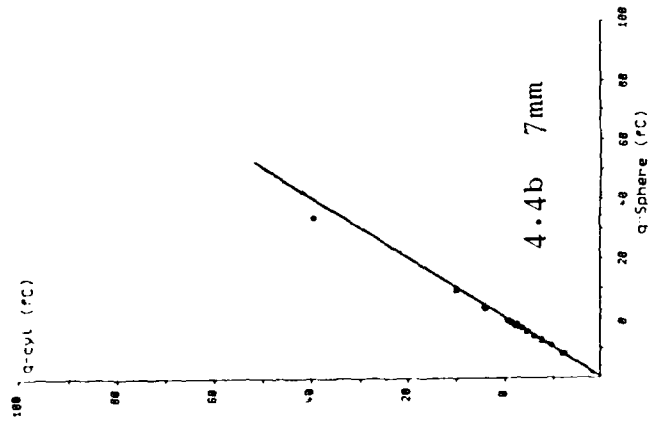
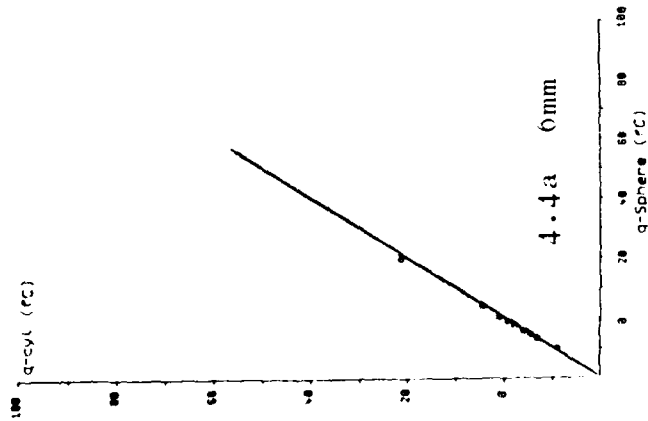


Figure 4.4  
Falling sphere  
charge versus  
calculated charge  
to a cylinder.  
Negative charge  
regime

which plot the ratio of actual to theoretical charge per event against the total charge acquired by the sphere during its fall for the positive and negative regimes respectively. When the net charge on the sphere is greater than about  $\pm 10\text{pC}$ , it is possible to discern a decrease in the total charge transfer. When the charge on the sphere reaches about  $+50\text{ pC}$ , the charge transfer is only 60% of the charge transfer predicted by the equations of Chapter 2. The effect seems less noticeable with negative charging although it would be expected that the slopes for positive and negative charging would be the same.

#### 4.3.3 The charging of spherical targets carrying an initial charge.

Charges up to  $\pm 45\text{ pC}$  were placed on the ice spheres and the resulting charge after crystal interactions was measured. The measured charge per event was then compared with the predicted value from the equations of Chapter 2. When a sphere was under-going positive charging events and its initial charge was negative, the positive charge acquired could be two to three times larger than the predicted value unless the sphere collected sufficient charge to carry a net positive charge, when subsequent positive charge transfers were inhibited. A similar effect was observed at lower temperatures; when negative charging was occurring with an initial positive charge on the sphere, the charge per event was inhibited.

#### 4.4 Discussion and Conclusions

One purpose of this study was to determine whether the shape of the target could influence the charge per event.



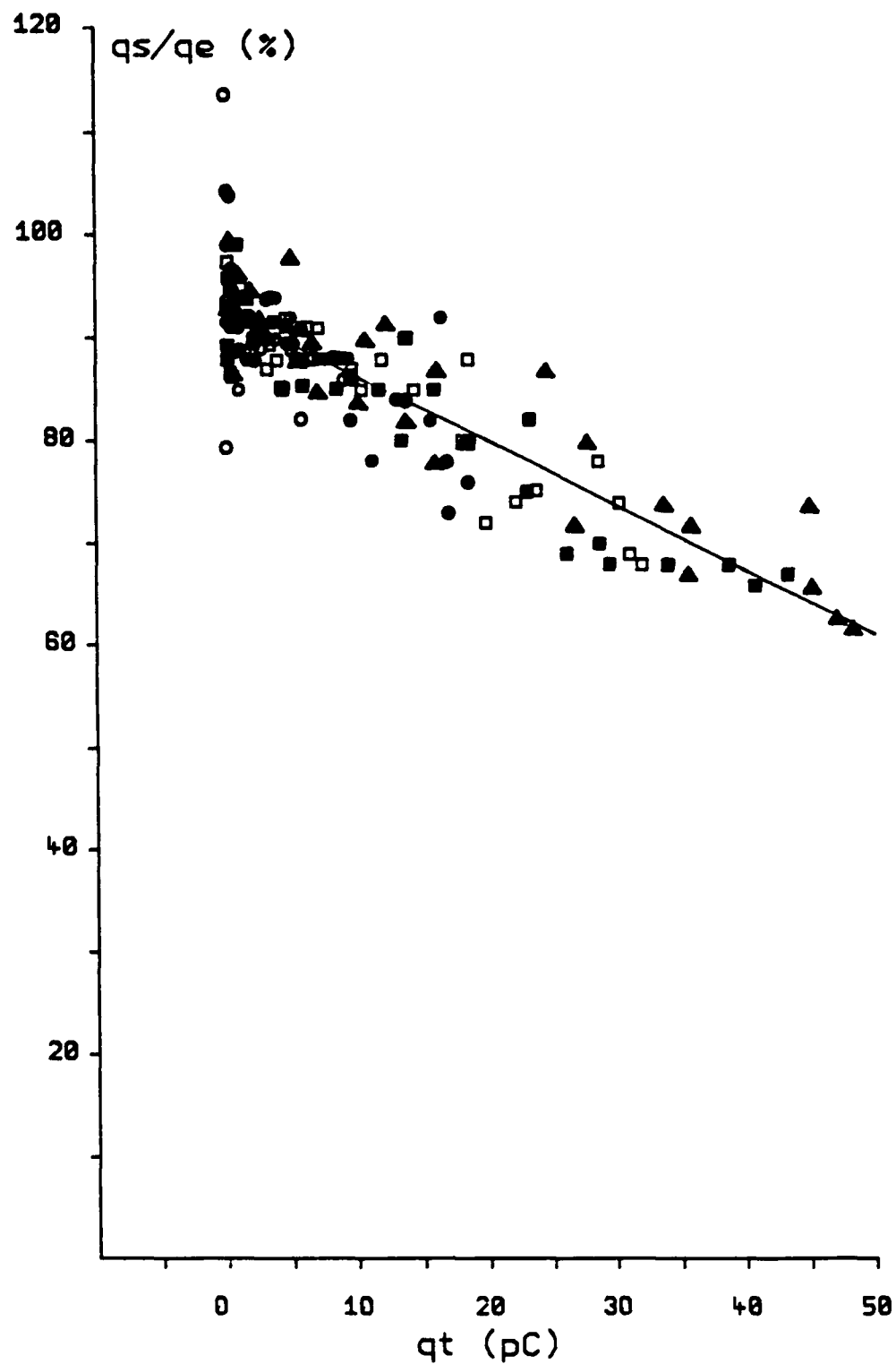


Figure 4.5 The ratio of actual to theoretical charge per event against total charge acquired by falling ice spheres for the positive charge regime

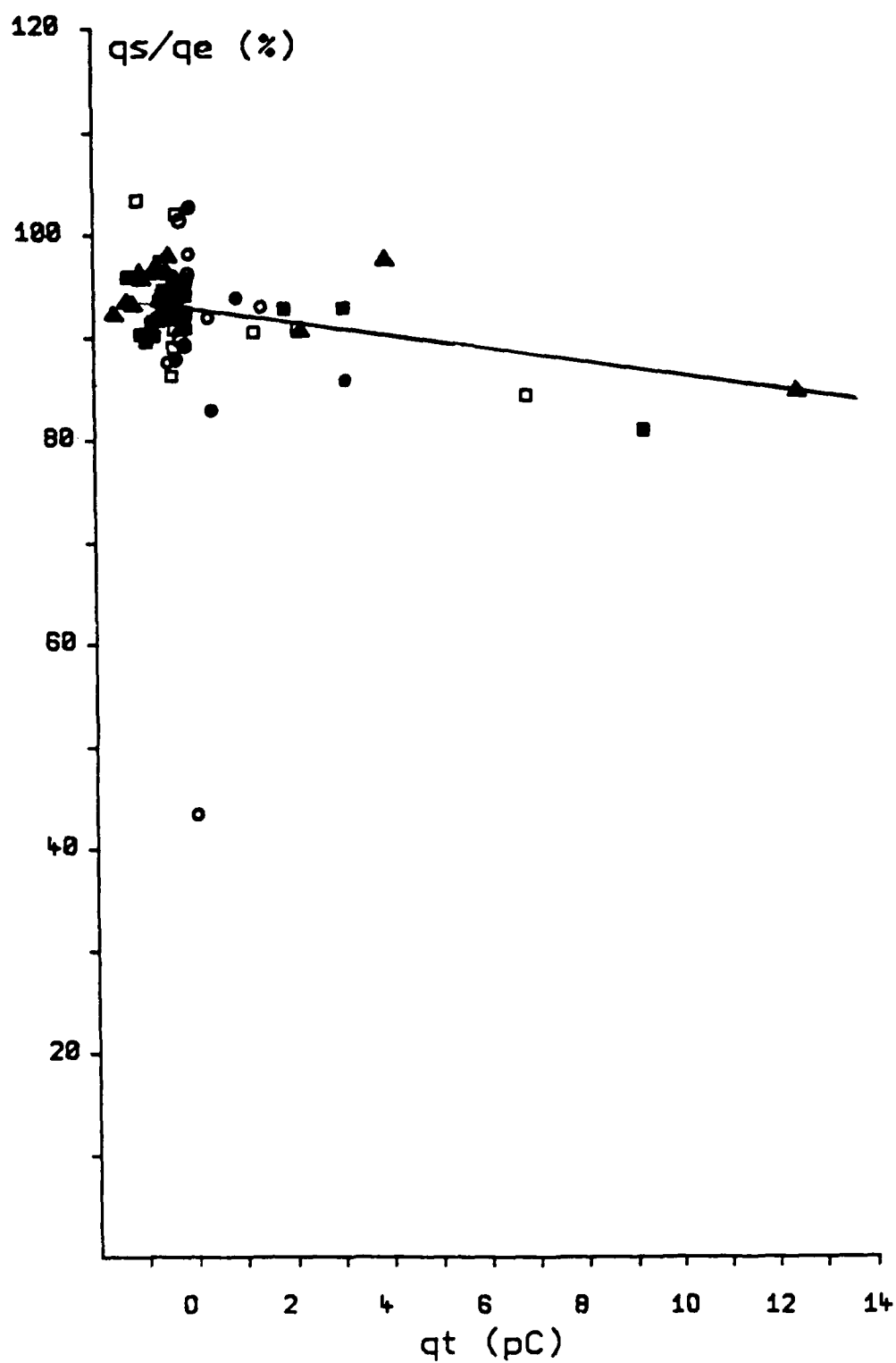


Figure 4.6 The ratio of actual to theoretical charge per event against total charge acquired by falling ice spheres for the negative charge regime

Figures 4.3 and 4.4 show that the charge acquired by the falling spheres is less than the expected value, however, this is due to the inhibiting effect of the charge remaining on the spheres during subsequent interactions with ice crystals. There is no evidence that using target rods on a rotating apparatus rather than freely falling spheres, has lead to erroneous values of charge transfer. However, the discovery that a pre-existing or acquired charge can affect subsequent charge transfers is important.

The limiting effect of an initial charge was observed in some preliminary experiments when a cylindrical target was allowed to retain the charge produced during ice crystal interactions. The charge transfer was reduced to less than 30% of the expected value when the target charge reached +200 pC. They also observed that the charge transfer was increased when the target charge was opposite to that being produced during the interaction.

The fact that the charge transfer can be enhanced/inhibited can be used to help explain the presence of the lower positive charge centre. When an ice pellet near the top of a cloud is large enough, it will begin to fall against the updraft. During a fall of typically 6 km to near the  $-10^{\circ}\text{C}$  isotherm, the graupel particle will acquire a charge in the region of -100 pC. Positively charged particles have been observed near the base of the cloud, so these negatively charged particles must have reversed their sign and acquired substantial positive charge in a relatively small distance. For example, a 5 mm graupel particle may fall through ice crystals of diameter 300  $\mu\text{m}$  of concentration  $10^5 \text{ m}^{-3}$ . The charge acquired per km is +30 pC, assuming a

charge per event of +60 fC and an event probability of 0.25. Thus, the graupel would have to fall 5 km to neutralise the -100 pC initially carried and then acquire the observed 50 pC. The present results show that the positive charge transfer is enhanced by up to three times due to the presence of the negative charge. Thus, the initial charge of -100 pC could be neutralised in about 1.1 km (assuming a charge per event of +180 fC). The positive charging is significantly inhibited when the charge on the graupel reaches +50 pC, and it takes a further 1.6 km of fall for the graupel to acquire +50 pC. So, the graupel acquires a significant charge in only 2.7 km, which is within the observed distance between the lower positive charge center and the main negative charge center.

The significant reduction in charge transfer following the acquisition of charge is a new result which will need careful analysis in order to ensure that theoretical models of thunderstorm electrification calculate correctly the rate of generation of electric fields within the cloud.

## CHAPTER 5

### A THEORETICAL TREATMENT OF THE TRAJECTORY OF AN ICE CRYSTAL PAST A CYLINDRICAL TARGET

#### 5.1 Introduction

A survey of the literature reveals that theoretical studies of the motion of spherical particles in a fluid have been available for a number of years (eg Langmuir and Blodgett, 1946; Landahl and Hermann, 1949; Ranz and Wong, 1952; Davies and Peetz, 1955; Loffler and Muhr, 1972 and others). These studies have considered the flow past cylinders and spheres for water droplets and spherical smoke particles. These calculations cannot be applied to ice crystals due to the differences in drag on plate and columnar crystals compared with spheres of similar size.

In recent years there has been increased interest in developing numerical models of cloud dynamics with particular reference to thunderstorm electrification (Helsdon, 1988). These models have assumed that the collision efficiency of a soft hailstone for all sizes of ice crystals is 100%. This chapter describes the development of a computer model to calculate the trajectories of plate and columnar crystals in a fluid flow around a cylindrical target. The collision efficiency was then calculated and compared with the experimental results of Keith and Saunders (1989c) obtained under similar conditions.

## 5.2 Development of the Model

Davies and Aylward (1951) presented a theoretical model to describe the motion of spherical particles in a fluid flow; this present model is based on their work and is modified to account for the different drag on ice crystals. The model was developed initially for spherical particles so that comparisons could be made with previous results.

The drag force on a spherical particle, radius  $r$ , in Stokes flow in a medium of viscosity,  $n$ , is given by:  $D_0 = 6\pi r n U_0$ . The velocity  $U_0$  should be substituted with  $(Q' - q')$ , that is, the relative velocity of the particle travelling with velocity  $q'$ . The drag force on the particle changes its velocity and so an equation of motion can be produced thus,  $F = 6\pi r n (Q' - q')$ . The velocities resolve into components along the  $x$  and  $y$  axes, namely,  $U'$ ,  $V'$ ,  $u'$ ,  $v'$ , which are the fluid and particle resolute respectively. As the particle travels along the  $x$  axis towards the target it is displaced sideways in the  $y$  direction due to the flow around the target. Figure 5.1 shows the streamlines around the cylinder; the trajectory of an infinitely light particle would follow these streamlines. The equations of motion of the particle in the  $x$  and  $y$  directions are given below.

$$(m/6\pi r n) du'/dt' = U' - u' \quad (1a)$$

$$(m/6\pi r n) dv'/dt' = V' - v' \quad (1b)$$

These equations are made dimensionless by measuring the distances in terms of  $R$  and the velocities in terms of  $U_0$ . Thus,  $u = u'/U_0$ ;  $x = x'/R$ ;  $t = t'U_0/R$  etc where  $U_0$  is the free fluid velocity and  $R$  is the radius of the cylinder. Thus the equations reduce to:

$$P_S du/dt = U - u, \quad P_C dv/dt = V - v \quad (2a,b)$$

where  $P_S (= mU_0/6\pi r nR)$  is the dimensional particle parameter and

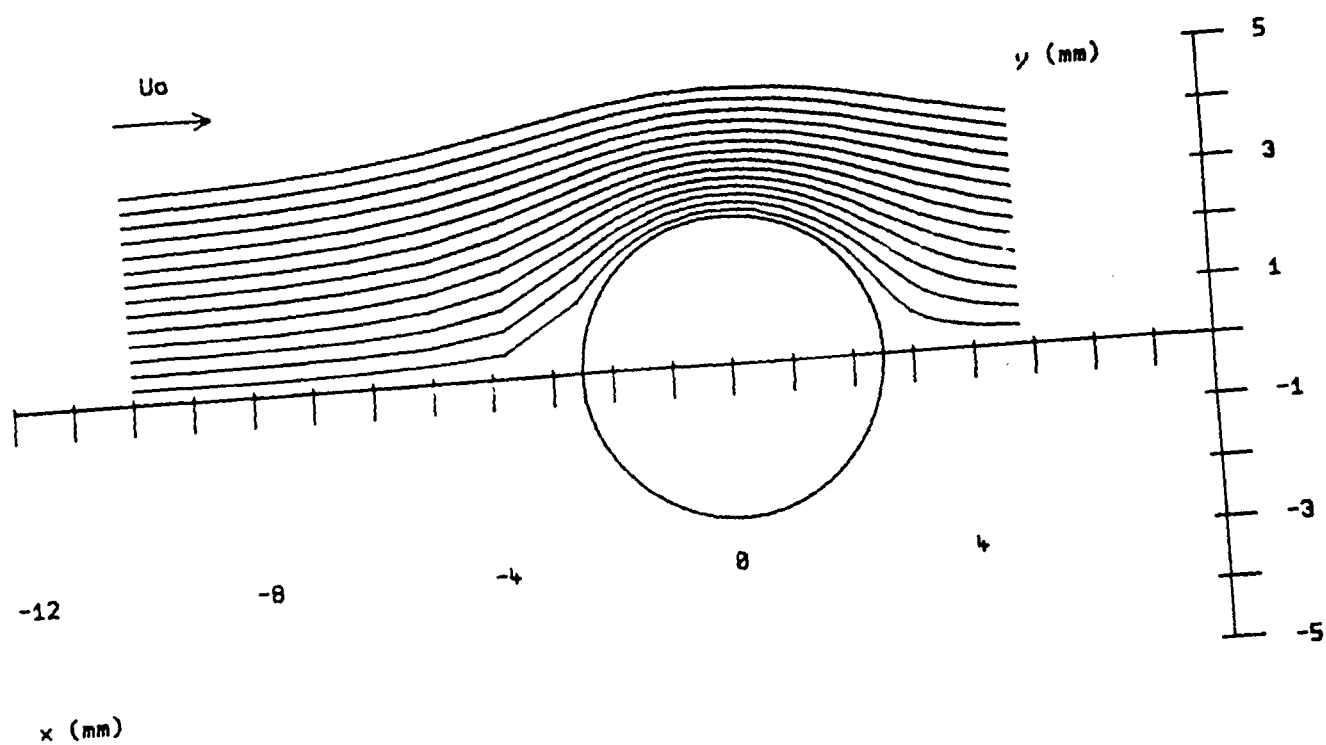


Figure 5.1 Streamlines around a cylindrical target

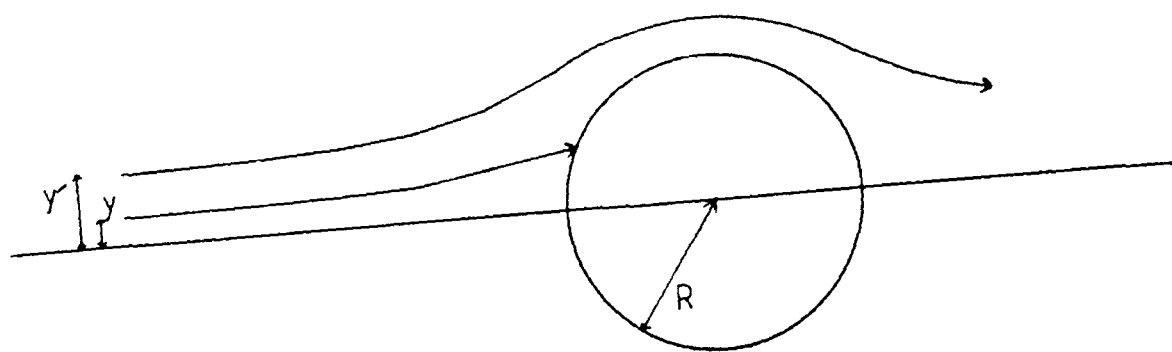


Figure 5.2 Two ice crystal trajectories showing a collision and a miss

is equal to the distance the particle would travel if injected into a stationary fluid with velocity  $U_0$  measured in units of  $R$ . It must be stressed at this point that  $P_S$  is the parameter applicable to spheres;  $P_P$  and  $P_C$  will be used to denote the parameters for plate and columnar crystals respectively and will be described later.

During a short time step  $t$  the particle will move a distance  $dx$ ,  $dy$  and there will be a change in velocity of  $du$ ,  $dv$ . However, at this stage the velocity changes are estimated and are denoted by  $d_1u$ ,  $d_1v$ . Thus,

$$dt = dx/(u_n + 0.5d_1u_n) = dy/(v_n + 0.5d_1v_n) \quad (3)$$

where  $n$  is the step number. This gives, for a known value of  $dx$ , a value of  $dy$  of

$$dy = dx(v_n + 0.5d_1v_n)/(u_n + 0.5d_1u_n) \quad (4)$$

The values of the fluid velocity  $U_n$ ,  $U_{n+1}$ ,  $V_n$  and  $V_{n+1}$  are interpolated from the flow field which allows a more accurate value of  $du_n$  to be calculated from equation 2a:

$$du_n = dt\{0.5(U_n + U_{n+1}) - (u_n + 0.5d_1u_n)\}/P_S \quad (5)$$

and combining with (3), gives:

$$du_n = (dx/P_S)((0.5(U_n + U_{n+1}))/((u_n + 0.5d_1u_n) - 1)) \quad (6)$$

Similarly from equations 2b and 3:

$$dv_n = (dx/P_S)((0.5(V_n + V_{n+1}))/((v_n + 0.5d_1v_n) - 1)) \quad (7)$$

The model assumes that the particle starts at a certain distance upstream of the target which is interpreted as the value of  $x$  where the particle velocity is 99% of the stream velocity. This distance was usually some eight target radii from the target. At large distances from the target the step length,  $dx$ , may be of the order of  $2R$  but as the particle approaches the target it is advisable to reduce the step length due to the deviation of the



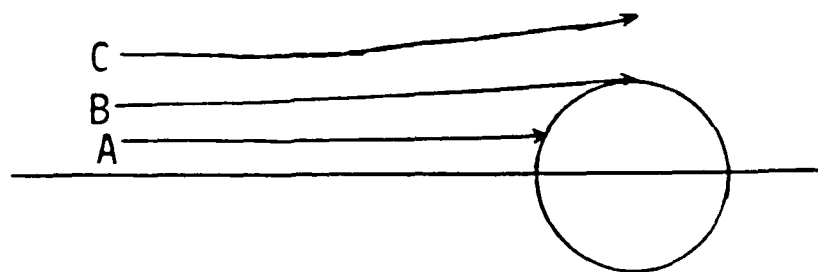
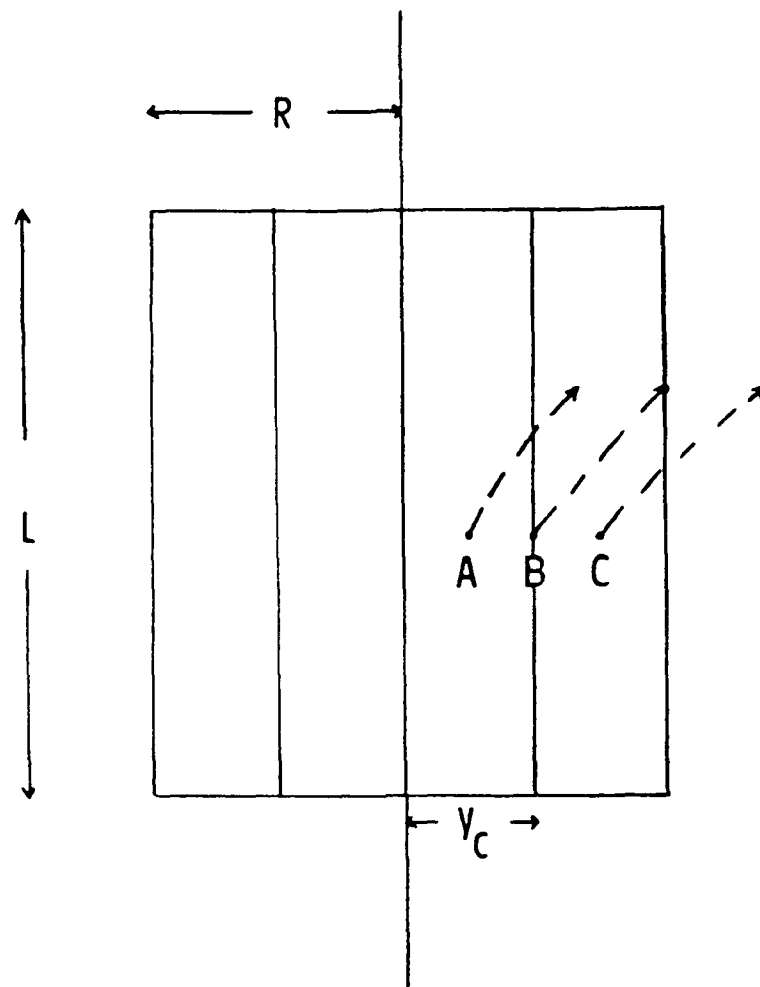


Figure 5.3 Schematic representation of the target A, a colliding trajectory B, the grazing trajectory and C, a miss trajectory

path in the  $y$  direction. Estimates for the values of  $d_1u_n$  and  $d_1v_n$  are made and a value for  $dy$  is calculated from equation 4. Values of the fluid velocity resolutions  $U_{n+1}$  and  $V_{n+1}$  are interpolated from the flow field and more accurate values of  $du_n$  and  $dv_n$  are determined from equations 6 and 7. If these values are comparable with the estimates then the model proceeds to the next value of  $n$ . If the values are not in good agreement the estimates are revised and the step is repeated. The particle will collide with the target if its center approaches within a distance of  $(1+r)$  of the cylinder center;  $r$  is the normalised value of the particle radius  $r'$  ( $r=r'/R$ ). Thus, the model continues to calculate the trajectory of the particles until the distance from the particle to the target center is less than the critical radius (ie a hit) or the particle misses the target completely. These two situations are shown in Figure 5.2. There is a critical trajectory (starting at  $y_C$ ) which causes the particle to just collide with the target; that is if  $y_1 < y_C$  the particle will hit and conversely if  $y_1 > y_C$  then the particle will miss completely. Figure 5.3 shows a two dimensional representation of a cylindrical target of radius  $R$  and length  $L$ . The area of the face is just  $2RL$ . Overlaid on the diagram are three values of  $y_1$  showing a hit, a miss and a glancing collision for the value  $y_C$ . Davies and Peetz (1965) defined the collision efficiency as that value of the initial starting position where the particle makes a grazing collision with the target; that is  $CE = y_C/R$ . This definition, however, is only suitable for particles of negligible radius. In this study, following the usual convention the collision efficiency is defined as the ratio of the collision cross section to the geometric cross section:

$$E = 2y_C L / 2(R+r')L = y_C / (R+r') \quad (8)$$

The values of the collision efficiency of a cylinder for spheres have been compared with the data of previous workers to ensure that the model gives the correct results. This gives confidence in the general scheme before applying the model to the problem of ice crystal trajectories.

The drag force for spheres given above does not account for viscous forces and these are now considered for ice crystals. Breach (1961) gives a second order equation for the drag coefficient for plate crystals of diameter  $2a$  and thickness  $2b$ . The thickness-diameter relationship is given by Pruppacher and Klett (1980):

$$C_D = (8m' / 3N_{RE})(1 + m'N_{RE}/48) \quad (9)$$

where  $m' = 12e^3 \{e(1-e)^{0.5} + (2e^2-1)\tan^{-1}(e/(1-e^2)^{0.5})\}$

and  $e = (1-(b/a)^2)^{0.5}$ . This leads to a particle parameter,

$$P_P = (3mU_O / 2.26m'aR)(1 + m'N_{RE}/48) \quad (10)$$

Columnar ice crystals can be idealised to cylinders and the particle parameter can be derived from the work of Jayaweera and Mason (1966). The parameter is given by:

$$P_C = (mU_O / 4\pi nLR)(\ln(2L/d) + 0.5) \quad (11)$$

where  $L$  and  $d$  are the length and diameter of the column respectively.

The particle parameters  $P_P$  and  $P_C$  are used in the model in place of  $P_S$  and the collision efficiencies were determined using the method described above.

### 5.3 Results

The trajectories for spheres were initially calculated to determine the model accuracy compared with previous models such

as those of Ranz and Wong (1952) and Loffler and Muhr (1972). The collision efficiencies calculated with this model were within 2-5% of those given previously, thus giving confidence in the model.

The particle size and mass determines its inertia, which is its resistance to a change in motion. If the particle is infinitely light it would follow the streamlines around the target except for the starting co-ordinate  $(-x,0)$ . As the particle inertia increases, its trajectory deviates more from the initial fluid streamline and tends to run parallel with the  $x$  axis. Figure 5.4 shows such a simulation; the particle has departed from the streamline and collided with the target.

Figures 5.5 and 5.6 show the relationship between the particle parameter  $P$  and the collision efficiency for plate and column crystals respectively. In both cases there is a rapid increase in efficiency with  $P$  which tails off as the efficiency approaches 95%.

Keith and Saunders (1989) measured the collision efficiency of a cylindrical target for plate and column crystals for different flow velocities. Briefly, an ice crystal cloud was drawn past a wet formvar covered glass target. The number of crystals replicated on the target surface was compared with the absolute concentration drawn past the target, the ratio giving the collision efficiency. These conditions were simulated by the model and the collision efficiency determined. A  $50\text{ }\mu\text{m}$  plate crystal was launched at the co-ordinates  $(-8,0.8)$  and  $(-8,0.84)$  into a  $3\text{ m s}^{-1}$  flow towards a target of radius  $2.5\text{ mm}$ . Figure 5.7 shows the trajectories of a  $50\text{ }\mu\text{m}$  plate for different starting co-ordinates. The impact velocity of the crystal

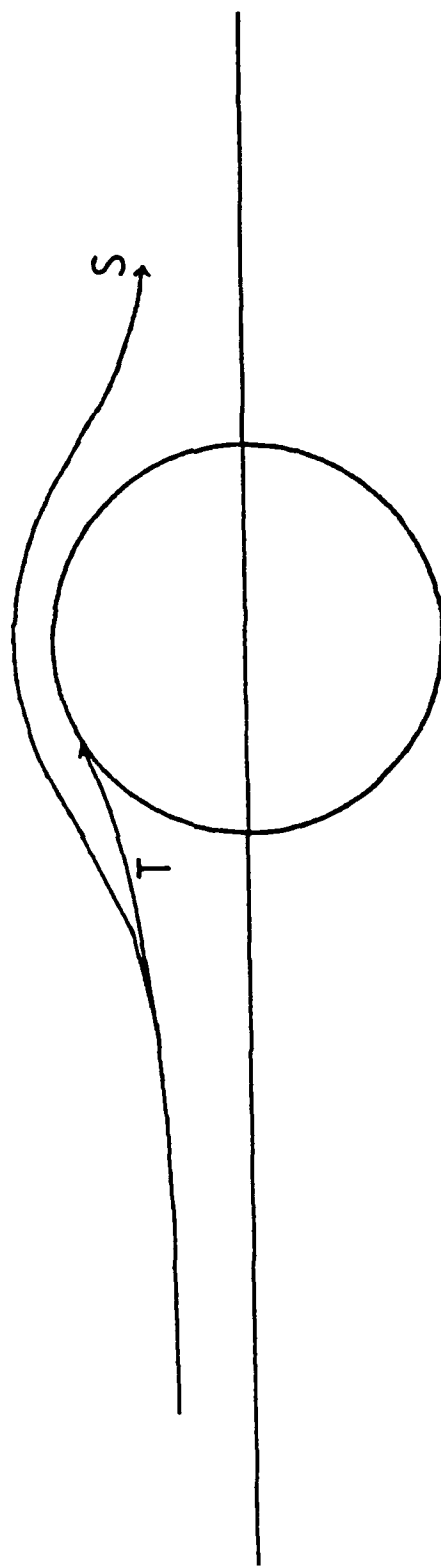


Figure 5.4 Departure of an ice crystal from the initial streamlines

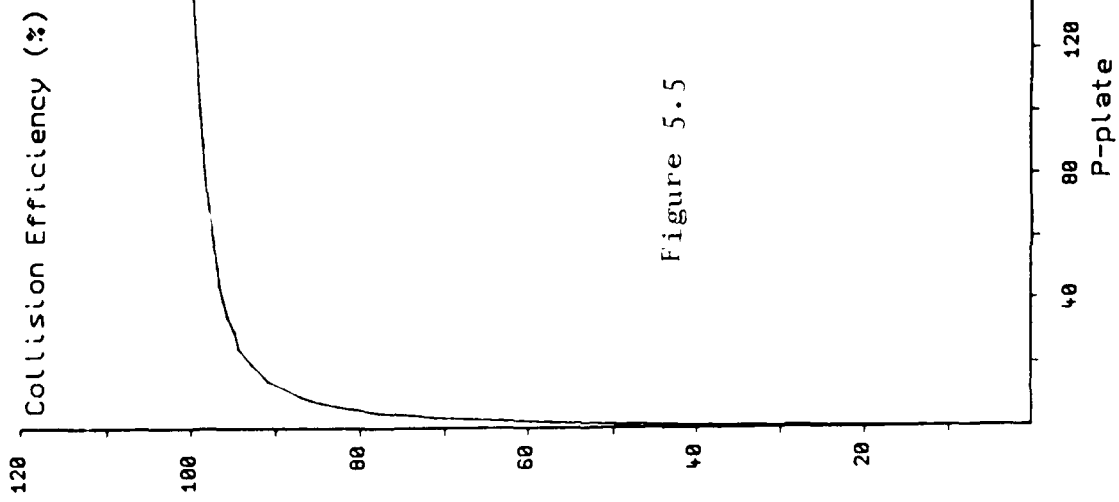


Figure 5.5

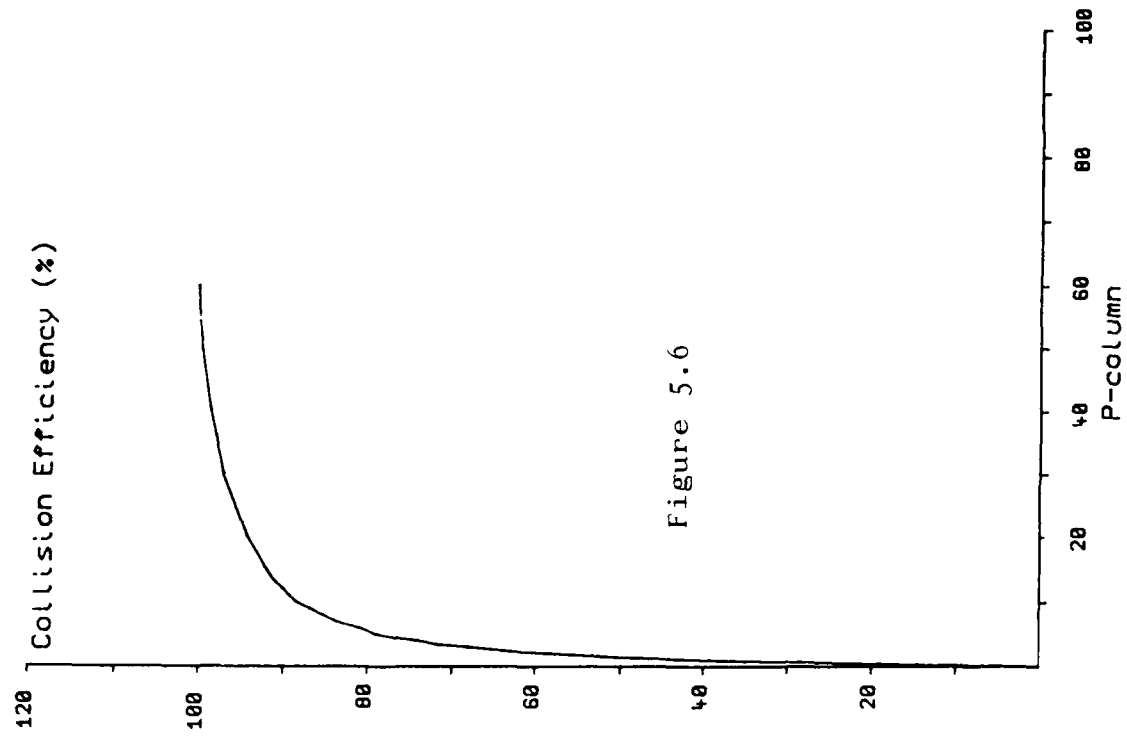


Figure 5.6

Variation of the collision efficiency with the particle parameter

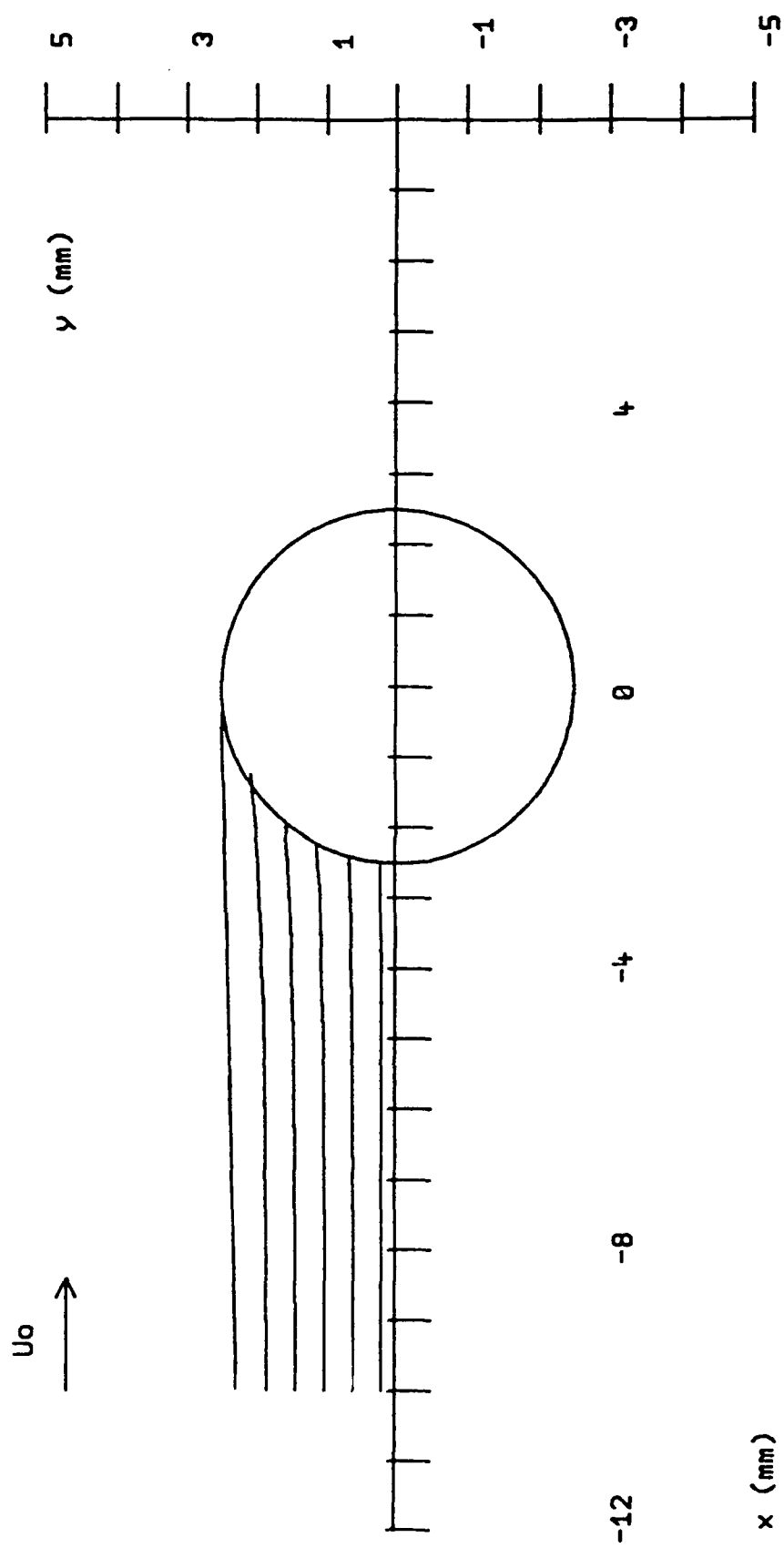


Figure 5.7 The trajectories of a 50  $\mu\text{m}$  plate crystal for different initial values of  $y$

increases from nearly zero (start co-ordinate  $(-8,0)$ ) to almost the free stream velocity for the grazing trajectory. The actual grazing trajectory co-ordinate was  $(-8,0.838)$  giving a collision efficiency of 83.8%.

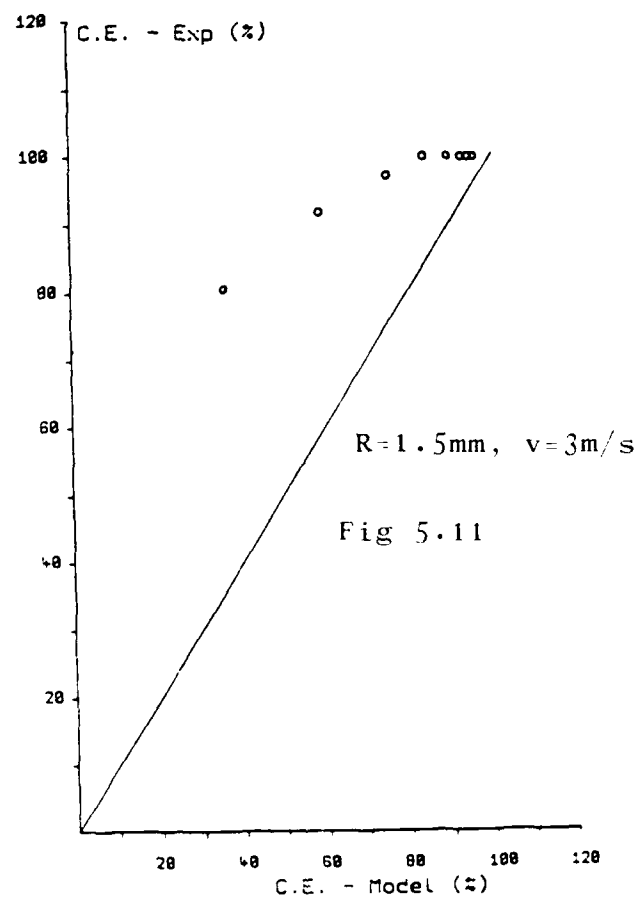
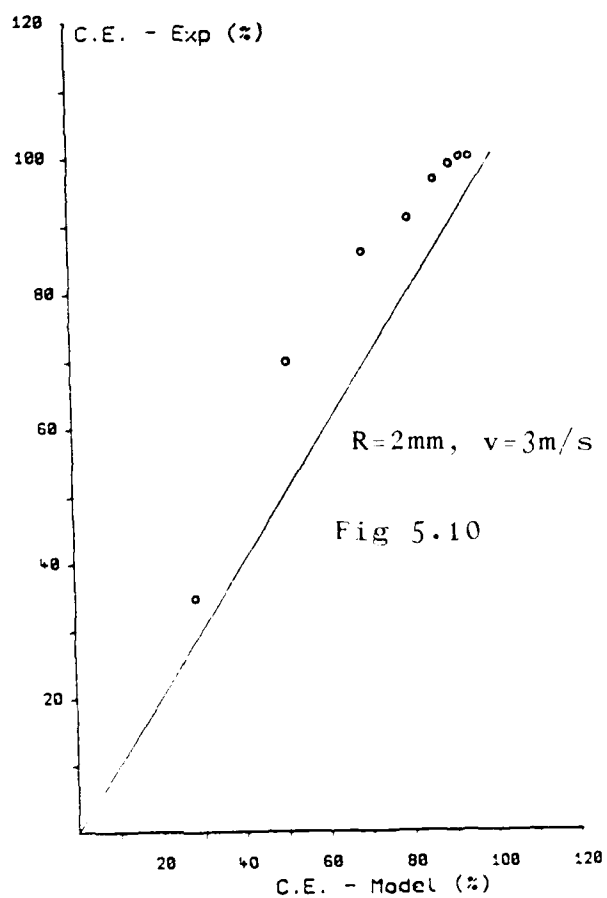
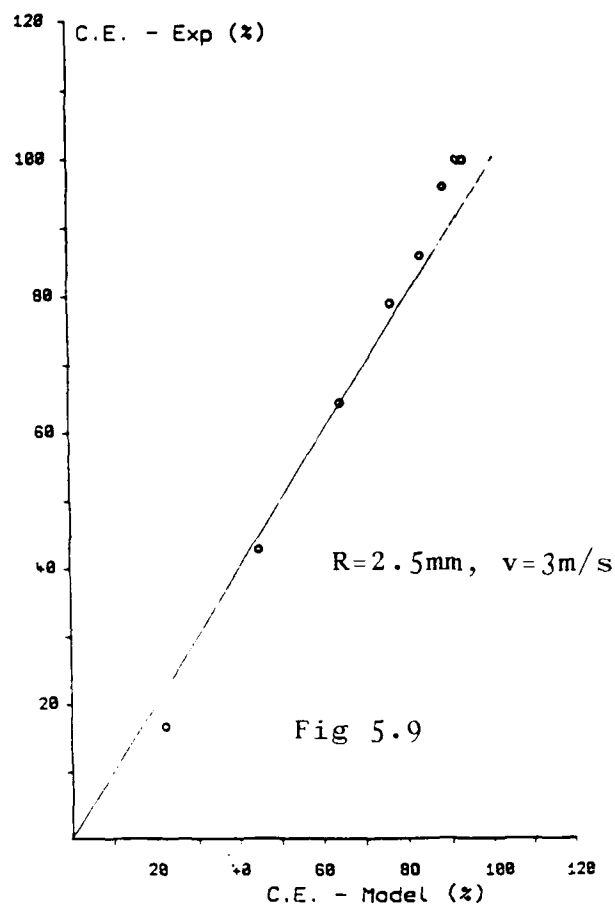
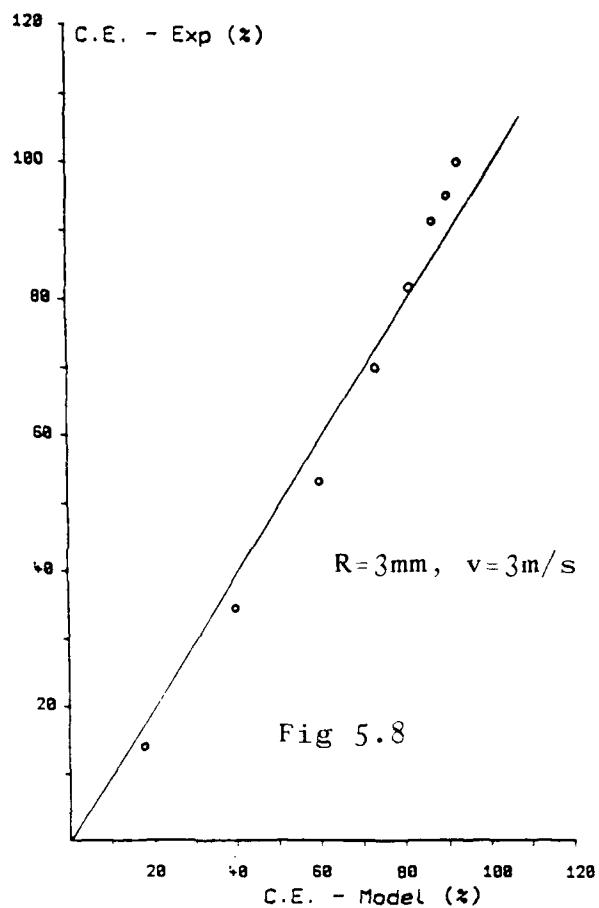
Figures 5.8-5.11 show the experimentally determined efficiency against that of the model for a flow speed of  $3 \text{ m s}^{-1}$  and target radii of 3, 2.5, 2 and 1.5 mm respectively. Also shown is a 1:1 line. The degree of fit is fairly good for the larger targets but is poor for the 1.5 mm target. Keith and Saunders also determined the collision efficiency of a 2.5 mm radius target for flow speeds of 4, 5 and  $6 \text{ m s}^{-1}$ ; the model results are shown in Figures 5.12-5.14. The agreement is again fairly good.

The above simulations were repeated for column crystals; the flow speed was  $3 \text{ m s}^{-1}$  and the large radii were 3, 2.5, 2 and 1.5 mm and the comparisons with the experimental data are shown in Figures 5.15-5.18. Again the agreement is good. Lastly, the target radius was set to 2.5 mm and the flow speed used was 4, 5 and  $6 \text{ m s}^{-1}$ ; the agreement is shown in Figures 5.19-5.21.

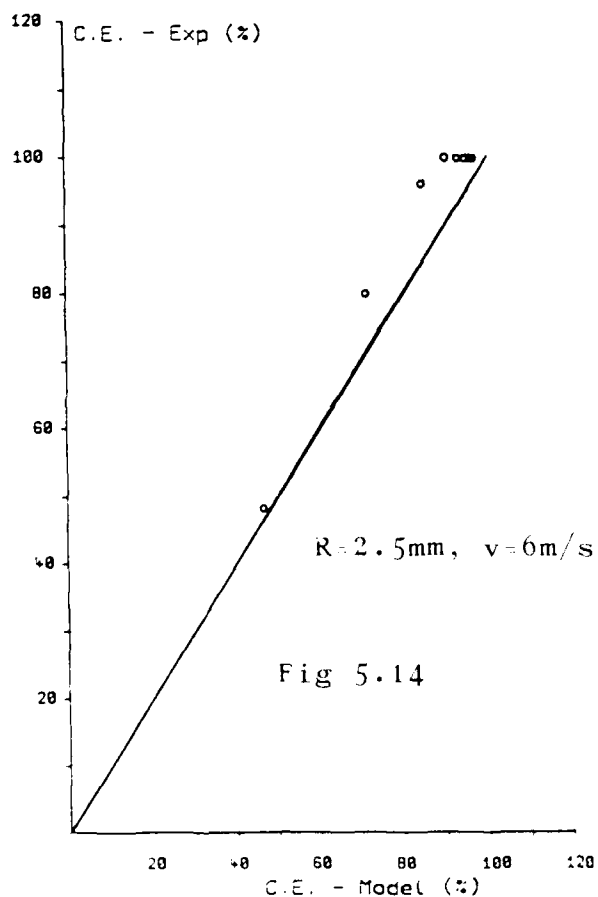
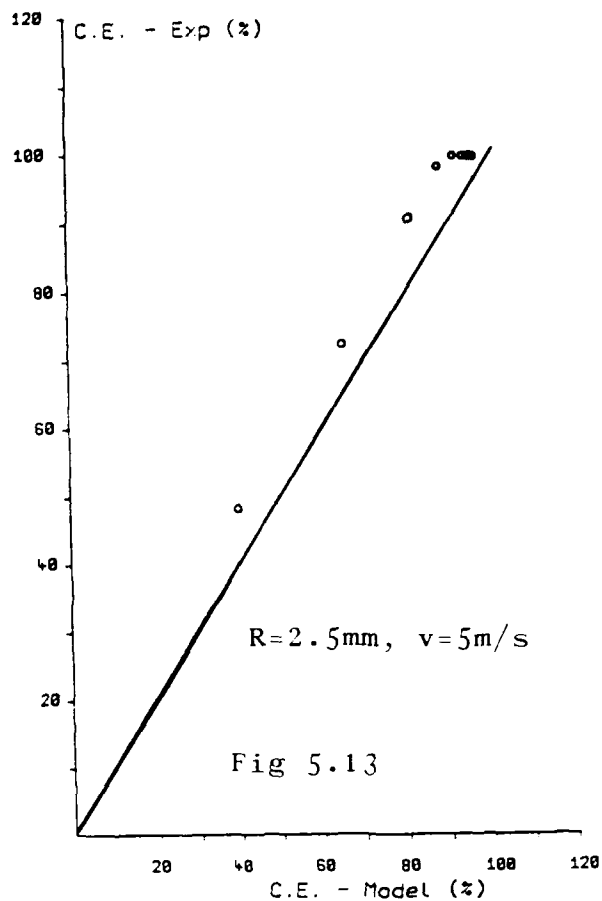
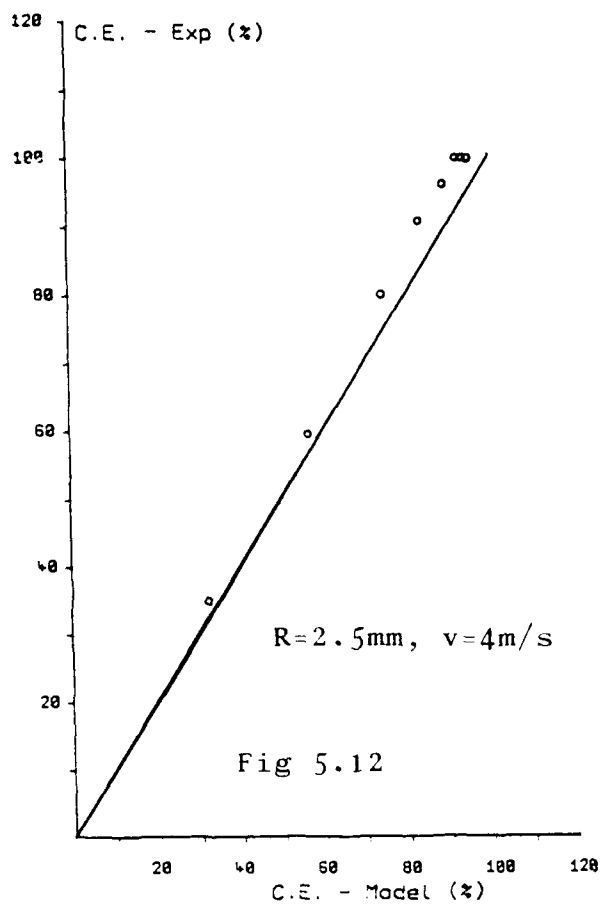
#### 5.4 Discussion and Conclusions

The model is the first to attempt to describe the motion of ice crystals past a cylindrical target. The fairly good agreement for larger targets, between the theoretical results and the experimental data of Keith and Saunders is surprising, considering the random tumbling motion of real ice crystals which have been observed in the laboratory. This random motion may account for the differences between the model and the experiment with the model consistently underestimating the collision

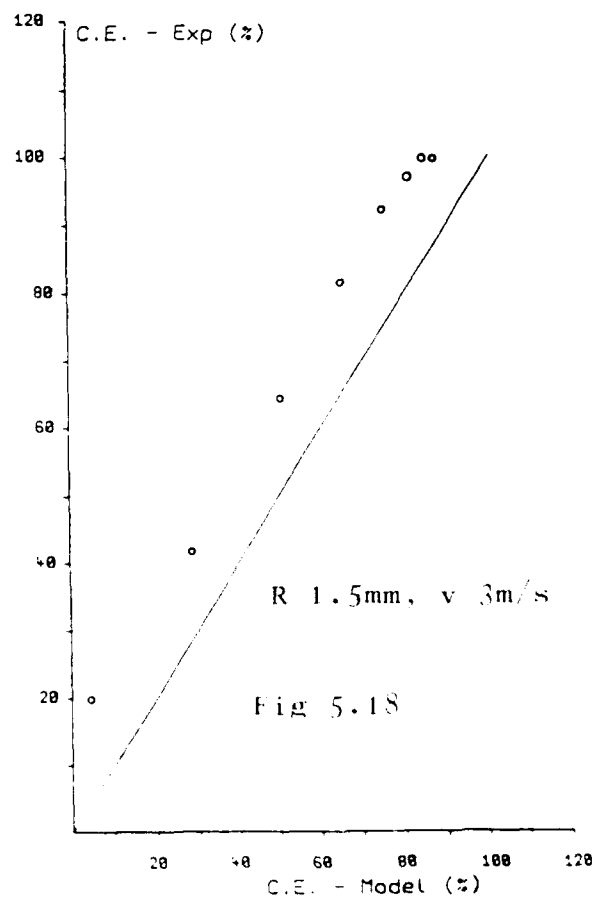
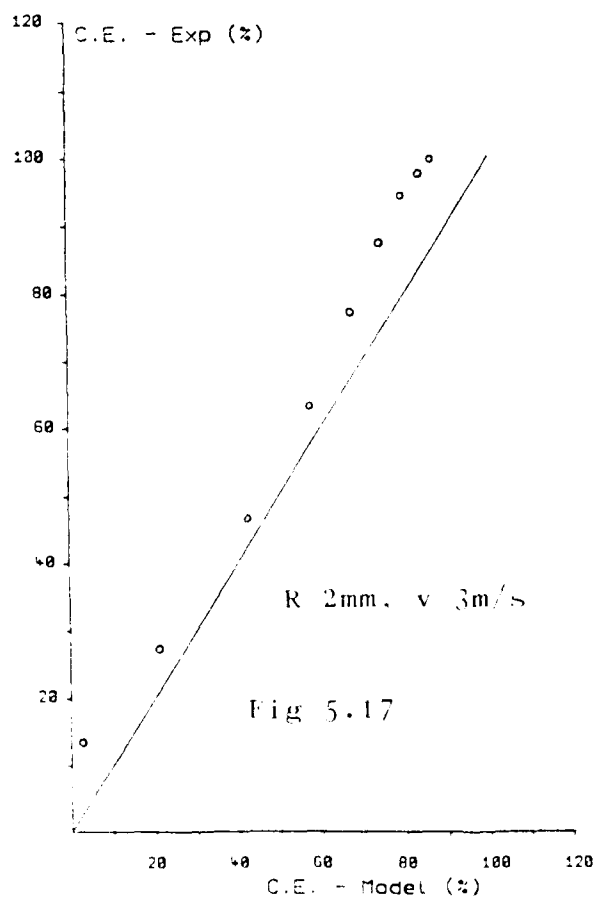
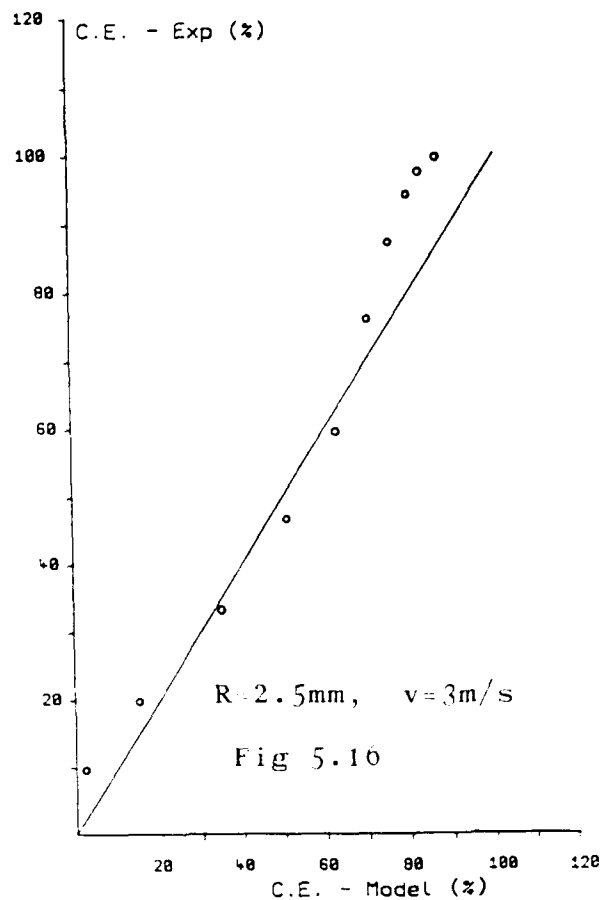
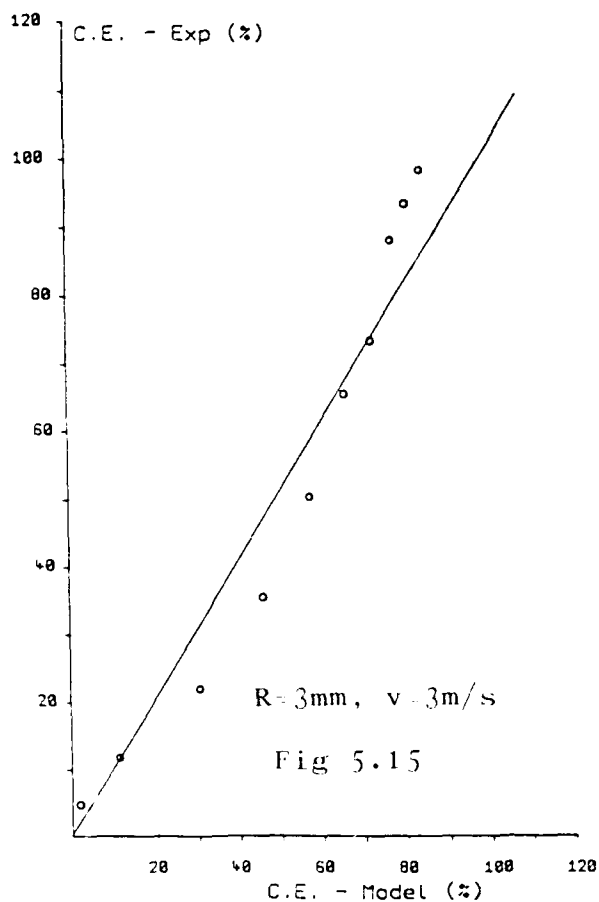




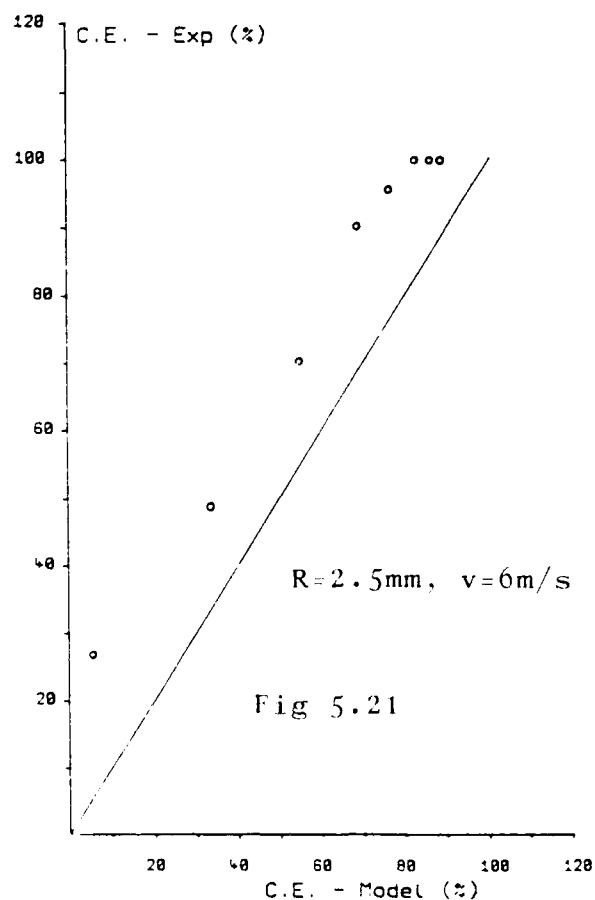
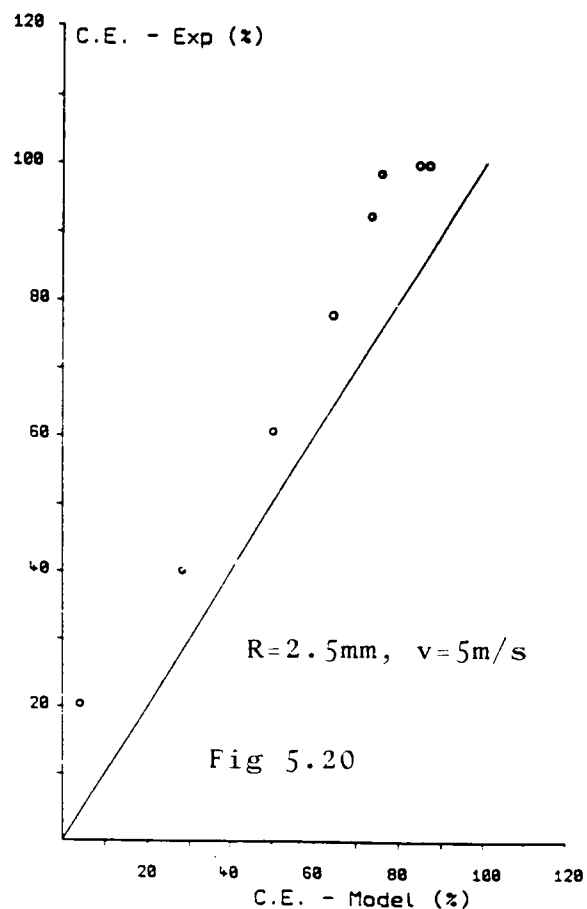
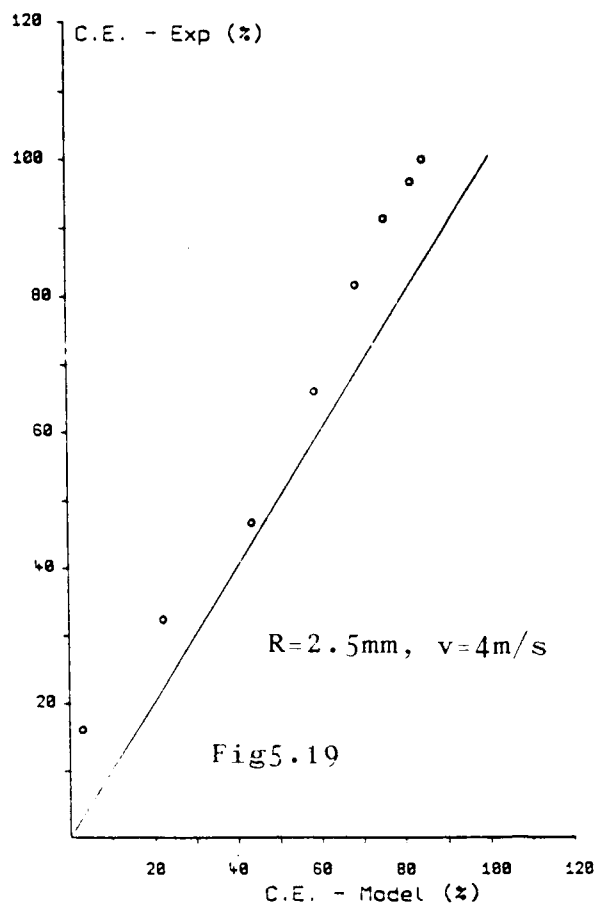
Comparison between the theoretical values of collision efficiency with the experimental values for plate crystals



Comparison between  
theoretical and  
experimental collision  
efficiencies for plate  
crystals



Comparison between theory and experimental collision efficiencies for column crystals



Comparison between  
theory and exper-  
imental collision  
efficiencies for  
column crystals

efficiency. Keith and Saunders state that there may be a maximum error of 5% in the experimental efficiencies due to the counting errors in the experiment.

These results are of importance to cloud modellers when considering the interactions between ice crystals and hailstones leading to thunderstorm electrification. The model and experimental results show that the efficiency is less than unity for small crystals and may reach 100% for very large crystals, whereas the cloud models have assumed a collision efficiency of 100% irrespective of size.

## CHAPTER 6

### THE HEAT TRANSFER OF A RIMING CYLINDER

#### 6.1 Introduction

When a hailstone or cylindrical target grows by the accretion of supercooled water droplets, the target temperature will be raised above the surrounding air temperature by an amount proportional to the accretion rate, due to latent heat release from the freezing droplets. The magnitude of temperature elevation above ambient is governed by the rate at which heat is transferred to the environment by convection and evaporation. The rate of heat loss is in turn governed by the value of the heat transfer factor,  $x$ , and the purpose of the experiments described here was to measure this coefficient as a function of the riming conditions.

#### 6.2 Historical Background

As early as 1925 Reiker performed experiments to determine the heat transfer from a hot cylinder when placed in a cooler airflow. He noted that when the flow changed from non-turbulent to turbulent the rate of heat transfer increased by as much as 40%. He also noted that for Reynolds numbers in the range  $10^3$  to  $10^4$  the heat transfer could be increased by placing longitudinal fins or grooves ( $1/10$  the diameter of the cylinder) on the target surface. McAdam (1942) also investigated the effect of turbulence on the heat transfer process; he found that the heat transfer increased by about 23-30% as the level of turbulence increased. Comings et al (1948), however, found that when the

turbulence intensity was increased from 1 to 7%, the heat transfer rose by 25% but further increase in the turbulence to 22% resulted in the heat transfer increasing by only another 5%. Geidt (1951) measured the rate of heat loss at the front and rear portions of a cylinder and found that the ratio of front to back-half heat transfer was a function of the turbulence; the ratio increased from 0.85 to 1.1 as the turbulence intensity rose. Further work by Kestin and Maeder (1957), Knudsen and Katz (1958) and Perkins and Leppert (1962) showed that the rate of heat transfer is a function of the turbulence level within the flow.

Ludlam (1951) considered the heat economy of a riming cylinder. The surface temperature is determined by a balance between the rate at which heat is released on freezing and the rate at which heat can be liberated to the environment through forced convection and evaporation. The heat transfer depends on the turbulence and the roughness of the surface. Macklin (1961) investigated the riming process and found that there are five types of rime ice; namely, clear, milky, opaque, kernel and feathery. The nature of the rime ice is dependent on the temperature of the rime, the impact velocity of the droplets and the liquid water content leading to clear rime ice at temperatures close to 0°C and feathery rime at much lower temperatures. The incidence of air bubbles in the ice, and air gaps within the actual structure of the rime, accounts for the increasing opacity with decreasing temperature. As the impact velocity increases, the effect is to shift the type of rime ice to that type normally found at higher temperatures. The reasons for this are two-fold; firstly, the accretion rate is increased and so the surface is warmer, and, secondly, the droplets spread more on impact and

tend to fill in the air gaps. List (1963a) criticised Macklin's paper for using a heat transfer factor of 0.24 which applies to a smooth surface. List introduced a factor  $0.24\bar{U}$  where  $\bar{U}=1$  for smooth ice, but may exceed 2 for a rimed surface. Macklin replied that he noted Reiker's observations but criticised List for introducing the factor without justification. List (1963b) derived an equation to describe the heat balance of a riming hailstone; he used a factor  $\bar{U}$  which he attributed to surface roughness but he did not give any values. Macklin (1964), commenting on List's results (1963b), stated that there was less than a 5% increase in heat transfer due to surface roughness; however, these experiments were conducted such that the surface temperature was close to  $0^{\circ}\text{C}$  in which case the rime ice was smooth.

Macklin and Payne (1967) presented equations to determine the surface temperature of a riming cylinder. The equation is based on the work of Ludlam (1951) but includes the effect of ventilation. They stated that the value of the heat transfer factor,  $x$ , was dependent on the airstream turbulence and the surface roughness but did not give any indication as to the possible dependency. The equation is given below, together with the symbols.

$$Ewv2R(L_f + c_w(T_a - T_m) + c_i(T_m - T_s)) = \\ x \text{ Re}^{0.5} (\text{Pr}^{1/3} k(T_s - T_a) + \text{Sc}^{1/3} L_v D(p_s - p_e))$$

$C_p$  = Specific heat of air (J/Kg K)

$c_i$  = Specific heat of ice (J/Kg K)

$c_w$  = Specific heat of water (J/Kg K)

$D$  = Diffusion of water vapor in air ( $\text{m}^2/\text{s}$ )



E	=	Collision efficiency
k	=	Thermal conductivity of air (J/m s °C)
L <sub>f</sub>	=	Latent heat of fusion (J/kg)
L <sub>v</sub>	=	Latent heat of vaporisation (J/kg)
P	=	Density of air (kg/m <sup>3</sup> )
P <sub>e</sub>	=	Saturation vapor density wrt water (kg/m <sup>3</sup> )
P <sub>s</sub>	=	Saturation vapor density wrt ice (Kg/m <sup>3</sup> )
Pr	=	Prandtl number = $C_p \nu P / k$
R	=	Radius of cylinder (m)
Re	=	Reynolds number = $2Rv/\nu$
Sc	=	Schmidt number = $\nu/D$
T <sub>a</sub>	=	Air temperature (°C)
T <sub>m</sub>	=	Melting temperature (°C)
T <sub>s</sub>	=	Rime surface temperature (°C)
v	=	Air velocity (m/s)
w	=	Liquid water content (kg/m <sup>3</sup> )
$\nu$	=	kinematic viscosity of air (m <sup>2</sup> /s)
x	=	Heat transfer factor

The left-hand side of the equation deals with the rate of heat production by the freezing water droplets, whereas the right-hand side determines the rate at which heat is being transferred to the environment by forced convection and evaporation. Thus, given measurements of T<sub>a</sub>, T<sub>s</sub> and Ew the value of x can be easily calculated. This paper describes experiments to determine the exact effect of the surface roughness on the heat transfer coefficient.

### 6.3 Experimental Procedure

The experimental apparatus is shown in Figure 6.1 and consists of a U-tube which is symmetrical about the x-axis. A 5mm diameter cylindrical target was placed in each of the arms as shown. Various tests were performed to confirm that the flow past each target was the same. A 5 mm wide platinum temperature sensor was attached to one of the targets (the targets will now be known as the sensor target and the reference target). The sensor has a sensitivity of  $4 \text{ mV} = 1^\circ\text{C}$  and the output to a chart recorder could be resolved to  $0.25 \text{ mV}$ . The tubes protruded into a large cloud chamber situated within the cold-room which has an effective operating temperature range of  $0$  to  $-38^\circ\text{C}$ . Water vapor was introduced into the chamber from a boiler, which formed a cloud of supercooled droplets. The cloud temperature was measured with a thermocouple. The cloud was drawn past the targets at velocity  $v$  with the rime temperature being monitored continuously. Care was taken to ensure that the depth of rime over the sensor did not exceed  $2 \text{ mm}$  and so a reliable value of the rime surface temperature was obtained. After a known time, usually one minute, the rime was scraped off the reference target and weighed. The rate at which rime was accreted, (the rime accretion rate, RAR) was calculated, from which the effective liquid water content,  $E_w$ , was determined.

$$\text{RAR (mg cm}^{-2} \text{ min}^{-1}) = 6E_w v \text{ (g m}^{-3} \text{ m s}^{-1}).$$

The effective liquid water content is made up of that portion of the droplet spectrum which strikes the target and is affected by the droplet collision efficiency. The experiments were performed at flow speeds of  $3$  and  $6 \text{ m s}^{-1}$  and at temperatures between  $-2.5$  and  $-32^\circ\text{C}$ . The total liquid water content

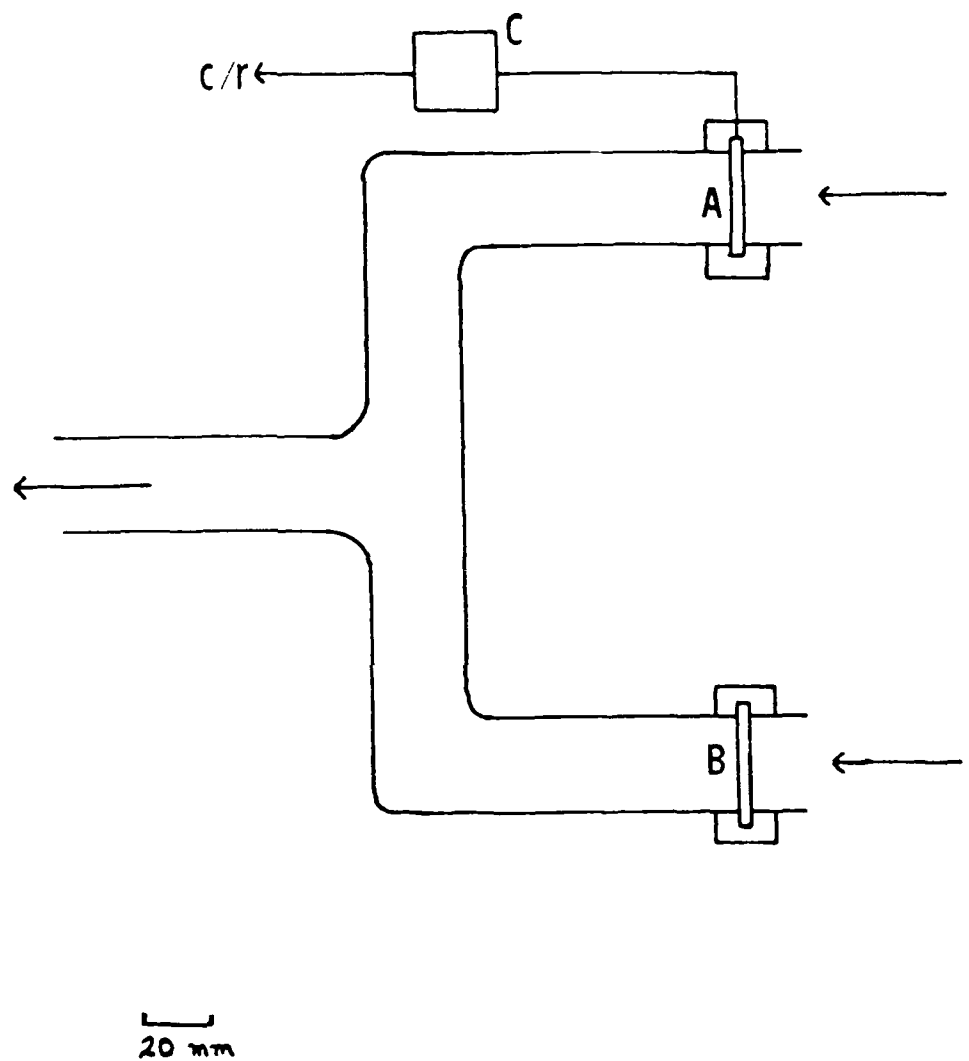


Figure 6.1 The heat transfer apparatus.

- A - Sensor target
- B - Reference target
- C - Sensor circuit

within the chamber ranged from  $0.2$  to  $9 \text{ g m}^{-3}$ . Thus, it was possible to determine the three unknown parameters in equation 1; that is,  $T_a$ ,  $T_s$  and  $E_w$ .

#### 6.4 Results

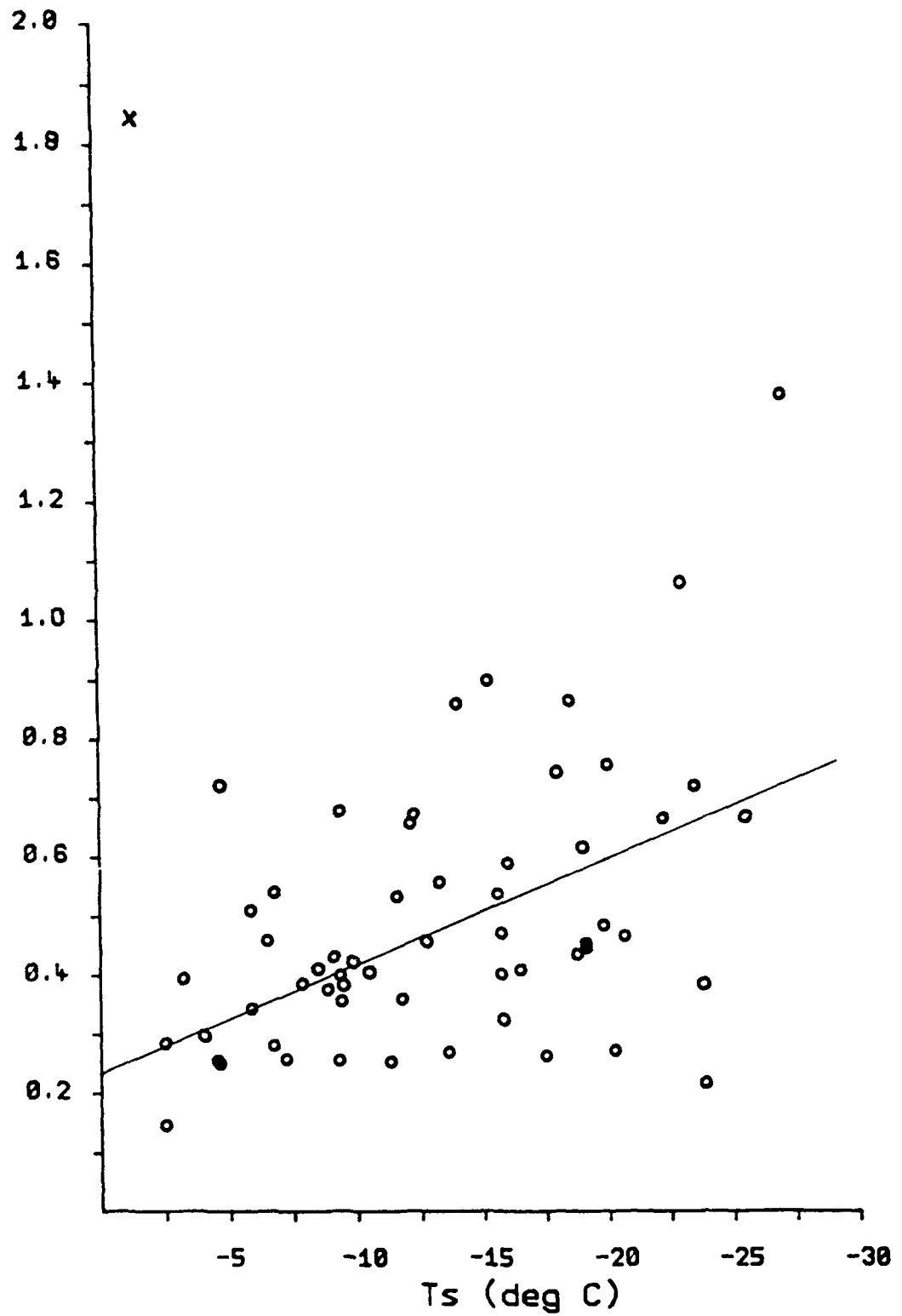
Figures 6.2 and 6.3 show measurements of the rime surface temperature against  $x$  for velocities of  $6$  and  $3 \text{ m s}^{-1}$  respectively. It can be seen that there is a broad spread in the results due to the random growth patterns of the rime for similar experimental conditions. The target grew in the dry growth regime (Macklin, 1961) at all times, although wet growth could be achieved when the air temperature was higher than  $-6^\circ\text{C}$ . The equations of the lines in Figures 2 and 3 are:-

$$x = 0.24 - 0.19T_s \text{ at } 6\text{m/s and } x = 0.24 - 0.035T_s \text{ at } 3\text{m/s.}$$

Hence an approximate relationship between the flow speed, the rime surface temperature and the heat transfer coefficient could be determined with the normalised parameter  $G = v_0 T_s / v$  where  $v_0 = 3 \text{ m s}^{-1}$ .

#### 6.5 Discussion

The results presented here show that the surface roughness has a profound effect on the value of  $x$ . At high temperatures of around  $-2$  to  $-6^\circ\text{C}$  the target is covered with smooth clear ice and the value of  $x$  is approximately  $0.3$ , which is in close agreement with the value of  $0.28$  given by Macklin. As the nature of the rime ice changes from kernel to feathery ice at colder temperatures, the value of  $x$  increased from about  $0.5$  to  $1.5$ . An empirical formula giving  $x$  for particular values of the parameter  $G$



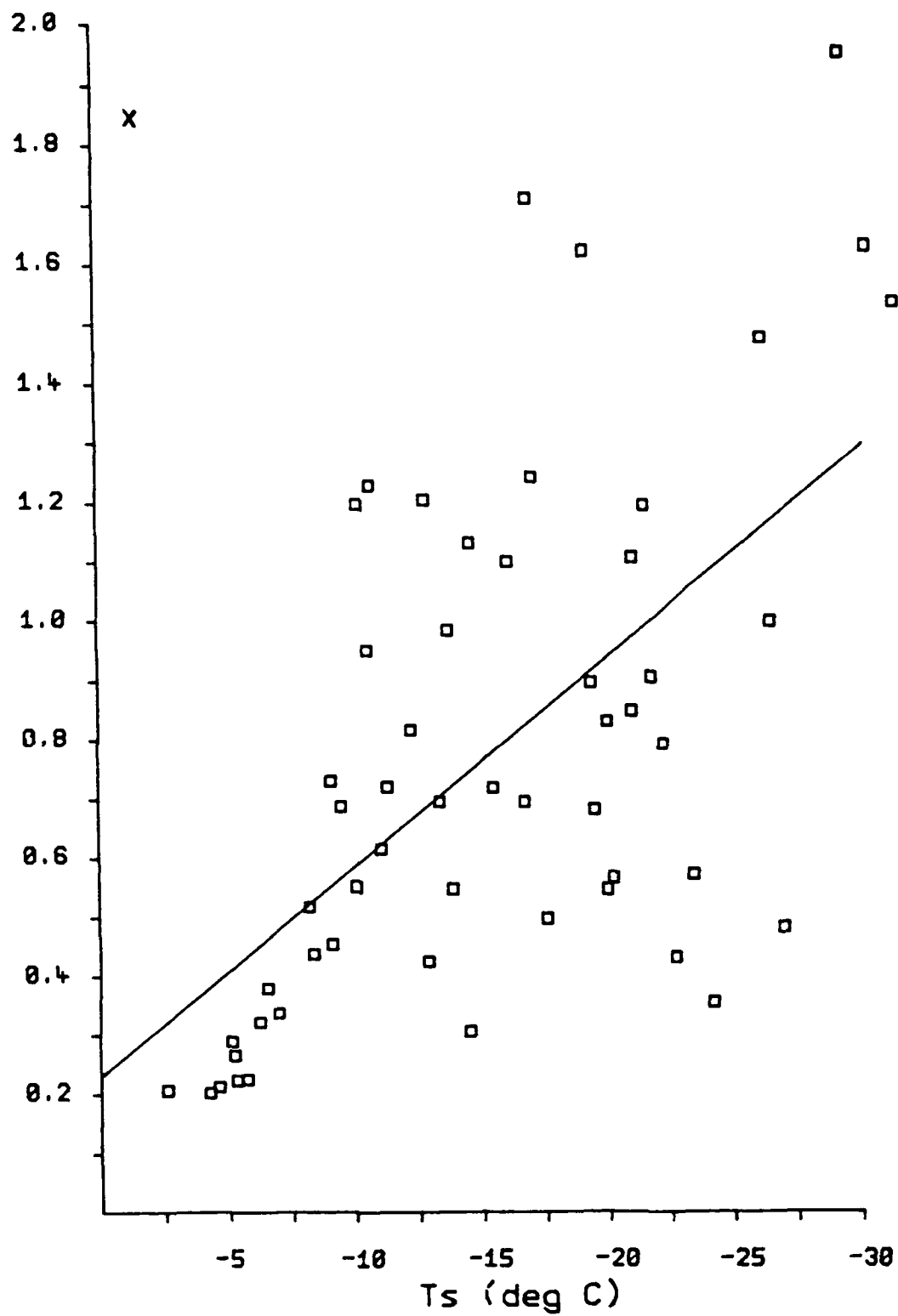


Figure 6.3 Variation of  $x$  with surface temperature at a flow velocity of 3 m/s

( $G = v_0 T_s / v$ ) is given below, valid in the range 3 to 6 m/s.

$$x = 0.24 - 0.035G$$

The main sources of error in these experiments were in determining the mass of rime collected (0.03% to 3.6%), the flow velocity (1.6% to 3.3%) and the rime surface temperature (0.42% to 6%). An upper limit of the uncertainty can be calculated by taking the square root of the sum of the squares of the maximum individual errors, which gives  $\pm 8\%$ .

A consequence of the increase of  $x$  with decreasing temperature is that the target can experience very high rime accretion rates at low temperatures without a significant increase in the rime surface temperature. For example, at an air temperature of  $-31.9^\circ\text{C}$  and flow speed of  $3 \text{ m s}^{-1}$  the target temperature is  $-31.4^\circ\text{C}$  for an effective liquid water content of  $0.9 \text{ g m}^{-3}$ . The calculated value of  $x$  is 1.57 for these conditions. At higher temperatures with less pronounced feather growth this rime accretion rate would lead to a rise in rime surface temperature of about  $1.5^\circ\text{C}$ . This is important when considering the growth of small graupel particles (soft hailstones) in the supercooled regions of a cloud. Browning et al (1963) have shown that the surface temperature of low-density graupel will be no more than a few degrees above ambient. As the graupel diameter increases, the accretion rate increases and the surface temperature can approach  $0^\circ\text{C}$ . Thus, there is an important difference in the growth of graupel and hailstones in that the surface temperature of the hailstone will almost always be close to  $0^\circ\text{C}$ , whereas the graupel temperature will be close to ambient. This difference in surface temperature is critical when considering thunderstorm electrification due to charge generation when ice crystals make

rebounding collisions with graupel particles. If the surface of the graupel is wet, then its adhesion efficiency is unity and the ice crystals cannot rebound, and so no charge is generated. However, it has been shown here that small graupel particles can experience very high liquid water contents without entering the wet growth regime, and so charge transfer will occur in conditions which hitherto have been thought to preclude charge transfer.

#### 6.6 Conclusion

It has been shown that the surface roughness of a riming hailstone target affects the heat transfer. The presence of feathers on the rime surface leads to pronounced increases in the target's ability to dissipate heat into the environment. The value of  $x$  ranges from 0.3 at high surface temperatures to almost 2 at lower temperatures. Thus small graupel particles will not undergo wet growth until the liquid water content reaches high values.



## CHAPTER 7

### THE SCAVENGING OF HIGH ALTITUDE AEROSOL BY SMALL ICE CRYSTALS

#### 7.1 Introduction

Following concern about the injection of particulate material by nuclear explosions and volcanic events, there have been several global models developed for the theoretical investigation of the removal of high altitude aerosol from the atmosphere. These models lack a knowledge of the scavenging efficiencies of the small ice crystals associated with cirrus clouds and storm ice anvils which are the only hydrometeors that could remove the injected particles.

In the past there have been a number of practical studies into the scavenging efficiencies of large ice crystals and snowflakes. A comparison of the extrapolated results of these findings and the theoretical models of Martin et al (1980) for the small crystal situation has been made. It was found that, in general, the extrapolated results gave efficiencies that were significantly higher than the predicted values. This difference was found to be enhanced as the crystal diameter decreased.

Experiments used small ice plates grown at  $-18.5^{\circ}\text{C}$  in a cloud chamber, which were then permitted to fall through a dense aerosol cloud, to provide the first direct measurements of the scavenging efficiencies of these small crystals under cloud conditions. Initial results are presented for non-disperse NaCl aerosol particles of size  $4 - 6\text{ }\mu\text{m}$ .

Airborne surveys such as those of Heymsfield (1975a,b,c), have revealed that the predominant habits of ice crystals in

cirrus clouds and thunderstorm anvils are a mixture of bullet rosettes and plates. The mean size was found to be 300-500  $\mu\text{m}$  with a mean concentration of  $10^6 \text{ m}^{-3}$ . Examination of the air beneath the clouds showed that the crystals survived falls of 4-5 km with concentrations of  $10^3 - 10^4 \text{ m}^{-3}$ . Hall and Pruppacher (1976) found these observations to be consistent with the accepted theories of crystal growth and evaporation.

The size range of aerosols of greatest importance is 0.1  $\mu\text{m}$  to 10.0  $\mu\text{m}$ ; the lower limit being derived from Brownian coagulation and the upper limit from the fact that particles above this size have sufficient Stoke's deposition velocity to fall out relatively quickly as was first pointed out by Greenfield (1957).

## 7.2 Previous Investigations

Analysis of the scavenging problem by ice crystals has been tackled by theoretical investigation and by experimental work.

### 7.2.1 Theoretical Investigation

Analysis of the situation is usually undertaken by considering the aerosol motion to be determined by a superposition of forces. An initial assumption is made that the ice crystal falls in a steady state, offering maximum resistance to the direction of the motion. The magnitude of the scavenging is then the sum of:

- i. Impaction - aerosols leave the flow of air around the crystal because of the momentum, and then impact on the crystal. This becomes the dominant mechanism for aerosol  $> 7-8 \mu\text{m}$  in size.
- ii. Interception - the mass centers of the aerosol particles

would follow the flow of air around the crystal but their physical size causes capture. This is the dominant mechanism of capture for aerosols in the size range  $0.5 < \text{diameter} < 8 \mu\text{m}$ .

iii. Brownian Deposition - this is the collection due to the Brownian motion of the aerosol which becomes modified by the flow of air around the collector and is the main collection mechanism for particles  $< 0.5 \mu\text{m}$ .

iv. Electrostatic Effects - charges on the aerosol or ice crystals are generally assumed to act as point charges with the normal distance<sup>2</sup> relation.

v. Phoretic Effects - these are enhancements of the collection efficiency due to gradients of temperature and vapor pressure around the collector. The magnitude of the effects are complex functions of the respective fields (see Pruppacher and Klett, 1980). The effects have been shown to alter the collection of particles smaller than  $1 \mu\text{m}$  as shown, for example, by Martin et al (1980 a, b).

This last point was disputed by Vittori (1973), who preferred a description of a growing crystal in terms of flushes of droplets rather than a steady field. This point has not been resolved, apart from the adoption of the field description for the purposes of constructing models.

Sophisticated models using the above approach have been developed by Martin et al (1980 a, b) for plate crystals, and by Miller and Wang (1989) for column crystals.

#### 7.2.2 Practical Studies

There have been two major sets of experimental work done on the scavenging efficiency of ice crystals. These are detailed in

Knutson et al (1976) and Murakami et al (1985 a, b, c). In both of these studies, large crystals ( $> 1$  mm) were allowed to fall through an aerosol chamber which was either opened to snowfall directly, or the crystals were collected from the ground and then introduced into the chamber. In these cases, the temperature, humidity, pressure, electric charge and aerodynamics were quite different to the conditions present in the clouds of interest.

### 7.3 Comparison of Results

In order to compare the existing practical results and theory, the empirical equations contained in the above studies have been modified as far as possible to match the conditions used by Martin et al (1980a). Two sets of results are shown displaying this data: Figure 7.1 displays the scavenging efficiency of a  $427.6 \mu\text{m}$  diameter plate crystal for a range of particle sizes; Figure 7.2 shows the equivalent data for an ice crystal with a diameter of  $101.2 \mu\text{m}$ . The first point to note is the much closer agreement between the data sets (up to  $1 \mu\text{m}$ ) for the larger crystal than for the smaller one. Martin et al (1980a) used a constant thickness ratio of 0.05 for their ice crystals. This differs from the results of Ono (1969) who showed that smaller diameter crystals have a greater thickness ratio, 0.15 - 0.3 being appropriate for crystals of  $100 \mu\text{m}$ .

In the extrapolation of the Murakami et al results, the following method has been used. The Best number was first calculated from the equation given by Jayaweera and Ryan (1972) for the atmospheric conditions set by Martin et al. This value was then used to derive the Reynolds number, using the empirical study of Heymsfield and Kajikawa (1987). The terminal velocities

Data for 427.6 um dia crystal (600mb)

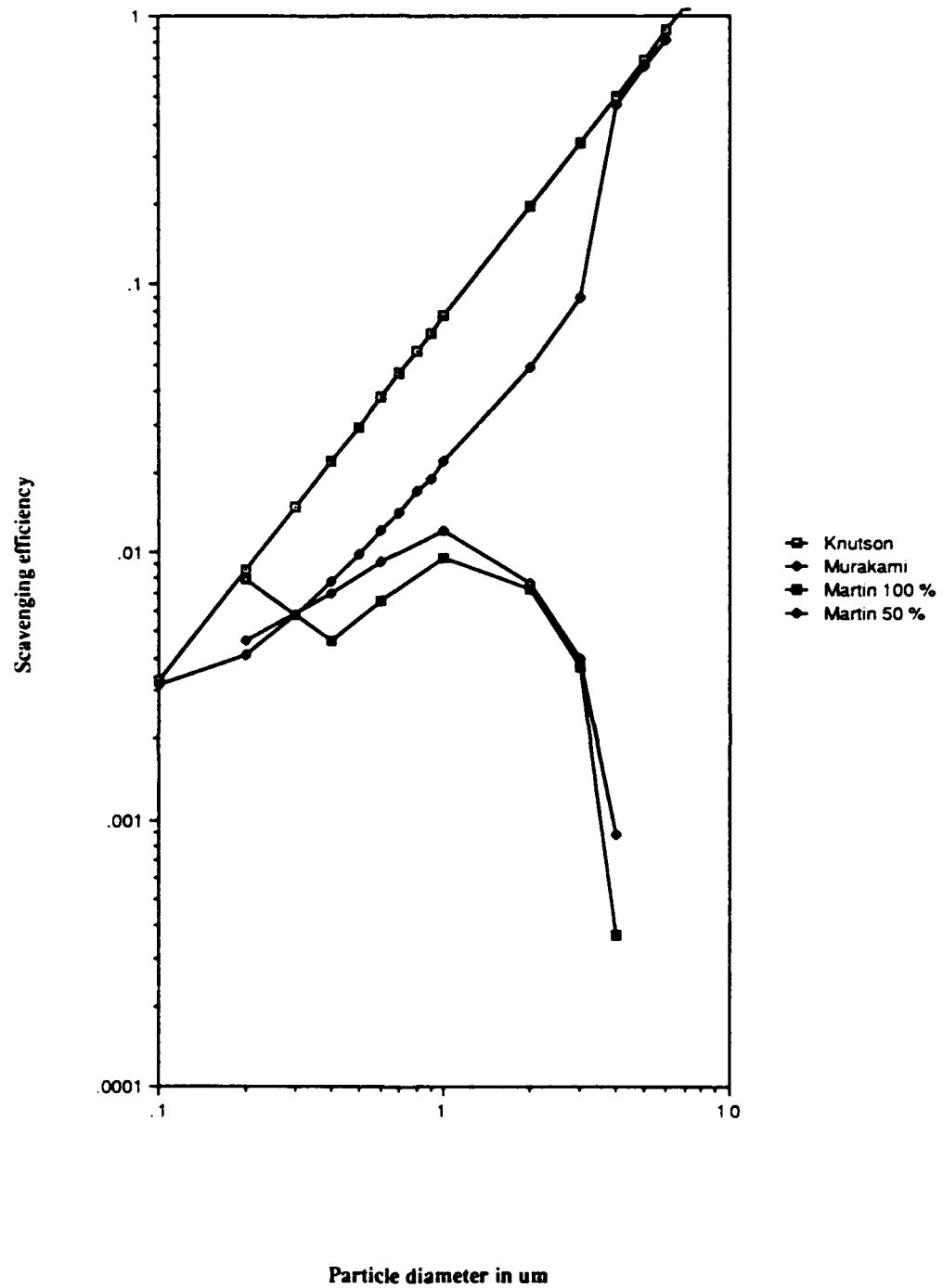


Figure 7.1

Data for 101.2 um dia crystal (600mb)

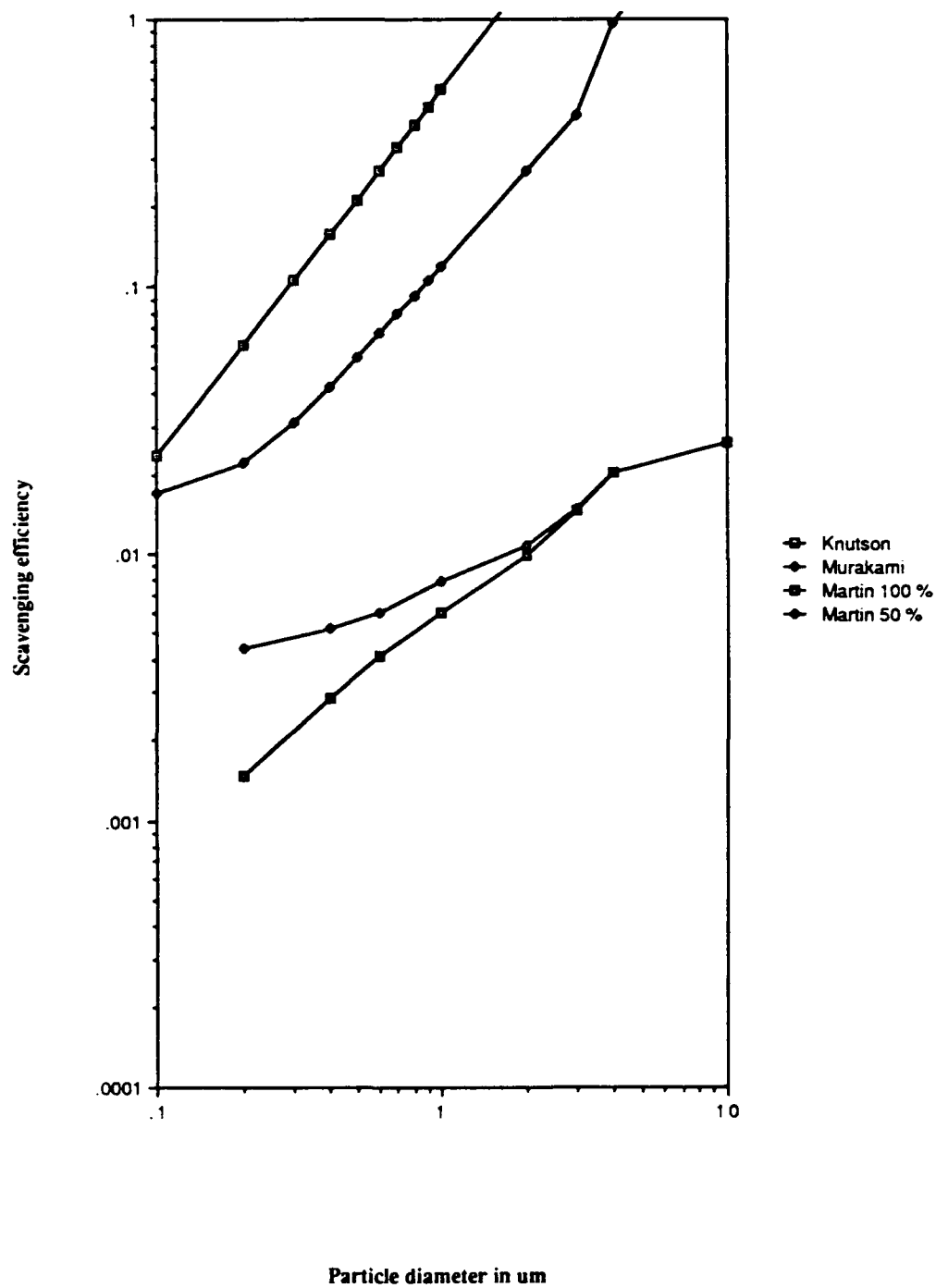


Figure 7.2

were then deduced using their method and the volume/diameter relation given by Davis (1974) for pla type plates with an ice density of  $920 \text{ kg m}^{-3}$ . This method gives thickness ratios of: 0.16, 0.118 and 0.07 for crystals of 101, 175 and 427  $\mu\text{m}$  diameter respectively. These differences result in higher Reynolds numbers and higher terminal velocities for the crystals than predicted by the thin crystal assumption. Crystals of these dimensions were observed as components of T and V shaped aggregates replicated on the sample slides, although a rigorous study has not been made.

#### 7.4 Present Experiment

Noting the disagreement between theory and extrapolated practical results, it was decided that the cirrus conditions of 300 - 500  $\mu\text{m}$  crystals falling through unsaturated air could be better investigated in a cold room environment.

The experiment shown in Figure 7.3 was set up inside a cold room maintained at  $-27^\circ\text{C}$ . The temperature and vapor supply were adjusted to provide conditions in the upper of the two chambers suitable for the growth of simple hexagonal plate crystals. The mean size of the droplets, 12  $\mu\text{m}$ , is set by the size of the water vapor inlet (Mossop, 1984).

When the temperatures had been stabilised and the upper cloud was established, a mono-disperse aerosol cloud was produced from a salt solution, by use of a Berglund-Liu generator and introduced into the lower chamber. The generator produces a mono-disperse stream of droplets by forcing a steady flow of solution through a small vibrating orifice. Assuming that the liquid (50% distilled water, 50% ethanol) evaporates completely,

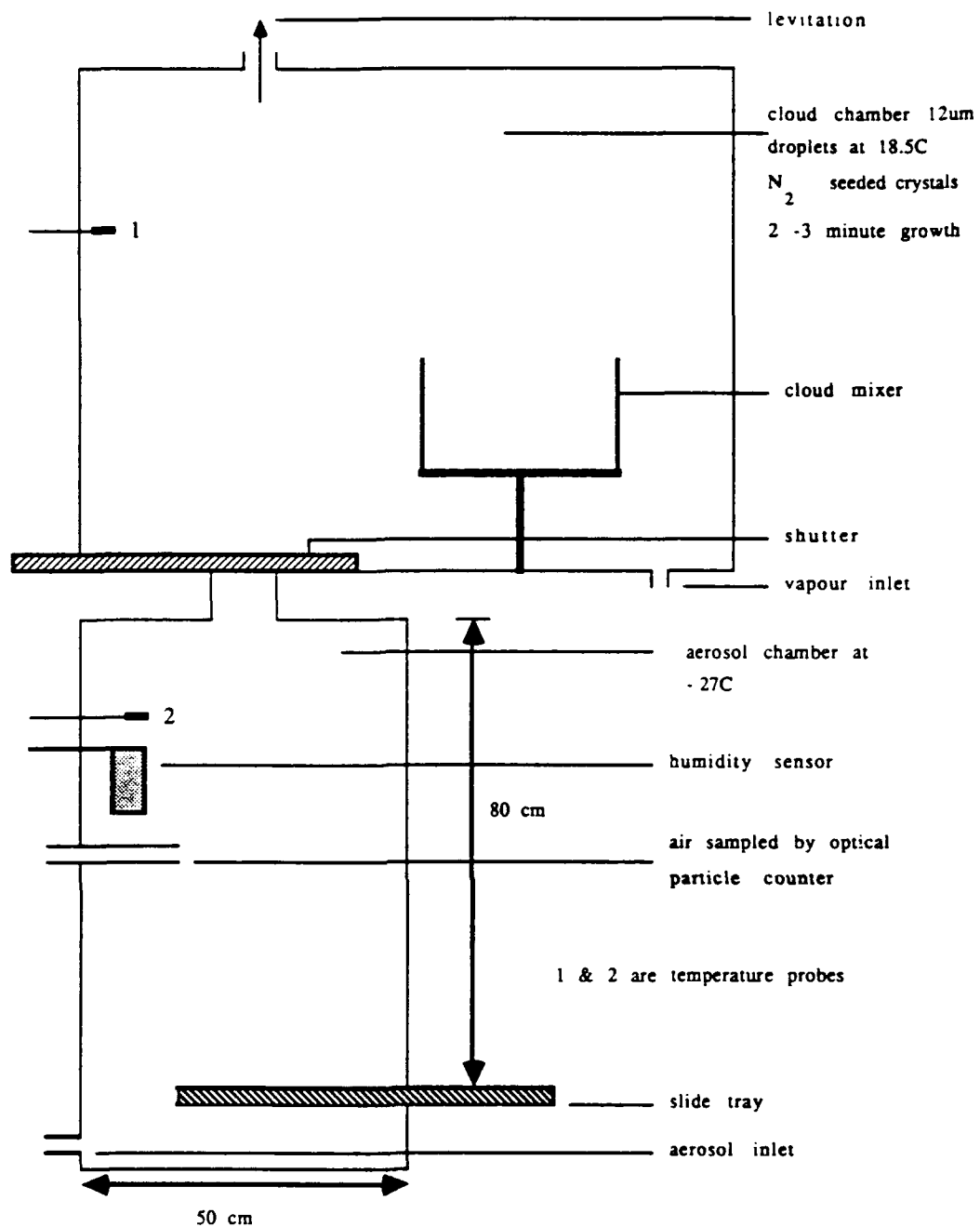


Diagram of Experiment

Figure 7.3



an aerosol produced from the dissolved salt will have a size determined by the flow rate through the orifice, the frequency of vibration of the orifice plate, and the concentration of the solute in the liquid mixture. (For example, if a 40  $\mu\text{m}$  droplet is produced, a concentration of 0.001 by volume of NaCl is needed to produce a 4  $\mu\text{m}$  crystal.) The size of the aerosol was verified by visual inspection under a microscope, while a series of electron micrographs verified their cubic or near cubic structure. Evaporation of the liquid was found to be complete, unless it was attempted to grow aerosols of 10  $\mu\text{m}$  or larger which required the evaporation of larger liquid drops. The ethanol is used to speed up the evaporation process and is needed to reduce the viscosity of the liquid in the narrow tubes of the aerosol generator. Typical concentration values attained for a 4  $\mu\text{m}$  salt aerosol were approximately  $10^7 \text{ m}^{-3}$ .

After the aerosol cloud had reached the desired level of concentration, the optical particle counter (Climet CI - 208) was removed, so as not to deplete the particle concentration in the lower chamber. At the same time, the particle generator was disconnected.

The upper cloud was seeded by the brief insertion of a rod from a flask of liquid nitrogen. As soon as the crystals could be seen (as points of light in a light beam), the cloud was stirred for a few seconds to provide an even distribution throughout the chamber. The crystals were then levitated whilst growing, by drawing air slowing from the top of the chamber. The assumption was made that no particle deposition occurred while the ice crystals were growing. When the droplet cloud cleared, due to the crystal growth, the levitation was stopped,

the shutter opened and the crystals allowed to fall through the lower cloud onto microscope slides. The slides were pre-coated with formvar which had dried. Once the ice crystals had landed, the formvar was reactivated with a fine mist of chloroform from a perfume bottle. The slides were then placed inside a desiccator to avoid contamination while the chloroform evaporated. They were later brought up to room temperature slowly, when the cold room was switched off.

During each run, the temperature in the two chambers was monitored by thermocouples. The upper chamber was warmer than the lower, due to the introduction of water vapor into the upper chamber while the lower chamber was positioned directly in front of the cooling fan. The humidity of the lower chamber was noted by use of a carbon film sensor. The humidity at the time of the crystal drop was found to be about 75% with respect to water at -27°C during a normal run.

The resultant slides were scanned with a binocular microscope, the crystal replicas sized into 10  $\mu\text{m}$  bins and the number of replicas with a scavenged salt particle noted.

The experimental scavenging efficiency was defined with relation to the mean diameter of each bin.

$$E = (N_{cp}/N_c) * (1/(A_c * V_s))$$

where,  $N_{cp}$  = a number of aerosol particles captured

$N_c$  = number of crystals sampled

$A_c$  = aerosol concentration

$V_s$  = volume swept by disc of mean bin size through height of fall.

## 7.5 Results

The results for four separate runs are shown in Figure 7.4, together with the extrapolated Murakami et al (1985) results, along with the predictions of Martin et al (1980), for an aerosol of 4-5  $\mu\text{m}$  diameter. The results are shown on a linear scale to show the scatter of the experimental data. Each point shown represents approximately 1000 ice crystal replicas in that particular size range. Points corresponding to smaller numbers of replicas are subject to significant statistical variability and thus the data are being reserved until the sample set can be increased in size. The adoption of the linear scale hides the variation within Martin et al values; these show a decrease in scavenging efficiency of roughly an order of magnitude for each increase of 100  $\mu\text{m}$  in crystal diameter.

Figure 7.5 shows a linear fit by least squares to the experimental data. The first two points of Martin et al's results are included in the fit. In Figure 7.6, a logarithmic fit to the data including the first three of Martin's points shows good correlation.

Although the experiments were performed at atmospheric pressure, the results have been plotted directly with those of Martin et al, because it was found that the extrapolated results of Murakami et al were insensitive to a pressure change of 600 - 1000 mb for the size of aerosol of interest. This insensitivity is due to the fact that for the aerosol in the range 1 - 10  $\mu\text{m}$  the major scavenging mechanism is interception.

Comparison plot of 4-6  $\mu\text{m}$  data

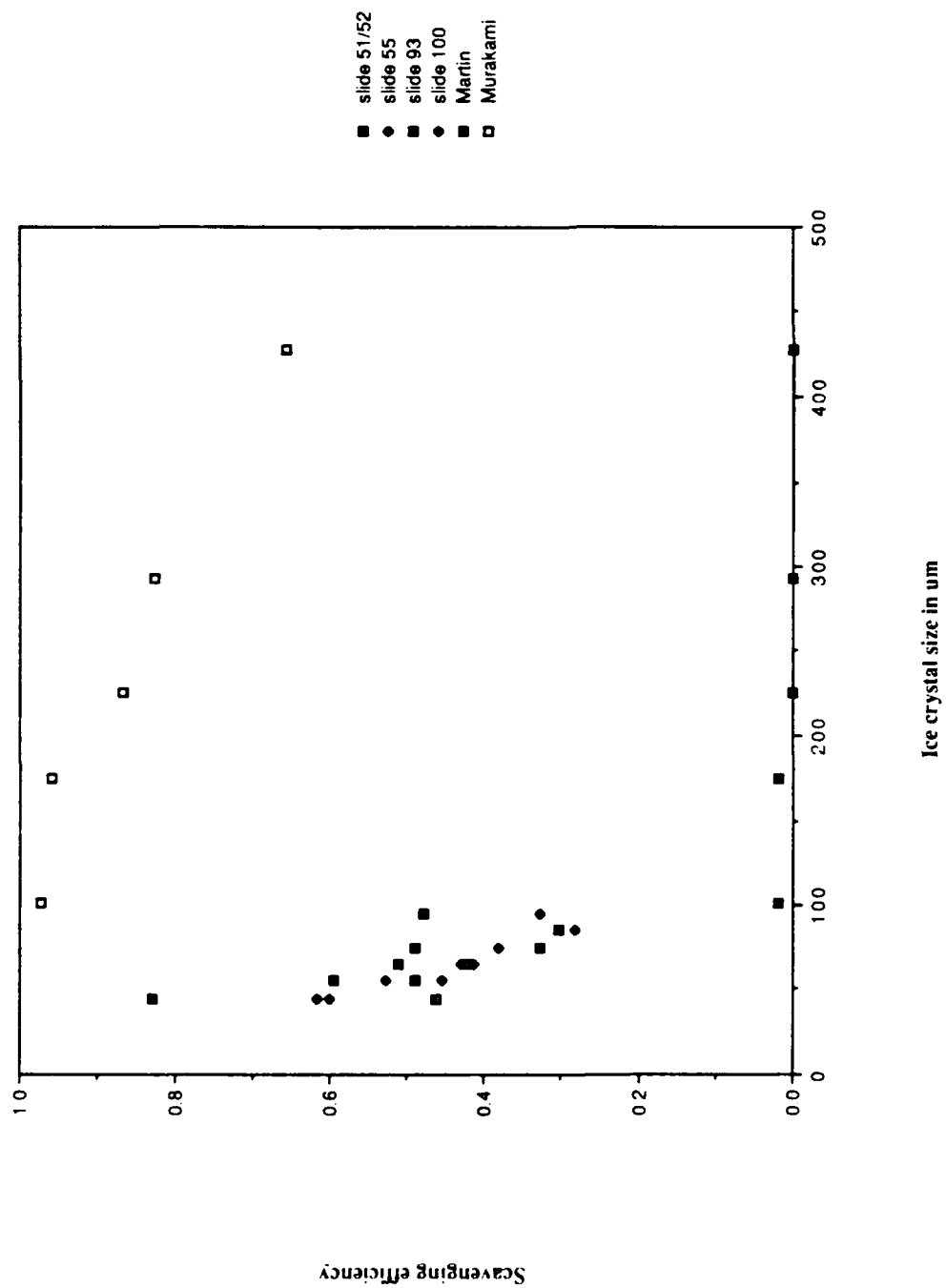


Figure 7.4

linear fit to 4-6 um data

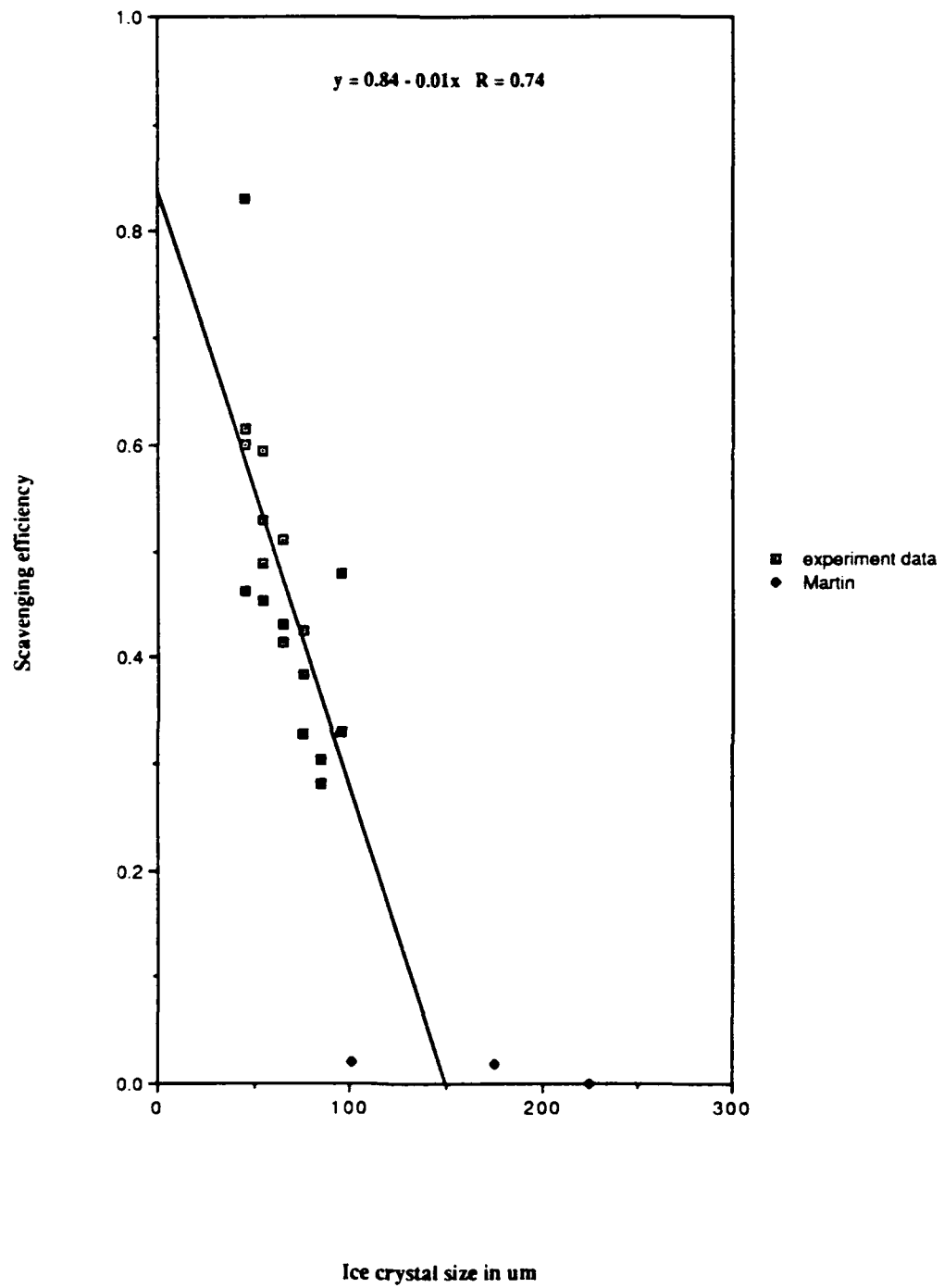


Figure 7.5

log fit to 4-6 um data

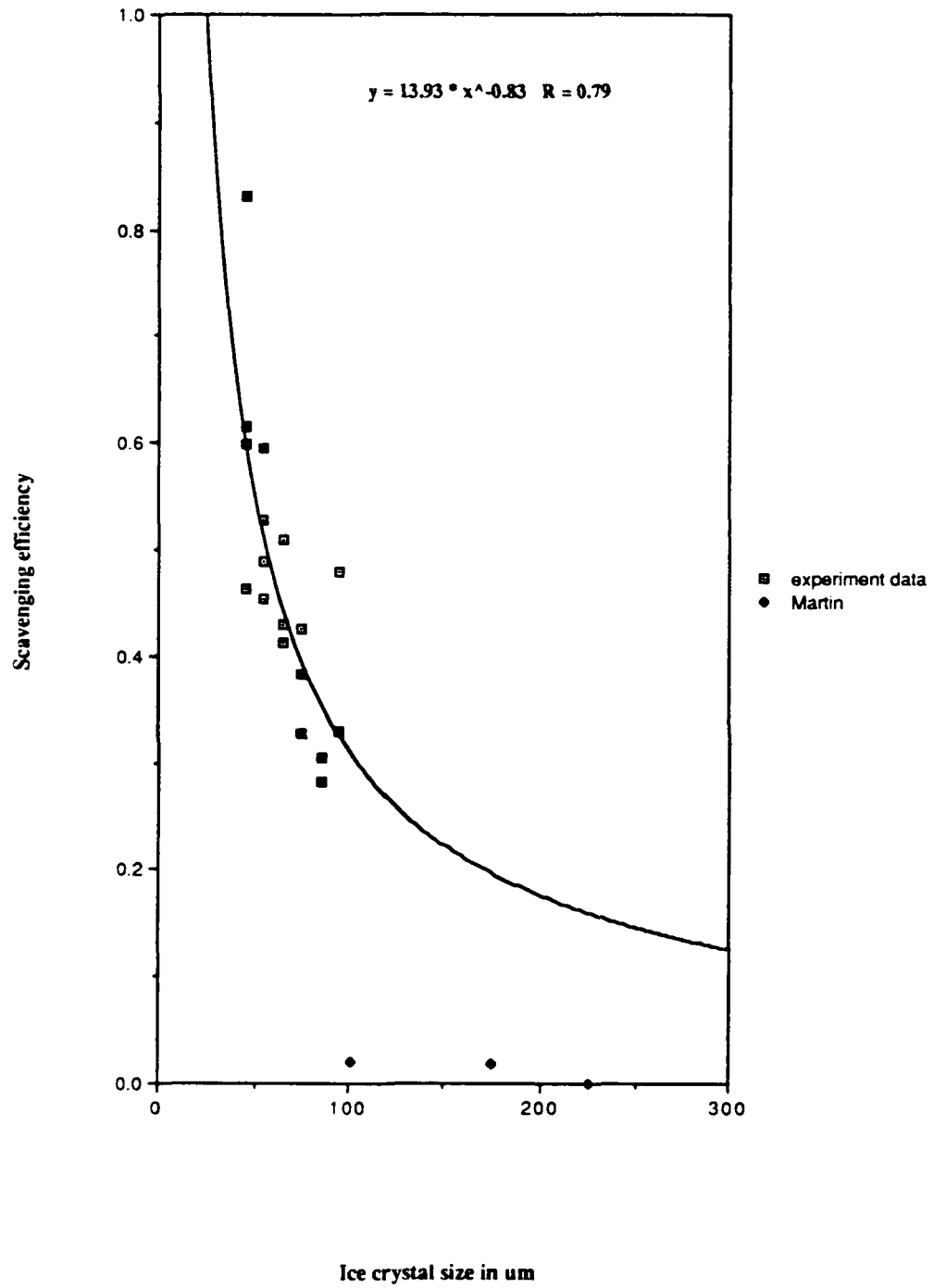


Figure 7.6

## 7.6 Experimental Limitations

The experimental results lie at the smaller end of the crystal size region examined by theory. However, they are directly applicable to the situation of evaporating ice crystals falling below cirrus clouds. The experimental observations need to be extended to larger crystal sizes, to check if the apparent fit to the theoretical predictions is real. The small plates examined to date were chosen because the growth of simple plate crystals greater than about 100  $\mu\text{m}$  is difficult in the cloud chamber used. Larger crystals can be grown but, to increase the rate of growth, more water vapour is used which tends to result in dendritic crystals. This type of crystal would be expected to exhibit a high scavenging efficiency, because of the increased edge/area ratio, (see "Experiments on aerosol scavenging by natural snow crystals." Lew et al 1986 a, b).

The microscope has a resolution limit of about 1  $\mu\text{m}$ , thus the lower decade of aerosol size of interest cannot be examined by this method.

## 7.7 Conclusions

From the current experiments, a scavenging efficiency for 4 - 5  $\mu\text{m}$  aerosol of between 82% and 24% has been found for ice crystals in the size range 40 - 100  $\mu\text{m}$  during a fall through air which was < 75% saturated with respect to water. There is a good correlation between crystal size and efficiency with fits to both a logarithmic and linear relationship. The use of large ice crystals in later experiments will show if the results so far observed fit the projection of the results of Martin et al.

## CHAPTER 8

### THUNDERSTORM CHARGING: CALCULATIONS OF THE EFFECT OF ICE CRYSTAL SIZE AND GRAUPEL VELOCITY

#### 8.1 Introduction

A one dimensional model of a developing thunderstorm has been adapted to in order to test the importance of various charge transfer parameters to the electrical development of the storm. The charge transfer data are taken from earlier laboratory measurements obtained when ice crystals rebound off soft-hail particles in the presence of supercooled water droplets. The experiments showed that the charge transfer depends on ice crystal size and impact velocity, so a range of size and velocity dependences have been tested in the model. The calculations have been performed using initial conditions from three storm cases having a range of storm severities. The processes by which thunderstorms become electrified are still under debate. Chapter 3 summarises the current ideas which include (i) the convection of charge, (2) the transfer of induced charges between particles colliding in the pre-existing electric field and (3) collisions between ice crystals and graupel pellets in the presence of cloud liquid water. This latter process has recently undergone extensive laboratory investigations by Jayaratne et al (1983) and Keith and Saunders (1989a), who showed that the amount of charge transferred depends on the ice crystal size and on the impact velocity. However, a number of models of electric field development in thunderstorms, such as those of Illingworth and



Latham (1977), Rawlins (1982) and Helsdon and Farley (1987), have included ice/ice interactions but have only used one value of charge transfer for all interactions. Keith and Saunders (1989a) found that for ice crystals up to a size,  $d$ , of 125  $\mu\text{m}$ , the charge transfer is proportional to  $d^{3.4}$  with a velocity dependence of  $v^{2.8}$ . For larger crystals the size dependence decreased. Other workers have found similar relationships; Marshall, Latham and Saunders (1978) found a  $d^2$  dependence over a wide range of sizes, while Gaskell and Illingworth (1980) using frozen ice spheres found  $d^{1.7}$  fitted their data with a linear velocity dependence. This paper makes a first attempt to determine the effect on the overall charging rate within thunderstorms of a range of reasonable values of the size and velocity dependencies.

The laboratory experiments give results of the form

$$q = Ad^av^b \quad (1)$$

where  $q$  is the charge transfer to the graupel pellet when ice crystals rebound from it;  $A$  is a constant which depends on the particular values of  $a$  and  $b$  used for the size and velocity dependencies. The coefficients are given in Table 8.1. The sign of the charge transfer also depends on temperature and cloud liquid water content. In this paper, only the negative charging of hailstones is considered; the laboratory experiments show that this occurs at temperatures below about  $-17^\circ\text{C}$  for typical values of cloud liquid water content. The negatively charged regions of thunderstorms are generally found at temperatures below about  $-17^\circ\text{C}$  (Krehbiel et al., 1979).

A one dimensional Lagrangian cloud model, (Andreev, 1976) has been adapted for the present purpose. Calculations have been

performed for values of  $a = 1, 2, 3, 4$  when  $b = 2.8$  and for  $b = 1, 2, 3$  when  $a = 2$ ; these cover the range of values determined in the laboratory experiments. Data from three storm days in the Thracian lowlands of Bulgaria have been used which produced three intensities of precipitation on the ground: 73/7/10 - light hail, 72/5/21 - hail that produced damage and 76/6/8 - rain.

## 8.2 MODEL DESCRIPTION

The convective cloud is modelled by an ascending spherical thermal above cloud base which entrains air at all levels from a cloudless environment. The entrainment is modelled by the parameter  $\alpha$  where  $\alpha = 0.6/R(Z)$  and  $R(Z) = R_0 + (0.2)Z$ ;  $R_0$  and  $R(Z)$  are the radii of the thermal at the condensation level (cloud base) and at height  $Z$  above cloud base respectively. The thermal is driven by the buoyancy force reduced by the entrainment and the weight of the hydrometeors present. The vertical temperature structure takes into account cooling as the thermal ascends, entrainment of environmental air and the heat released by the microphysical processes included in the models.

The microphysical processes are described using the bulk parameterisation scheme used by Andreev (1976). Four categories of hydrometeor are included; cloud and rain drops, ice crystals and graupel. The cloud drops and ice crystals are uniformly distributed and are limited to 200 $\mu$ m diameter and so have negligible fall velocities and move upwards with the air. The Marshall-Palmer distribution (1948) is used for the rain drops and a similar version for the graupel:

$$N(D_i) = N_0 e^{-\lambda D_i} \quad (2)$$

where  $N(D_i)$  is the number of graupel particles of diameter  $D_i$  per

unit volume of air per unit particle diameter.  $N_0$  is a constant taken as  $3 \times 10^{-4} \text{ cm}^{-4}$  as used by Orville and Kopp (1977), being an appropriate value for a graupel distribution.  $\lambda$  depends on the cloud ice content represented by the graupel and is given by

$$\lambda = (\pi d_H N_0 / S_{pf})^{0.25} \quad (3)$$

where  $d_H$  is the density of a hail particle ( $\text{g/m}^3$ ) and  $S_{pf}$  is the graupel ice content ( $\text{g/m}^3$ ).

In the model cloud, droplets form by condensation; all the water vapor in excess of the saturation mixing ratio with respect to water is immediately condensed out, as in Cotton (1972). Raindrops are formed by auto-conversion of the cloud droplets and they grow by collisions and coalescence with cloud drops (Kessler, 1969). Below  $0^\circ\text{C}$ , ice crystals originate by heterogeneous freezing at the expense of cloud droplets, their concentration being given by Fletcher (1962);

$$n = 10^{-2} e^{-0.6\Delta T} \text{ m}^{-3} \quad (4)$$

where  $\Delta T$  is the supercooling. An enhanced ice crystal concentration may be obtained by multiplying  $n$  by  $E_H$  where  $E_H$  is the ratio of observed ice crystals to ice nuclei as found by Hobbs (1969) and as used in Cotton's model (1972). ( $E_H = 21544 \times 10^{-T/6}$  where  $T$  is the supercooling in the range 4 to  $26^\circ\text{C}$ .)

Crystals grow by deposition and by collecting cloud droplets. Graupel particles are formed by drop freezing (Bigg, 1953) and by contact nucleation of droplets by ice crystals (Cotton, 1972), and they grow by coalescence with cloud and raindrops, (Wisner et al., 1972). The model takes account of the reduction of mass of the drops and crystals due to the entrainment of environmental air. All particles having a terminal velocity greater than the updraught velocity fall out, as in Cotton

(1972).

In the calculation of the charging rate per unit volume of cloud the following assumptions are made:

1. All the graupel are in the riming stage.
2. Ice crystals and graupel are uncharged before all impacts.
3. The size and fall velocity of the crystals are negligible compared with the graupel. The terminal velocity,  $V_D$  of graupel of diameter  $D$  is given by

$$V_D = (4g d_H D / 3C\rho)^{0.5} \quad (5)$$

where  $g$  is the acceleration due to gravity, the drag coefficient,  $C = 0.6$  and  $\rho$  is the density of air.

4. The charges on the ice crystals and graupel do not effect the cloud microphysics or dynamics.
5. The charge  $q$  gained by a soft hailstone per separating crystal event is  $3fC$  for  $d = 125\mu\text{m}$  and  $V = 3 \text{ m/s}$  from the data of Keith and Saunders (1989a). With these assumptions, the charging rate of a single hail pellet of diameter  $D$ , becomes:

$$dQ/dt = E_r (\pi D^2 / 4) V_D n q \quad (6)$$

where  $E_r$  is the fraction of crystals in the path of the hailstone that collide and then rebound resulting in charge transfer. From equations 1, 2, 3, 5 and 6, the charging rate per unit volume of cloud becomes:

$$\frac{dQ}{dt} = \frac{\pi}{4} A E_r N_0 n \left( \frac{4gd_H}{3C\rho} \right)^{\frac{b+1}{2}} d^a \int e^{-\lambda D} D^{\frac{b+5}{2}} dD \quad (7)$$

Equation 7 is integrated over all graupel diameters for  $a = 1, 2, 3, 4$  when  $b = 2.8$  and for  $b = 1, 2, 3$  when  $a = 2$ . The resulting equations have coefficients as given in Table 8.1 and are of the form:

Table 8.1

Eqn.	a	b	A	c	d	e	f	B
8	1	2.8	$1.1 \times 10^{-2}$	1.9	0.675	-0.225	1.225	6.9
9	2	2.8	$8.9 \times 10^{-9}$	1.9	0.675	-0.225	1.225	6.9
10	3	2.8	$7.1 \times 10^{-5}$	1.9	0.675	-0.225	1.225	6.9
11	4	2.8	0.57	1.9	0.675	-0.225	1.225	6.9
12	2	1	$6.4 \times 10^{-8}$	1	0	0	1	2
13	2	2	$2.1 \times 10^{-8}$	1.5	0.375	-0.125	1.125	3.9
14	2	3	$7.1 \times 10^{-9}$	2	0.75	-0.025	1.25	8.01

---


$$dQ/dt = BAE_r(g/C\rho)^c d_H^d N_0^e n S_{pf}^f d^a$$


---

The values of B given are from gamma functions for each case. The differential equation for the specific humidity in the cloud, the thermal velocity, the temperature in the cloud T, the liquid water content of the cloud and rain drops, the ice content of the crystals and graupel  $S_{pf}$ , are numerically integrated by the Runge-Kutta method. The values of  $S_{pf}$ , T, V, n and d calculated at each step are used to calculate dQ/dt. A is determined from Equation 1 based on assumption 5 and it takes different values depending on the values of a and b chosen.  $E_r$  is taken as 0.3 which is a value based on the laboratory work of Keith and Saunders (1989c) and is an average taken over the range of crystal sizes of relevance in this calculation. The calculations are carried out for the thermal ascending from cloud base to the height where the velocity is zero in time steps corresponding to height changes of 5m.

The model has been run using sounding data, Table 8.2, for

TABLE 8.2

10 July 1973			21 May 1972			8 June 1976		
Z(m)	T(°C)	RH%	Z(m)	T(°C)	RH%	Z(m)	T(°C)	RH%
1800	12.9	60	1900	10.8	68	2000	7.8	82
2850	5.7	74	3540	-4.3	49	4010	-6.7	74
3350	2.2	70	3830	-6.5	43	5450	-14.7	58
6000	-13.6	59	4365	-7.3	31	5990	-17.7	59
9000	-35.4	31	5760	-12.7	31	6890	-24.6	55
10720	-49.6	31	7400	-15.9	38	7370	-28.0	46
11220	-54.0	31	8650	-24.6	44	9450	-31.4	48
12060	-52.9	43	9390	-31.0	49	9890	-34.8	48
			10000	-36.6	52	10100	-34.8	47
			10600	-41.0	57	10450	-36.7	45
						11240	-40.5	42

the three cases under study. No atmospheric electrical measurements were made. A radar was in operation which provided estimates of the vertical extent of the storms through values of the maximum height of the radar reflectivity,  $H_{\max}$ . Ground based records of the damage cause by the precipitation are available. For 73/7/10 there was hail on the ground and  $H_{\max}$  was approximately 12 km. Hail causing damage was noted on 72/5/21 when  $H_{\max}$  was 11.6 km, and on 76/7/8 rain at the ground was observed with  $H_{\max}$  9.7 km.

The model makes use of values of  $R_0$  and the vertical velocity at cloud base  $W_0$  which were chosen so that the height of the convective level in the model agreed with the observed values of  $H_{\max}$ , which was effectively the height of the cloud top to

within an error of 550 m. For each of the three cases,  $R_0 = 5$  km and  $W_0 = 5$  m/s were found to be appropriate. The cloud condensation level and the temperature difference between the cloud and its surroundings were determined from the sounding.

The ability of the model used to predict the microphysical and dynamical characteristics of cumulus clouds has been tested and verified. In the three cases studied: (1) hail, (2) damaging hail, and (3) rain, the maximum updraught velocity of 20, 37 and  $16.5 \text{ m s}^{-1}$  respectively, are similar to those found in typical cumuli. The formation of large hail requiring a strong updraught over a large vertical extent of cloud is modelled appropriately with updraught velocities exceeding  $15 \text{ m s}^{-1}$  over vertical depths of (1) 7110 m, (2) 8935 m, and (3) 1625 m for the three cloud cases. The maximum contents are modelled:- (1)  $0.14 \text{ g m}^{-3}$  at  $-21^\circ\text{C}$ , (2)  $3.1 \text{ g m}^{-3}$  at  $-28^\circ\text{C}$  and (3)  $0.1 \text{ g m}^{-3}$  at  $-14^\circ\text{C}$ , which agrees with the concept that for hail to reach the ground, a longer growth time with a greater height above freezing level is required. Similarly, predicted ice crystal contents are realistic and in line with the predictions of other models.

It is known that the simulation of precipitation by one dimensional Lagrangian models must be considered critically. Mitzeva (1988) analysed the ability of the model to agree with observed precipitation intensities. Using stepwise discriminant analysis of thermodynamic and microphysical parameters for 268 storms over the Thracian lowlands, the model discriminated correctly between rain at the ground and hail in over 90% of the cases. From 163 hail cases, 88% were correctly classified as hail or damaging hail cases. The cases chosen for analysis in this paper were classified correctly.

### 8.3 RESULTS

Figure 8.1 presents the charging rate in the cloud as a function of altitude and temperature for the three cases. It shows an increase with an increase in the value of "b" and with storm severity. Figure 8.2 shows that as "a" increases, the charging rate apparently decreases; however, it must be remembered here that the value of A is different for each case. Again, higher charging rates occur with the more severe storms. In all cases, the charging rate is low at temperatures above  $-17^{\circ}\text{C}$  because of the low ice crystal concentration developed by the model. The effect of higher crystal concentrations can be seen in Figure 8.3, where the crystal generation equation (4) has been enhanced by the factor  $E_H$ . The calculations have been performed for  $a = 2$  and  $b = 2.8$  for these case studies. The effect in each case is to extend the charging regime to higher temperatures. It should be noted that above about  $-17^{\circ}\text{C}$  the experiments show that the charge transfer reverses sign. However, sign reversal is not shown and is not yet included in the model.

### 8.4 DISCUSSION

Clearly, the initial data from the soundings reflects the subsequent intensity of the thunderstorm electrification processes. The highest charging rates occur in the most vigorous storms, particularly when there is sufficient hail produced to cause damage. The values of charging rates calculated are dependent on the values of the parameters "a" and "b". The value of "a" is found from the laboratory experiments to be dependent on



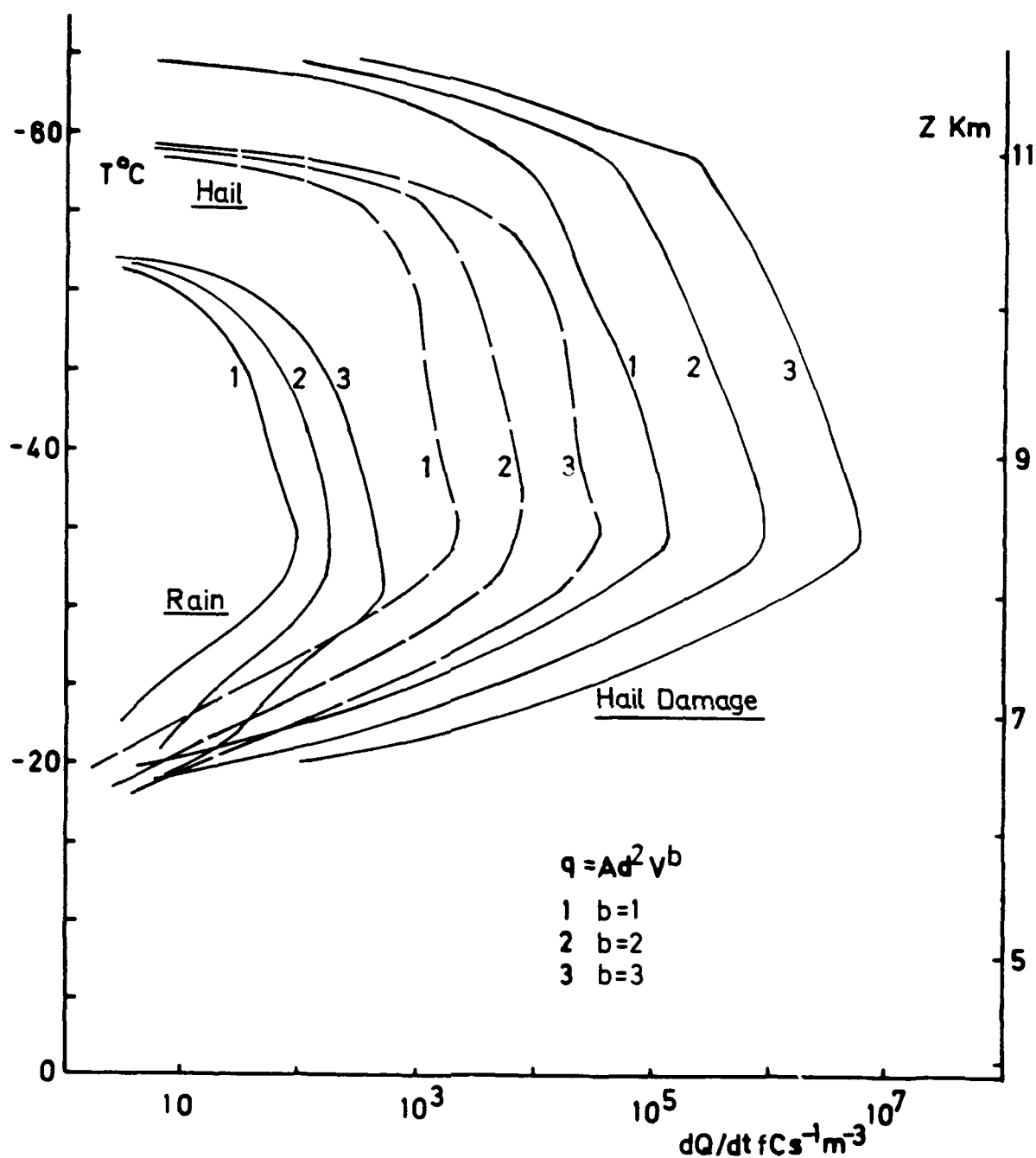


Figure 8.1 Charging rate for hail, hail damage and rain cases ( $a=2$ ,  $b=1,2,3$ )

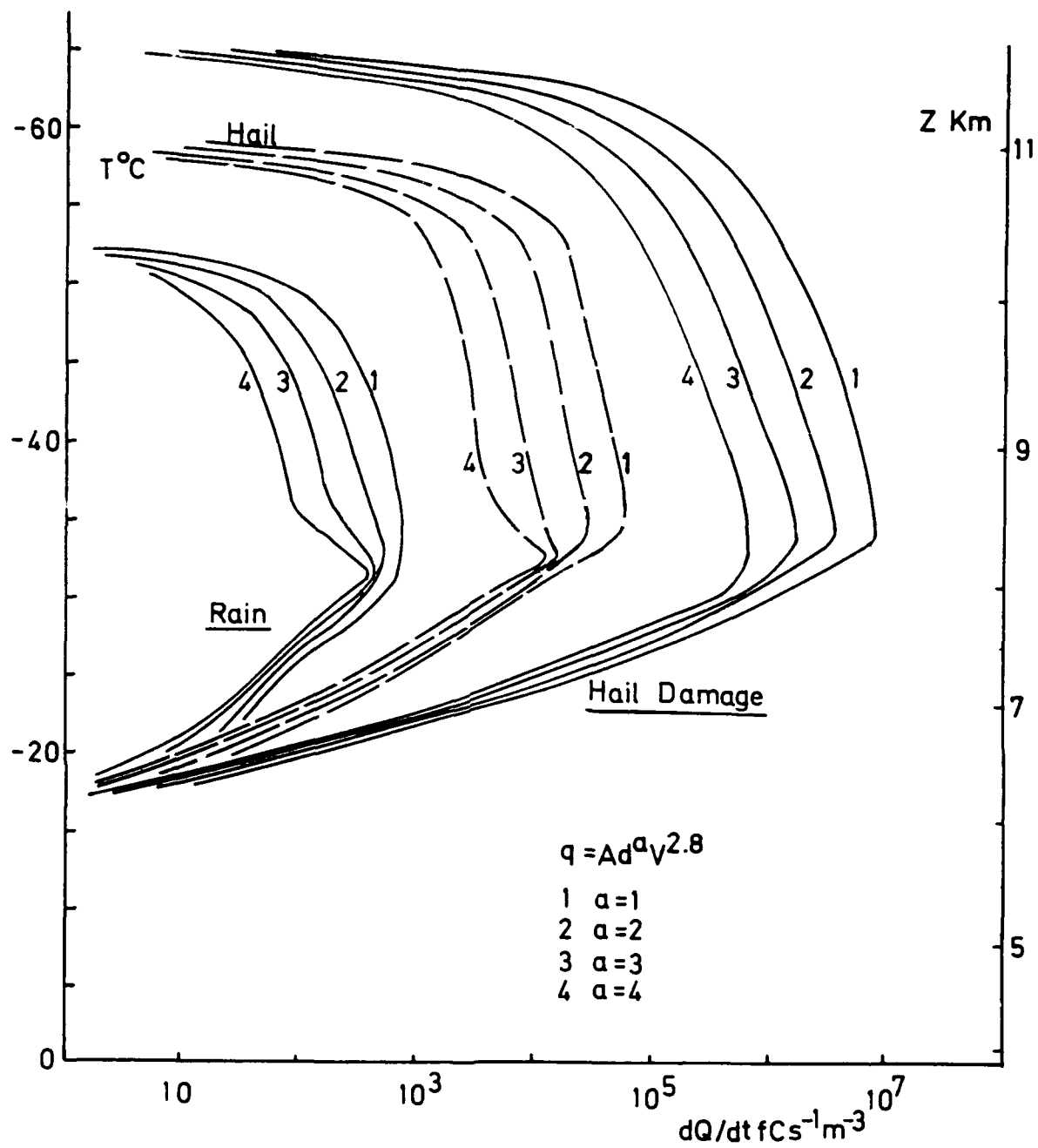


Figure 8.2 Charging rate for hail, hail damage and rain cases ( $b=2.8$ ,  $a=1,2,3,4$ )

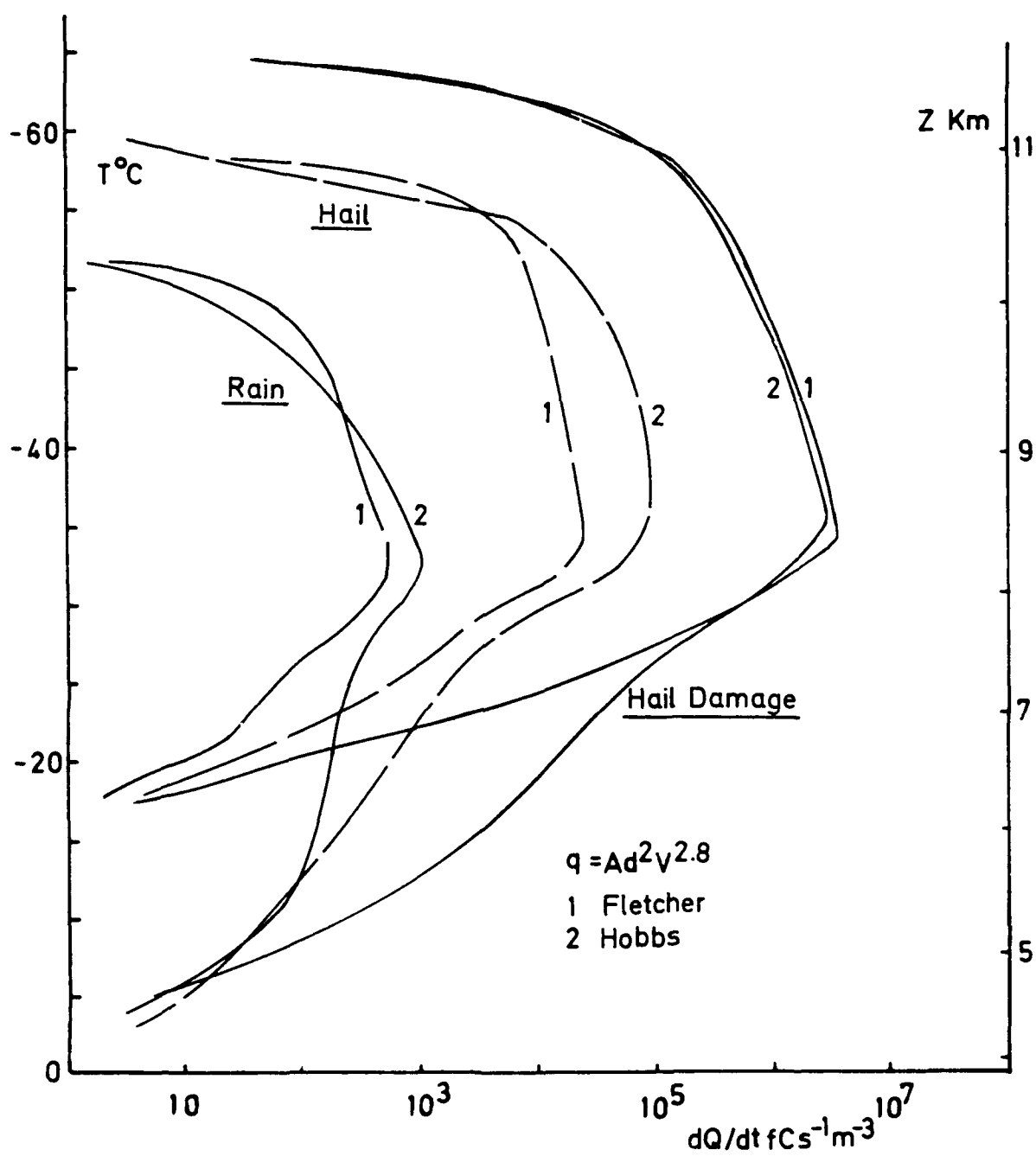


Figure 8.3 Charging rate for hail, hail damage and rain cases ( $a=2$ ,  $b=2.8$ ) with enhanced ice crystal concentrations

crystal size, and so, strictly, different values of "a" and hence "A" should be used as the crystals in the model grow. The inclusion of this feature awaits a more sophisticated model. The dependence of charge transfer on velocity is fairly independent of crystal size and hence the results shown here of the strong effect of the value of "b" on the charging rate are valid. However, the greatest effect on the charging rates is produced by the pre-existing environmental conditions. The maximum charging rates vary by about three orders of magnitude between the hail damage case and the rain only case, whereas the range of velocity parameter "b" values chosen, produces maximum charging rates varying over one order of magnitude. It is reassuring that nature is not so dependent on particular values of parameters concerned with crystal size and velocity, as a range of values has been obtained from laboratory measurements.

Cloud development in the model has been continued to regions below  $-40^{\circ}\text{C}$  where all the liquid water in the cloud has been frozen. However, the laboratory measurements of charge transfer have been performed at higher temperatures, and so data applicable to these regions are not available. It is reasonable to use the laboratory data at temperatures as low as  $-35^{\circ}\text{C}$  where the model predicts the maximum charging rate to occur. Further work is required to determine values of charge transfer over the whole range of conditions of atmospheric interest. The model considers ice crystals to be uniformly distributed and to be spheres of less than  $200\text{ }\mu\text{m}$  diameter. Laboratory work has now been extended to larger crystals and these results can be included in a future version of the model.

The maximum charging rates occur at the  $-30$  to  $-35^{\circ}\text{C}$  temper-

ature levels in the model. In thunderstorms, the negative hail falls against the updraft to form the negative charge region which is commonly observed between the  $-15$  and  $-30^{\circ}\text{C}$  levels. The positively charged ice crystals are carried in the updraught to the top of the cloud and produce the upper positive charge. Thus the classic Wilson dipole is produced. The requirements of any thunderstorm charge transfer mechanism are that it should be able to generate charge at a minimum rate of between  $10^4$  and  $10^5$   $\text{fC/s m}^3$  in order to account for the observed rates of electrical development. It is commonly noted that the most vigorous and most electrified storms produce hail, and so it is significant that the model predicts realistic charging rates in these cases. The conclusion is that thunderstorm charging may be due to interactions between particles of the ice phase, but that precise dependence of the charging rate on crystal size and impact velocity, while important, is not a critical requirement of an adequate charging mechanism.

## CHAPTER 9

### DISCUSSION AND SUGGESTIONS FOR FUTURE WORK.

The work reported in Chapter 2 extends our knowledge of thunderstorm charging rates through the laboratory measurements of charge transfer during ice crystal collisions with graupel pellets. A wide variety of realistic cloud conditions have been investigated and the sign and magnitude of the charge transfer is found to be a sensitive function of the cloud parameters. The results have been formulated so that they can be included in numerical models of the electric field development in thunderstorms. A first attempt at this is described in Chapter 8 in which a one-dimensional model is used. For a more accurate assessment, three dimensional models are more appropriate.

In Chapter 3, a discussion is presented of the charge transfer mechanism when ice crystals bounce off ice targets. The results are in qualitative agreement with the concept of two competing mechanisms, one causing positive charging and the other, negative. Which mechanism dominates depends on the cloud conditions. In general, at low temperatures, graupel pellets charge negatively due to either a contact potential difference with the interacting ice crystals or a surface charge difference due to charges on dislocations in the ice. At higher temperatures, positive charging may be due to negative surface charges on the graupel pellet because its surface is warmer than the interior while it grows by vapor diffusion. Neither of these mechanisms is completely formulated, and more work is needed to show whether there is in fact a contact potential difference between ice crystals and the graupel surface. Also, the heat

balance of a growing surface needs careful analysis - can an adequate temperature gradient be maintained across the surface layers to account for the observed charging? An outstanding problem is the need to fit into the charging mechanism scheme the results of the effect of doping the rime ice with realistic concentrations of salts. The initial measurements were made back in 1983 in UMIST, but because of the complexity of the results obtained, they have effectively been ignored. More laboratory work is needed into the effects on the surface of riming particles of impurities in the super-cooled droplet cloud. Also needing study is the question of whether the nature of the ice crystal itself is important. Two recent communications to me have indicated that there is a disagreement on this question which needs resolving.

Although the early electrification of thunderclouds cannot be accounted for by the induction mechanism, there is still the possibility that the mechanism may be active later in the storm lifetime. Experiments are in hand at present to determine whether there is any possibility that water droplets may bounce off the underside of graupel pellets and thus remove induced charge which, upon gravitational separation of the particles, will lead to the growth of the electric field. The possibility that ice crystals may also separate induced charge in the same way was discounted following experiments. However, these experiments were performed with a dry, evaporating ice surface; graupel pellets are in fact growing and so will have a mobile molecular layer on their surface which could have sufficient electrical conductivity to give some inductive charging. Further experiments are needed in this area.

Aircraft measurements of the electric field and charges carried on precipitation particles in thunderstorms have provided information about the rate of development of cloud electrification and the location of the charges in the context of the precipitation types. However, the sample volume of any charge probe on an aircraft is very small, of order 100 liters per second, and with a detectable charged particle concentration of order one per liter, the sample statistics are poor. More information is therefore needed on the charges on particles, their locations and their sizes.

The work described in Chapter 4 confirmed that the experimental techniques used in the UMIST work are valid - moving rod targets can adequately simulate riming graupel pellets. Of note is the discovery that the pre-existing charge on the graupel can affect subsequent charge transfer. While a falling graupel pellet is young it will charge at a high rate, however when its charge reaches 10 pC, the charging rate is around 80% of the uncharged rate. These results have yet to be included in models of the rate of electrical development of thunderclouds.

Other work described here is a theoretical study of the collision efficiency of graupel pellets for ice crystals. The theoretical predictions tie in fairly well with our earlier laboratory studies and may be used in numerical models of cloud electrification. Also studied was the value of the heat transfer coefficient of a riming graupel pellet. The surface roughness of rime is dependent on temperature and on impact velocity. The rougher the rime the greater is its ability to dissipate the latent heat released by the freezing droplets. The consequence is that in conditions of high water accretion when wet growth may



be expected, it should be possible for the rime to continue to experience dry growth. A more detailed study is needed, together with a theoretical treatment, in order to know better the precise conditions on the surface of a riming graupel pellet. Chapter 7 deals with an important problem in the atmosphere, namely the removal of particulates. The cold room cloud facility was used to grow ice crystals which were then allowed to fall through 4 - 5  $\mu\text{m}$  aerosol particles and to scavenge them. The small crystals used here simulated the evaporating conditions beneath a cirrus layer. More work is need to extend the studies to larger ice crystals.

Applications to the USAF for further funding in these areas are in hand. The PI is involved in electrical studies of cumulus clouds over the Cape in the Summer of 1991 when the field work and predictions from the laboratory experiments come together. Also, more laboratory work is envisaged along the lines outlined above. There is a possibility of liaison with Dr Boulay of ONERA, Paris, who has developed a novel technique for determining the nature and position of charge layers in insulators. If his techniques can be used with ice, then our questions concerning surface layers of charge may be resolved.

## REFERENCES

- Andreev B., Microphysical effects of a dynamical model of an active isolated element of convection, *Bulg. Geophys. J.*, 2, 17-27, 1976.
- Avila, E. E., J. M. Caranti and M. Lamfri, Charge reversal in individual ice-ice collisions, *Proc. Int. Conf. Atmos. Elec.*, Uppsala, 245-250, 1988.
- Baker, B., M. B. Baker, E. R. Jayaratne, J. Latham and C. P. R. Saunders, The influence of diffusional growth rate on the charge transfer accompanying rebounding collisions between ice crystals and hailstones, *Q. J. R. Meteorol. Soc.*, 114, 1193-1215.
- Baker, M. B. and J. G. Dash, Charge transfer in thunderstorms and the surface melting of ice, *J. Crystal Growth.*, 97, 770-776, 1989.
- Bigg E. K., The Supercooling of Water, *Proc. Phys. Soc.*, London, B66, 688-794, 1953.
- Breach, D. R., Slow flow past ellipsoids of revolution, *J. Fluid Mech.*, 10, 306-314, 1961.
- Browning K. A., F. H. Ludlam and W. C. Macklin, The density and structure of hailstones, *Quart. J. Roy. Met. Soc.*, 89, 75-84, 1963.
- Bryant, G. W. and B. J. Mason, Etch pits and dislocations in ice crystals, *Phil. Mag.*, 5, 1221-1227, 1960.
- Buser, O. and A. N. Aufdermaur, Electrification by collision of ice particles on ice or metal targets. Electrical processes in atmospheres, Steinkopf, Darmstadt, 1977.
- Caranti, J. M. and A. J. Illingworth, Surface potentials of ice and thunderstorm charge separation, *Nature*, 283, 44-46, 1980.
- Caranti, J. M., A study of the electrical properties of ice, PhD thesis, Manchester, 1982.
- Caranti, J. M., A. J. Illingworth and S. J. Marsh, The charging of ice by differences in contact potential, *J. Geophys. Res.*, 90, 6041-6046, 1985.
- Christian, H., C. R. Holmes, J. W. Bullock, W. Gaskell, A. J. Illingworth and J. Latham, Airborne and ground-based studies of thunderstorms in the vicinity of Langmuir Laboratory, *Q. J. R. Meteorol. Soc.*, 106, 159-174, 1980.
- Church, C. R., The electrification of hail. PhD thesis, Univ. Durham, 1966.
- Comings E. W., J. T. Clapp and J. F. Taylor, Air turbulence and transfer process, *Ing. End. Chem*, 40, 1076-1082, 1948.

Cotton W. R., Numerical simulation of precipitation development in supercooled cumuli, Part 2, Monthly Weather Rev., 100, 764-784, 1972.

Cross, J. D. and P. A. Speare., Electrical aspects of the evaporation of ice, Brit. J. Appl. Phys., 2, 1021-1025, 1969.

Cross, J. D., The effect of impurities on the surface structure of evaporating ice, J. Glac., 10, 287-292, 1971.

Davies C. N. and M. Aylward, The trajectories of heavy solid particles in a two dimensional jet of ideal fluid impinging normally upon a plate, Proc. Roy. Soc., B64, 889-911, 1951.

Davies C. N. and C. V. Peetz, Impingement of particles on a transverse cylinder, Proc. Roy. Soc., A234, 269-295, 1956.

Davis, C. I., The ice nucleating characteristics of various AgI aerosols. PhD Thesis, Dept Mech Eng, University of Wyoming, USA, 1974 (or see Pruppacher and Klett, 1980, page 40).

Dye, J. E., Jones, J. J., Winn, W. P., Cerni, T.A., Gardiner, B., Lamb, D., Pitter, R. L., Hallett, J. and C. P. R. Saunders., Early electrification and precipitation development in a small isolated Montana thunderstorm, J. Geophys. Res., 91, 1231-1247, 1986.

Dye, J. E., J. J. Jones, A. J. Weinheimer and W. P. Winn, Observations within two regions of charge during initial thunderstorm electrification, Q. J. R. Meteorol. Soc., 114, 1271-1290, 1988.

Elster, J. and H. Geitel, Zur influenzetheorie der Niederschlagselektrizitat, Phys. Z. 14, 1287-1292, 1913.

Findeisen, W., Uber die Entstehung der Gewittelektrizitat, Meteor. Zeit, 57, 201, 1940.

Fletcher N. H., The physics of rainclouds, CUP, p386, 1962.

Fletcher, N. H., Surface structure of water and ice. II. A revised model, Phil. Mag., 18, 1287-1300, 1973.

Fukuda, A. and A. Higashi, X-ray diffraction topographical studies of dislocations in natural large ice single crystals, Jpn. J. Appl. Phys., 8, 993-999, 1986.

Furukawa, Y., M. Yamamoto and T Kuroda, Ellipsometric study of the transition layer on the surface of an ice crystal, J. Crystal Growth, 82, 665-677, 1987.

Gardiner, B., D. Lamb, R. L. Pitter, J. Hallett and C P R Saunders, Measurement of initial potential gradient and particle charges in a Montana summer storm, J. Geophys. Res., 90, (D4), 6079-6086, 1985.

Gaskell, W., A. J. Illingworth, J. Latham and C. B. Moore, Airborne studies of electric fields and the charge and size of precipitation elements in thunderstorms, Q. J. R. Meteorol. Soc., 14, 447-460, 1978.

Gaskell, W. and A. J. Illingworth, Charge transfer accompanying individual collisions between ice particles and its role in thunderstorm electrification, Q. J. R. Meteorol. Soc., 106, 841-854, 1980.

Gaskell, W., A laboratory study of the inductive theory of thunderstorm electrification, Q. J. R. Meteorol. Soc., 107, 955-966, 1981.

Geidt A., Effect of turbulence level of incident air on local heat transfer and skin friction on a cylinder, J. Aero. Sci., 18, 725-730, 1951.

Greenfield, S. M., Rain scavenging of radioactive particulate matter from the atmosphere, J Met., 14, 115-125, 1957.

Hall W. D. and H. R. Pruppacher, The survival of ice particles falling from cirrus clouds in subsaturated air, J. Atmos. Sci., 33, 1995-2006, 1976.

Hallett, J. and C. P. R. Saunders, Charge separation associated with secondary ice crystal production, J. Atmos. Sci., 36, 2230-2235, 1979.

Helsdon J. H. and R. D. Farley, A numerical modeling study of a Montana thunderstorm: 1 Model results versus observations involving non-electrical aspects, J. Geophys. Res. 92, 5645-5659, 1987a.

-----A numerical modelling study of a Montana thunderstorm: 2 Model results versus observations involving electrical aspects, J. Geophys. Res. 92, 5661-5675.

Heymsfield A., Cirrus uncinus generating cells and the evolution of cirriform clouds, 1. Aircraft observations of the growth of the ice phase, J. Atmos. Sci., 32, 799-808, 1975a.

Heymsfield A., Cirrus uncinus generating cells and the evolution of cirriform clouds. 2. The structure and circulations of the cirrus uncinus head, J. Atmos. Sci., 32, 809-819, 1975b.

Heymsfield A., Cirrus uncinus generating cells and the evolution of cirraform clouds. 3. Numerical computations of the growth of the ice phase, J. Atmos. Sci., 32, 820-830, 1975c.

Heymsfield A. and M. Kajikawa, An improved approach to calculating terminal velocities of plate-like crystals and graupel, J. Atmos. Sci., 44, 1088-1099, 1987.

Higashi, A., M. Oguro and A. Fukuda, Growth of ice single crystals from the melt, with special reference to dislocation structure, J. Cryst. Growth, 3, 728-732, 1968.

- Hobbs P. V., Ice multiplication in clouds, J. Atmos. Sci., 26, 315-318, 1969.
- Illingworth, A. J. and J. M. Caranti, Ice conductivity restraints on the inductive theory of thunderstorm electrification, J. Geophys. Res., 90, 6033-6039, 1985.
- Illingworth A. J. and Latham J., Calculations of electric field growth structure and charge distributions in thunderstorms, Quart. J. Roy. Met. Soc., 103, 281-295, 1977.
- Itagaki, K., X-ray topographic study of vibrating dislocations in ice under an AC electric field, Adv. X-Ray Anal., 13, 526-538, 1970.
- Itagaki, K., Charged dislocations in ice, Int. Conf. Physics and Chemistry of Ice, Ottawa, Ont., 73.1-73.4, 1972.
- Itagaki, K., Possibility of anomalous relaxation due to the charged dislocation process, J. Phys. Chem., 87, 4261-4264, 1986.
- Jayarathne, E. R. and C. P. R. Saunders, Thunderstorm electrification: the effect of cloud droplets, J. Geophys. Res., 90, 13063-13066, 1985.
- Jayarathne, E. R., C. P. R. Saunders and J. Hallett, Laboratory studies of the charging of soft hail during ice crystal interactions, Q. J. R. Meteorol. Soc., 109, 609-630, 1983.
- Jayaweera K. O. L. F. and B. J. Mason, The behaviour of freely falling cylinders and cones in a viscous fluid, J. Fluid Mech., 22, 709-720, 1966.
- Jayaweera K. O. L. F. and B. F. Ryan, Terminal velocities of ice crystals, Quart. J. Roy. Met. Soc., 98, 193-197, 1972.
- Keith, W. D., C. S. Mill and C. P. R. Saunders, A hot-wire instrument to measure liquid water content for use in the laboratory, J. Phys. E., 19, 436-438, 1986.
- Keith, W. D. and C. P. R. Saunders, Charge transfer during multiple large ice crystal interactions with a riming target, J. Geophys. Res., 94, 13103-13106, 1989a.
- Keith, W. D. and C. P. R. Saunders, The effect of centrifugal acceleration on the charging of a riming hailstone, Meteorol. Phys., 41, 55-61, 1989b.
- Keith, W. D. and C. P. R. Saunders, The collection efficiency of a cylindrical target for ice crystals, Atmos. Res., 23, 83-95, 1989c.
- Keith, W. D. and C. P. R. Saunders, Further laboratory studies of the charging of graupel during ice crystal interactions, Atmos. Res., 25, 445-464, 1990.
- Kestin J. and P. F. Maeder, The influence of turbulence on heat transfer from cylinders, NACA TN-4018, 1957.

- Knudsen J. G. and D. L. Katz, Fluid Dynamics and Heat Transfer, McGraw-Hill Book Co., 1958.
- Knutson E. O., S. K. Sood and J. D. Stockholm, Aerosol collection by snow and ice crystals, Atmos. Environ, 10, 395-402, 1976.
- Krehbiel, P. R., M. Brook and R. A. McCrory, An analysis of the charge structure of lightning discharges to ground, J. Geophys. Res., 84, 2432-2456, 1979.
- Krehbiel, P. R., The electrical structure of thunderstorms. In The Earth's Electrical Environment, Nat. Ac. Press., Washington DC, 90-113, 1986.
- Landahl H. D. and R. G. Hermann, Sampling of liquid aerosol by wires, cylinders and slides and the efficiency of impaction of the droplets, J. Coll. Sci., 4, 103-136, 1949.
- Langmuir I. and K. B. Blodgett, A Mathematical investigation of water droplet trajectories, U. S. Army Tech. Rep. No. 5418, 1946.
- Latham, J. and B. J. Mason, Electrical charging of hail pellets in a polarizing electric field, Proc. Roy. Soc. Lond., A 266, 387-401, 1962.
- Latham, J. and B. J. Mason, Generation of electric charge associated with the formation of soft hail in thunderclouds, Proc. Roy. Soc. Lond., A 260, 537-549, 1961.
- Latham, J., The electrification of frost deposits, Q. J. R. Meteorol. Soc., 89, 265-270, 1963.
- Levin, Z., A refined charge distribution in a stochastic electrical model of an infinite cloud., J. Atmos. Sci., 33, 1756-1762, 1976.
- Lew K. J., D. C. Montague, H. R. Pruppacher, and R. M. Rasmussen, A wind tunnel investigation on the riming of snowflakes; 1, Porous discs and large stellars, J. Atmos. Sci., 43, 2392-2409, 1986a.
- A wind tunnel investigation on the riming of snowflakes; 2. Natural and synthetic aggregates, J. Atmos. Sci., 43, 2410-2417, 1986b.
- List R., The accretion of ice on rotating cylinders, Quart. J. Roy. Met. Soc., 89, 552-555, 1963a.
- List R., General heat and mass exchange of spherical hailstones, J. Atmos. Sci., 20, 189-197, 1963b.
- Locatelli, J. D. and P. V. Hobbs, Fall speeds and masses of solid precipitation particles, J. Geophys. Res., 79, 2185-97, 1974.
- Löffler F and W. Muhr, Die Abscheidung von Feststoffteilchen und Tropfen an Kreiszyllindern infolge von Tragheitskreften, Chemie Ing-Techn., 44, 510-514, 1972.

- Ludlam F. H., The heat economy of a rimed cylinder, Quart. J. Roy. Met. Soc., 77, 663-666, 1951.
- Macklin W. C., Density and structure of ice formed by accretion, Quart. J. Roy. Met. Soc., 87, 30-50, 1962.
- Macklin W. C., Comments on "General heat and mass exchange of spherical hailstones", J. Atmos. Sci., 21, 189-197, 1964.
- Macklin, W. C. and Payne, G. S., A theoretical study of the ice accretion process, Q. J. R. Meteorol. Soc., 93, 195-213, 1967.
- Marshall J. S. and Palmer W. McK., The distribution of raindrops with size, J. of Met., 5, 165-166, 1948.
- Marshall, B. J. P., J. Latham and C. P. R. Saunders, A laboratory study of charge transfer accompanying the collision of ice crystals with a simulated hailstone, Quart. J. R. Met. Soc., 104, 163-178, 1978.
- Marshall, T. C., and W. P. Winn, Measurements of charged precipitation in a New Mexico thunderstorm: Lower charge centers, J. Geophys. Res., 87, 7141-7157, 1982.
- Martin J. J., P. K. Wang, H. R. Pruppacher and A. E. Hamielec, On the efficiency with which aerosol particles of radius  $> 0.1 \mu\text{m}$  are collected by simple ice crystal plates, Pure and Applied Phys., 188, 1109-1129, 1980a.
- Martin J. J., P. K. Wang and H. R. Pruppacher, A theoretical determination of the efficiency with which aerosol particles are collected by simple ice crystal plates, J. Atmos. Sci., 37, 1628-1638, 1980b.
- Mason, B. J., The generation of electric charges and fields in thunderstorms, Proc. Roy. Soc. Lond., A 415, 303-315, 1988.
- McAdam W. H., Heat Transmission, 2nd Ed., McGraw-Hill Book Co. 1942.
- McCappin, C. J. and W. C. Macklin, The crystalline structure of ice formed by droplet accretion, I. Fresh samples, J. Atmos. Sci., 41, 2437-2445, 1984.
- McKnight, C. V. and J. Hallett, X-ray topographic studies of dislocations in vapor-grown ice crystals, J. Glaciol., 21, 397-407, 1978.
- Miller N. K. and P. K. Wang, A theoretical determination of the efficiency with which aerosol particles are collected by falling columnar ice crystals, J. Atmos. Sci., 46, 1656-1663, 1989.
- Mitzeva R., Forecast precipitation type and hail intensity using a physical statistical method, Bulg. Geophys. J., 14, 26-34, 1988.

Moore, C. B., B. Vonnegut and D. N. Holden, Anomalous electric fields associated with clouds growing over a source of negative space charge, J. Geophys. Res., 94, 13127-13134, 1989.

Mossop S. C., Production of laboratory clouds. Quart. J. Roy. Met. Soc., 110, 275-279, 1984.

Murakami M., K. Kikuchi, and C. Magono, Experiments on aerosol scavenging by natural snow crystals. 1, Collection efficiencies of uncharged snow crystals for micron and sub-micron particles, J. Met. Soc. Japan, 63, 119-129, 1985a.

-----, Experiments on aerosol scavenging by natural snow crystals. 2, Attachment rate of 0.10 mm diameter particles to stationary snow crystals, J. Met. Soc. Japan, 63, 130-135, 1985b.

-----, Experiments on aerosol scavenging by natural snow crystals. 3, The effect of snow crystal charge on collection efficiency, J. Met. Soc. Japan, 63, 1127-1137, 1985c.

Ono A., The shape and riming properties of ice crystals in natural clouds, J. Atmos. Sci., 26, 138-147, 1969.

Orville H. O. and F. J. Kopp F J, Numerical simulation of the life history of a hailstorm, J. Atmos. Sci., 34, 1596-1618, 1977.

Perkins H. C. and Leppert G., Forced convection and heat transfer from a uniformly heated cylinder, J. Heat Transfer, 32, 257-263, 1962.

Pruppachar H. and J. D. Klett, Microphysics of clouds and precipitation, Reidel Publishing Corp., 1980.

Ranz, W. E. and J. B. Wong, Impaction of dust and smoke particles on surface and body collectors, Ind. Eng. Chem., 44, 1371-1381, 1952.

Rawlins F. A., A numerical study of thunderstorm electrification using a three dimensional model incorporating the ice phase, Q. J. Roy. Met. Soc., 108, 779-800, 1982.

Reiker H. Forschungs Geb. Ingenieures No. 269, 1925.

Reynolds, S. E., M. Brook and M. F. Courley, Thunderstorm charge separation, J. Met., 14, 426-436, 1957.

Sartor, J. D., Induction charging of clouds, J. Atmos. Sci., 38, 218-220, 1981.

Saunders, C. P. R. and C. C. Zhang, Rime density, radial forces and atmospheric electricity, Atmos. Res., 21, 101-111, 1987.

Sinha, N.K., Observations of basal dislocations in ice by etching and replicating, J. Glaciol., 21, 385-395, 1978.



Takahashi, T., Electric surface potential of growing ice crystals, J. Atmos. Sci., 27, 453-462, 1970.

Takahashi, T., Riming electrification of charge generation mechanism in thunderstorms, J. Atmos. Sci., 35, 1536-1548, 1978.

Vittori O., Scavenging of atmospheric particles by growing ice crystals: A contribution to a proposed mechanism, J. Atmos. Sci., 30, 321-324, 1973.

Vonnegut, B., Possible mechanism for the formation of thunderstorm electricity, Bull. Am. Met. Soc., 34, 378-381, 1953.

Williams, E. R., The tripole structure of thunderstorms, J. Geophys. Res., 94, 13151-13167, 1989.

Wilson, C. T. R., Investigations on lightning discharges and on the electric field of thunderstorms, Phil. Trans. R. Soc. A., 221. 73-115, 1920.

Wisner C., H. D. Orville and Myers, A numerical model of a hail-bearing cloud, J. Atmos. Sci., 29, 1160-1181, 1972.